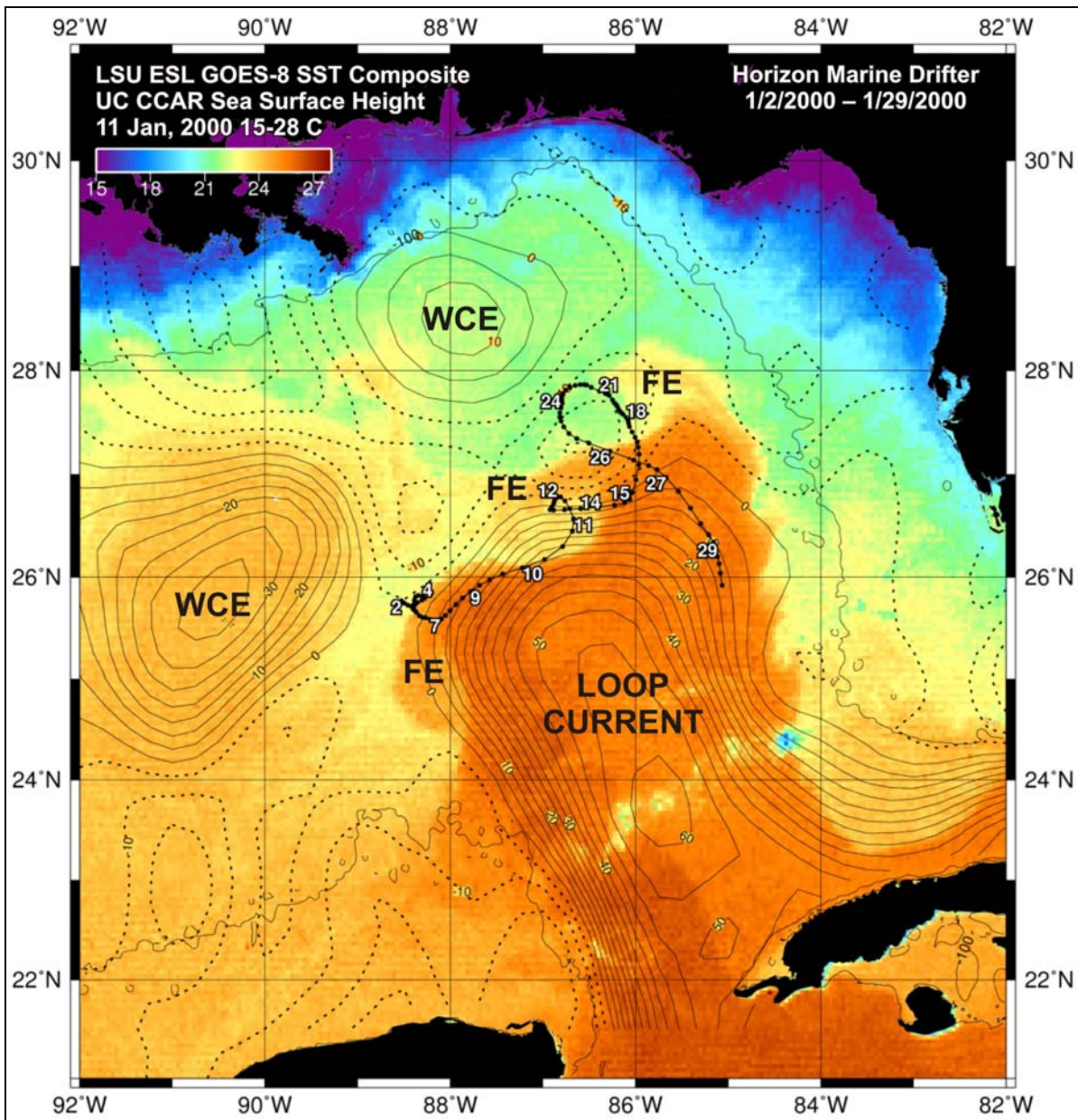**Coastal Marine Institute**

Loop Current Frontal Eddies Based on Satellite Remote-Sensing and Drifter Data

Coastal Marine Institute

Loop Current Frontal Eddies Based on Satellite Remote-Sensing and Drifter Data

Authors

Nan Walker
Robert Leben
Steve Anderson
Jim Feeney
Patrice Coholan
Neha Sharma

July 2009

DISCLAIMER

This report was prepared under contract between the Mineral Management Service (MMS), and the Coastal Marine Institute at Louisiana State University. This report has been technically reviewed by the MMS, and it has been approved for publication. Approval does not signify that the contents necessarily reflect the views and policies of MMS, nor does mention of trade names or commercial products constitute endorsement or recommendation for use. It is, however, exempt from review and compliance with the MMS editorial standards.

REPORT AVAILABILITY

CITATION

ACKNOWLEDGMENTS

ABOUT THE COVER

The cover depicts circulation during a northward intrusion of the Loop Current in January 2000 using GOES SST imagery, gridded SSH data, and drifter measurements.

TABLE OF CONTENTS

LIST OF FIGURES

x

LIST OF TABLES

ABBREVIATIONS AND ACRONYMS

ADCP   Acoustic Doppler Current Profiler
ARGOS   Global Satellite-based Location and Data Collection System
AVHRR   Advanced Very High Resolution Radiometer
AXBT   Airborne Expendable Bathythermograph
CE   Cyclonic Eddy
CB   Campeche Bank
CCAR   Colorado Center for Astrodynamics Research
ESL   Earth Scan Laboratory
FHD   Far Horizon Drifter
FS   Florida Straits
GOES   Geostationary Environmental Satellite
GoM   Gulf of Mexico
GPS   Global Positioning System
GVAR   Goes Variable
LC   Loop Current
LCFE   Loop Current Frontal Eddy
LSU   Louisiana State University
MMS   Minerals Management Service
NOAA   National Oceanic and Atmospheric Administration
OCM   Ocean Color Monitor
POES   Polar Orbiting Environmental Satellite
RMS   Root Mean Square Error
SSH   Sea Surface Height
SST   Sea Surface Temperature
TRW   Topographic Rossby Wave
UTC   Universal Time Coordinated
WCE   Warm Core Eddy
YC   Yucatan Channel

1.0 INTRODUCTION

1.1 Introduction, Motivation, Goals and Key Questions

The over-arching goal of this project was to develop and apply new remote sensing methodologies to improve upon the surveillance of ocean features and the understanding of near surface circulation processes in the Gulf of Mexico (GoM). The Loop Current (LC) and its associated eddies are the most energetic ocean circulation features in the GoM, exhibiting surface current velocities of 1-2 m/s. As oil and gas exploration and drilling moves into deeper water, a better understanding of circulation processes and energetic current events associated with the LC will increase in importance for the effective management of these offshore activities.

The more specific goal of this project was to apply these new techniques to improve understanding of the basic characteristics of Loop Current Frontal Eddy (LCFE) cyclones, specifically where they develop, how they evolve as they travel around the LC, frequency of occurrence, and how they affect circulation throughout the water column in areas of oil and gas operations. Steady progress on understanding aspects of their circulation has been made (for example Cochrane (1972); Paluszkiewicz et al. (1983); Vukovich and Maul (1985); Vukovich (1988); Fratantoni et al. (1998); Walker et al. (2003) and Schmitz et al. (2005)). Their importance is noteworthy as they play a crucial role in the separation process of warm core eddies (WCEs) (Cochrane 1972) and were implicated as possible trigger mechanisms for topographic Rossby waves (TRWs) along the Sigsbee Escarpment (SE) (Hamilton and Lugo-Fernandez 2001). Walker et al. (2005), McKone et al. (2007), and Walker et al. (2008) revealed the occurrence of several full water column current acceleration events lasting for a few to several days when a LCFE, moving along the NW margin of the LC, intensified rapidly over or east of the mooring. In these cases, the LCFE appeared to move over a pre-existing cyclone. These features have proved problematic for comprehensive study. The main reasons for this include their rapid motion, their relatively weak thermal signature in contrast to warm-core eddies, difficulty in resolving them both in space and time with satellite altimetry due to the narrowness of the altimeter tracks and the 10-30 day repeat coverage, and heavy cloud-cover over the GoM (Walker et al. 2003).

Three groups participated in this project: Louisiana State University, University of Colorado, and Horizon Marine Inc. Together, these groups provided the best methods currently available for studying LCFEs. Louisiana State University (Nan Walker) has expertise in remote sensing of sea surface temperature (SST) and ocean color and has developed a unique archive of GOES-8 and GOES-12 night-time "de-clouded" composite imagery (January 1996 to the present) for surveillance of circulation features in the GoM over short time-scales. The GOES "de-clouded" SST data provides a means of tracking the features on a daily basis, as the cyclones entrain relatively warm LC water in a counter-clockwise direction around their centers (Figure 1). In addition, the LCFEs often form upstream from LC meanders which are also apparent in the SST data. The advantage of Geostationary Operational Environmental Satellite (GOES) data is the excellent repeat coverage (every 15-30 minutes) which allows for substantial removal of clouds over short time periods and thus the potential of daily updates for tracking features of interest.

University of Colorado (Bob Leben) has expertise in the quantification and analysis of satellite-derived sea surface height (SSH) data in the GoM dating back to 1993. SSH data from several satellite altimeters enables tracking sea surface highs and lows, revealing the LC, warm- and cold-core eddies with updates of 10-30 days along narrow tracks. The advantage of the SSH data is the fact that it is an all-weather system, unaffected by cloud cover, and it yields unique dynamical information related to ocean circulation (Leben et al. 2002).
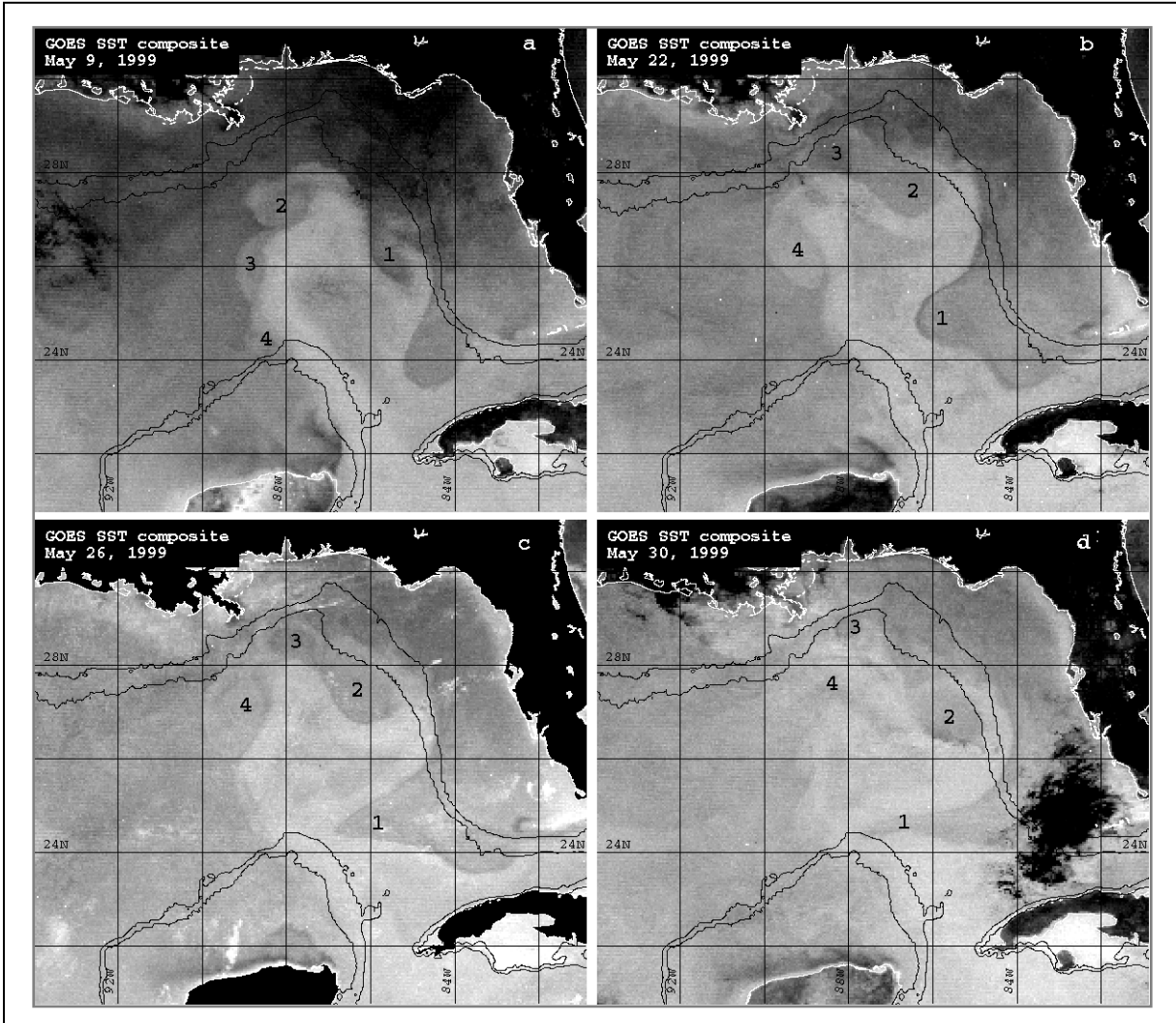
Figure 1. GOES SST composite images depicting the movement of LCFEs around the LC margin in May 1999. (a) May 9; (b) May 22; (c) May 26; (d) May 30. LCFEs are numbered 1 - 4. Lighter shades of gray represent higher SSTs. A 2 x 2 degree latitude/longitude grid is superimposed (modified from Walker et al., 2003).

Horizon Marine Inc. (Steve Anderson, Jim Feeney, Patrice Coholan, Neha Sharma) have operated the industry-supported Eddy Watch Program for over two decades and they provide expertise in quantifying near-surface velocities using drifting buoys which they deploy routinely in features of interest. In addition, they provided Eddy Watch reports, which summarize circulation of the LC and eddies in the GoM on a weekly basis. The main time period covered by this project was January 2001 through May 2004.

This project dovetailed with several MMS-sponsored programs including two LSU mooring programs along the SE (McKone et al. 2007); in the LC (Inoue et al. 2008), as well as the Exploratory Study which focused on the regional circulation along and offshore of the SE (Donohue et al. 2006). Our project provided satellite imagery, in support of these other programs and the field programs provided supporting measurements to aid in our data interpretation.

Our research focuses on answering these broad questions:

I.   How can we most effectively integrate and use the new advanced remote sensing data streams to improve upon the detection, tracking, understanding and prediction of circulation processes of LCFE cyclones that travel rapidly along the margin of the LC?

II.   By using the tools developed in I. can we improve on the available metrics that modelers need to be able to accurately characterize LCFE cyclones as they change in size, intensity, and speed around the margin of the LC?

III.   Do the new remote sensing tools provide observations that further our understanding of key processes that may lead to better prediction of surface and bottom current accelerations, LC intrusions and detachment of warm-core eddies, or hurricane intensity changes in the GoM?

Our research also attempts to evaluate the following hypotheses concerning LCFE cyclones.

H1.   LCFEs form as relatively small (< 50 km across) features and grow in spatial dimension and in intensity as they propagate downstream along the cyclonic shear margin of the LC.

H2.   LCFEs increase in speed as they move downstream along the margin of the LC.

H3.   When hurricanes move across LCFE cyclones, upwelling is enhanced leading to extreme cooling that may impact hurricane intensity.

1.2 Background Information

This investigation focuses on understanding the kinematics and horizontal/vertical structures of LCFEs as they move along the outer perimeter of the LC. These cyclones often play a crucial role in the separation process for warm core rings (Cochrane 1972; Leipper et al. 1972; Vukovich et al. 1979), they may provide a trigger mechanism for the generation of Topographic Rossby Waves as suggested by Hamilton and Lugo-Fernandez (2001), they may trigger surface to bottom flow accelerations as shown by McKone et al. (2007), and they may also play a role in the development of short-lived high velocity sub-surface jets (200-500m) that have been reported by the oil and gas industry. In addition, the upwelling of nutrients within these features makes them ideal spawning and recruitment regions for pelagic species such as the blue-fin tuna (Maul et al. 1984; Bakun 1996). As oil and gas exploration moves into deeper water, these frontal eddies will have more of an impact on operations and environmental management.

Before the availability of satellite measurements, Cochrane (1972) studied the separation of a warm core ring from the LC in May 1969. His ship-board measurements showed that the LC was constricted by two large cold meanders; one protruding eastward from the Campeche Bank, and the other protruding westward from the west Florida shelf. These meanders joined to form a cyclonic shear zone that separated the warm ring from the LC. In the study of a different event, Leipper et al. (1972) showed that the cold zone separating the anticyclonic eddy from the LC extended to a depth of at least 250 m. Vukovich et al. (1979) used five years of NOAA AVHRR satellite data (1973-1977) to study the kinematics of the LC and the separation of warm core rings. They found that ring separation was always preceded by the growth of a large meander off the southern part of the west Florida shelf along the east side of the LC. They also noted that smaller meanders moved along the LC boundary at an average speed of 28 km/day and with an average wavelength of 210 km. Vukovich (1988) reviewed five years of AVHRR satellite infrared data to show that wave-like cyclonic perturbations are largest and most prevalent north and east of the LC. He suggested that the cyclones either develop or intensify along the northwest side of the LC north of 27° N. He measured propagation speeds around the LC of 2 to 20 km/day with length scales of 100 to 250 km. Paluszkiewicz et al. (1983) named these cyclonic features "frontal eddies" and studied one of these features in detail using hydrographic, current meter mooring, and AVHRR satellite data. They obtained detailed physical and chemical measurements within a frontal eddy that affected the continental shelf southwest of Tampa in April 1982. The thermal infrared imagery provided an accurate spatial representation of the surface thermal properties and enabled tracking of the eddy for several days. The warm counter-flowing LC filament that eventually flowed over the shelf measured 220 km in length, extended at least 180 m deep, and remained attached to the LC as it moved southward at an approximate speed of 26 km/day over a 4-day period. They observed strong doming of isotherms within the cyclonic eddy and intensification of the doming over time, indicative of upwelling. Many of the characteristics of this LCFE were similar to some cyclones that had been observed along the shelf edge of the Gulf Stream (Lee et al. 1991; Lee and Atkinson 1983). In both cases, the frontal eddies consisted of counter-flowing warm near-surface filaments or streamers of the main current, separated from the main current by cooler water. The LC filament was deeper (60-180 m) than those reported along the edge of the Gulf Stream (15-20 m) (Lee et al. 1991). They concluded that these frontal features provide a major mechanism for upwelling along the margin

of the LC and for exchanging water between the west Florida continental slope and shelf (Paluszkiewicz et al. 1983).

The subsequent analysis of Vukovich and Maul (1985) provided detailed information from ship surveys on the sub-surface properties of cold-domed frontal eddies on the east side of the LC away from the Florida shelf. Doming of isotherms within the cyclones was clearly evident to a depth of 1000 m from one of the ship's survey. Geostrophic currents in excess of 100 cm/s were calculated along the LC side of the eddy where horizontal density gradients were greatest. Their observations suggest that a cyclone along the east side of the LC is always associated with separation of large anticyclonic rings; although they also noted that many of the cyclones dissipated locally. Lee et al. (1995) and Fratantoni et al. (1998) studied the quasi-stationary eddies near Dry Tortugas that form from southward moving LCFEs. They found that the longevity of Tortugas eddies is influenced by LC eddy shedding processes. Longevity is approximately double during eddy shedding events, when the LCFEs are entrained southwestward across the GoM, rather than moving southward into the Florida Straits (FS) where they initiate movement of Tortugas eddies.

Zavala-Hidalgo et al. (2003) studied regions of cyclonic circulation east of the Campeche Bank (CB) using SSH data along a Topex-Poseidon track running from 18º N, 84º W to 30.5º N, 90º W, a track which bisected the Yucatan Current. The cyclonic eddies that they studied were generated near 23.5º N and 86.5º W, which is a location usually occupied by the LC (Vukovich et al. 1979; Leben 2005). They showed that cyclone generation in this region is closely associated in time with the last stage in the shedding process of a LC anticyclone, an observation that supported previous research. The eight cyclones they detected over seven years persisted for varying lengths of time, ranging from 1.3 to 9.6 months. Some of these cyclones later moved northwards towards the Mississippi shelf break. The cyclones that they studied were large and persistent and formed when the LC was in a retracted state, or port-to-port situation, meaning that the LC flowed fairly directly from the Yucatan Channel (YC) to the FS (Schmitz et al., 2005).

In contrast, our study targets cyclones that are first apparent in SST imagery along the western margin of the LC as it flows in close proximity to the CB. These cyclones are initially quite small in size but can grow to large dimensions north and east of the LC (Figures 1, 2, and 3).

Schmitz (2003) and Schmitz et al. (2005) have used the term "embryonic shingles" to describe these small scale shear-edge features that become apparent in satellite imagery after the Yucatan Current enters the GoM. These shingles propagate northward or northwestward along the LC margin, depending upon the orientation of the LC. They appear in satellite SST imagery as meanders in the thermal front. Although Schmitz et al. (2005) gives unique names to cyclones on the west, north and east margins of the LC, we choose to use the term, LCFE, for all frontal cyclones regardless of size or location.

Several possible generation mechanisms for LCFE formation have been proposed and include topographic vortex stretching (Cochrane 1965), shear instability in the LC (Maul 1974 and 1977), baroclinic instabilities along the CB slope (Hurlbert 1986) and impingement of a Caribbean anticyclonic eddy on the Yucatan Current (Huang and Hsueh 2004).

Walker et al. (2003) studied LCFE kinematics based on their motion around the LC in May 1999. In Figure 1, a sequence of four GOES-8 "de-clouded" SST composite images from the sequence in May 1999 are shown to illustrate the movement and growth of four LCFEs over a three week period. The LCFEs are apparent as they advected warmer LC water around their centers of circulation. In addition, they grew in size upstream from large meanders in the LC which were also observable as deformation in the margin of the LC, an area of strong SST gradients. Although doming of cold water within the centers of these cyclones is a characteristic, the cool water does not reach the surface and thus is not usually detected in satellite IR imagery. Detailed analyses of eddy motion and spatial scales during May 1999 revealed that the LCFEs moved at variable speeds ranging from 5 to 36 km/day along the margin of the LC. Diameters of the four features which were tracked ranged from 64 to 224 km. A detailed analysis of LCFEs during 2000 and 2001 revealed the presence of 2 to 4 LCFEs at all times when the LC was visible (Walker et al. 2003).

The May sequence clearly reveals circulation changes associated with five LCFE cyclones which led to the near separation of a WCE by May 30. Initially on May 9, four LCFEs were clearly apparent (and numbered in Figure 1) along the margin of the LC- located to the east, north, northwest and west. A large unmarked cyclone (24º N, 85º W) was located downstream of LCFE 1 on May 9, and appears to be headed towards the FS. This feature is a classic Tortugas Eddy (Fratantoni et al. 1998). By 22 May, LCFE 2 and LCFE 4 had increased in size while LCFE 1 moved south from 26º N to 25º N. A close inspection of the May 22 image shows that a meander had formed upstream of LCFE 4 which led to deformation of the LC to the west. Likewise, LCFE 1 deformed the LC margin by moving westward also. By May 26, the LCFE 2 and 4 have grown in size and have propagated downstream, further deforming the LC. By May 30, separation of a LC warm-core eddy appears imminent as LCFE 1 continues to move westward between the southern and northern portion of the LC. However, the LC later surges northwest to recapture the warm eddy. This short time series provides a glimpse of how rapidly the LCFEs can grow, move and impact the structure of the LC.

Two additional GOES SST image composites with SSH overlays are provided in Figures 2 and 3 as further examples of the dynamic nature of the LC system. These examples depict two of the many configuration possibilities for the LC and its associated LCFEs and WCEs. On January 18, 2001, the LC was located in the eastern GoM with four main LCFEs along its perimeter, apparent in the SST image (Figure 2). This configuration is typical of a LC which has surged north into the GoM, with well-developed meanders and LCFEs. This configuration often leads to the separation of a WCE.

In contrast, Figure 3 shows the LC in a retracted state, south of 25º with a LCFE along its northeast margin (25º N, 84-85º W). A second region of low SSH, perhaps a LCFE, was apparent near 23º N, 87º W, adjacent to the CB, with an SSH value of -15 cm. A WCE had separated from the LC, with an abnormally large LCFE along its northern margin. The LC obviously loses LCFEs when WCEs separate from it. The SSH data reveals that this LCFE was abnormally large (> 200 km across), comparable in size to a WCE, with SSH of -30 cm. The interaction zone between this LCFE cyclone and a smaller WCE to the west of it (26º N, 91º N), provided a counter-rotating circulation that entrained near surface river and shelf water offshore.
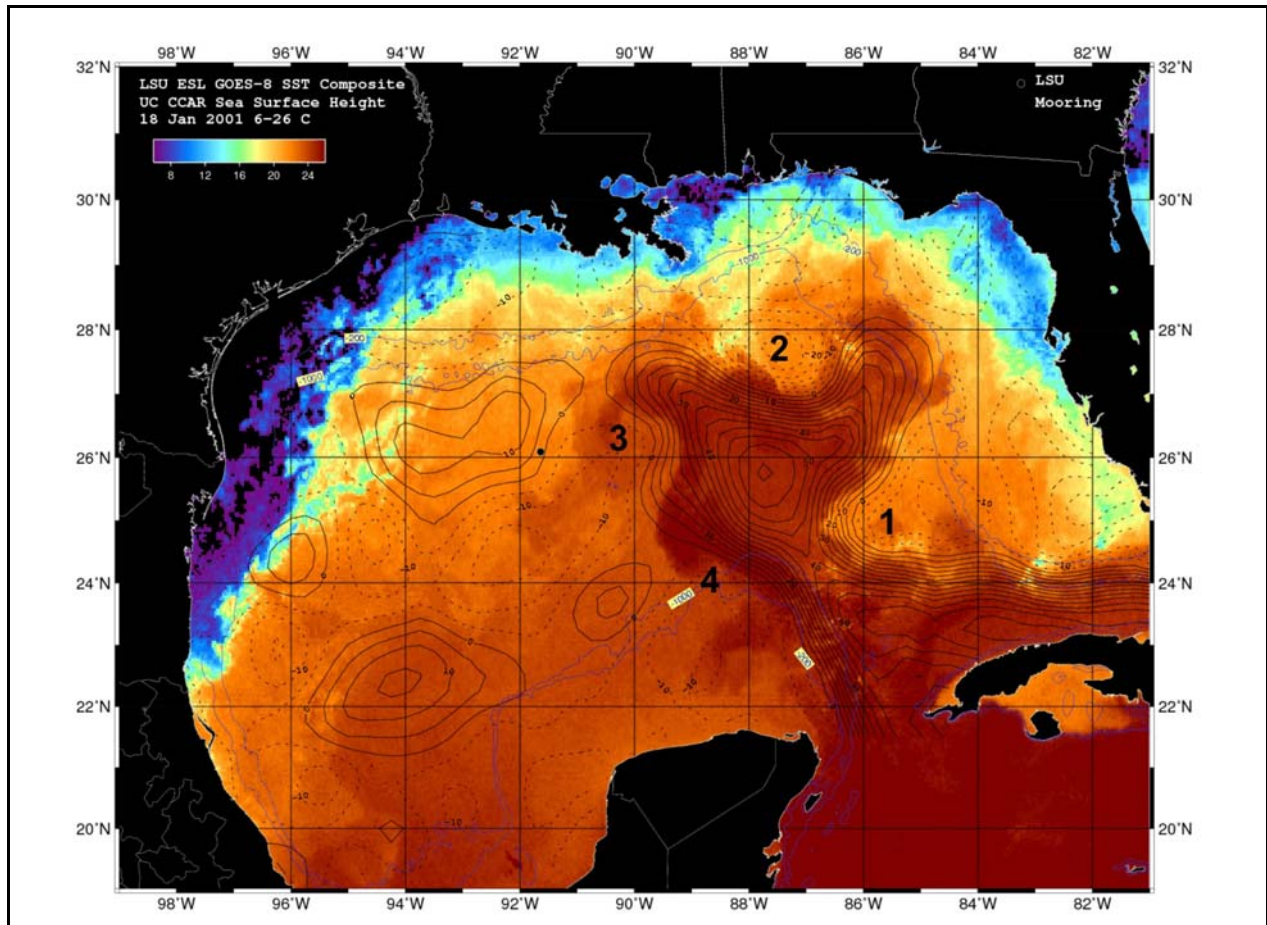
Figure 2.   GOES-8 SST composite image for January 18, 2001, showing the LC in the eastern GoM with four main LCFEs along its margin, numbered 1 to 4.
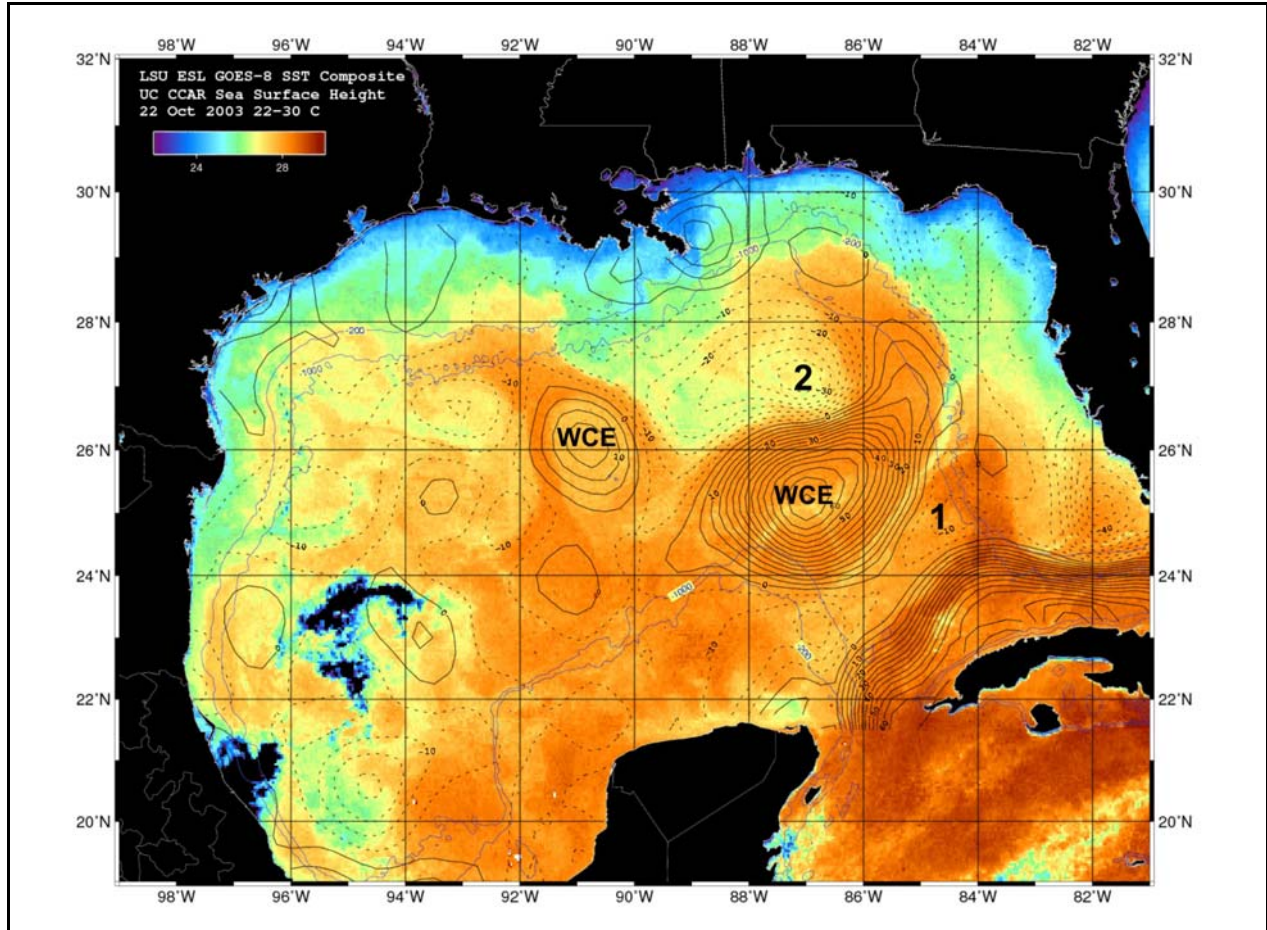
Figure 3. GOES-8 SST composite image for October 22, 2003, superimposed with gridded SSH data, showing the LC in a retracted state with at least one LCFE (1) passing between the LC and the WCE, which had recently separated. The WCE was bounded to the north by an abnormally large LCFE (2). A smaller older WCE was located west of this LCFE/WCE.

2.0 DATA AND METHODS

2.1 GOES SST Measurements and Image Composites

The GOES GVAR sensors provide high frequency repeat coverage which improves the potential for retrieving ocean temperature information over short time-scales (Legeckis et al. 1999; Walker et al. 2003). This study utilized both GOES-8 and GOES-12 measurements, obtained in real-time, using a ~3-meter geostationary antenna at the LSU Earth Scan Laboratory (http://www.esl.lsu.edu). Data calibration, navigation and registration were performed using a SeaSpace Terascan[TM] system. A unique aspect of the Walker et al. (2003) methodology is the use of the mid-IR channel (channel 2 at ~3.9 μm) rather than the thermal IR (channel 4 at ~11μm). Channel 2 is less contaminated by atmospheric water vapor than is channel 4, as is well illustrated by the comparison shown in Figure 4. Channel 2 data can be contaminated by solar reflections restricting its use to night-time. A "cloud-erasing" technique was performed by compositing sequences of 8-10 hours of night-time channel 2 data and retaining the warmest value for each pixel each night (i.e. the warmest pixel method). This technique assumes that the ocean is warmer than the atmosphere and eliminates much of the cloud contamination over the GoM, revealing ocean temperatures and features with much increased frequency. The sole use of night-time data improved the accuracy of the SST algorithm compared with previous studies. Linear regression of channel 2 data with buoy data in the GoM yielded R^2 values of 0.98 and the resulting SST algorithms (for GOES-8 and GOES-12) exhibited RMS values of <0.48º C, and biases near 0º C. These results were considerably better than those obtained by May et al. (1998) and Wu et al. (1999). We think our results showed improvement due to the sole use of channel 2 and night-time data, exclusively, which reduced diurnal surface warming effects during daylight hours.

The GOES night-time SST composites were used in this project as the main method for detecting LCFEs on a daily basis. A suite of GOES composite images, from January 2000 through June 2004, were provided on an Earth Scan Lab (ESL) web page (http://www.esl.lsu.edu/research/CMI-GOES) for project participants and other MMS-funded researchers. Animation of sequences of the night-time composite images provides a powerful method for visualizing the movement and growth of LCFEs around the margin of the LC, as well as other circulation features in the GoM. An interactive animation toolbox was provided on the ESL Web page as part of this project.
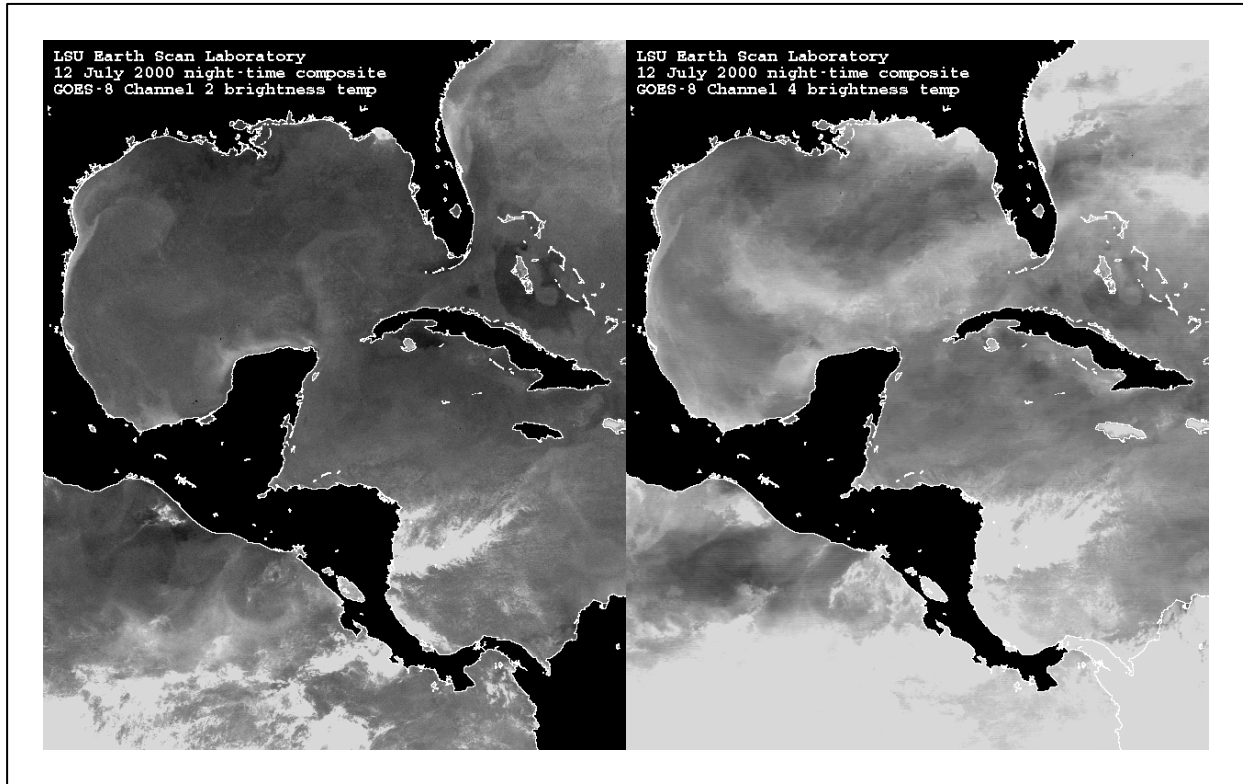
Figure 4. GOES-8 night-time image composites from (left panel) mid-IR channel 2 (3.8-4.0
μm) and (right panel) thermal-IR channel 4 (10.2-11.2 μm) brightness temperatures
(in degrees C) on July 12, 2000. Channel 2 reveals ocean temperature structure (LC
and coastal upwelling), whereas channel 4 reveals mainly atmospheric water vapor
and clouds (lower temperatures). Temperature range is 21-28º C with lighter gray
shades depicting lower temperature. (from Walker et al. 2003).

2.2 Sea Surface Height Sensors and Measurements

Satellite altimetry measures sea surface height (SSH) and is the only remote sensing technique that directly measures a dynamical variable of the ocean. Although the SSH is a surface measurement, it reflects the integrated variation of density throughout the water column. By referencing a mean surface and assuming a relation between SSH and vertical density structure, one can calculate the associated geophysical fluid dynamics such as the distribution and redistribution of mass and momentum in the ocean. Furthermore, unlike satellite thermal sensors, altimetry is an all-weather observation. This makes it a complementary remote sensing data product for synthesis with SST imagery and satellite tracked drifter records. Since 1992, altimeter measurements have provided nearly continuous monitoring of the Gulf of Mexico from the multi-satellite sampling afforded by altimeters aboard the NASA/CNES TOPEX/POSEIDON, ESA's ERS-1 and ERS-2 satellites. The addition of data from the U.S. Navy Geosat Follow-on (GFO) satellite, the NASA/CNES Jason-1 satellite and ESA's Envisat satellite in recent years further improved altimetric measurements. GFO became operational in late 2000. The most complete coverage with satellite altimeters was from October 2002 through October 2005, when, measurements from four satellites (Envisat/ERS-2, GFO, Jason and TOPEX/POSEIDON) were available (http://argo.colorado.edu/~realtime/welcome/).

Two main formats of SSH data were used in this study. Gridded data were obtained from the CCAR ftp site in quasi-real time and superimposed on the GOES SST composite images each day. These gridded data have a 60-100 km working spatial resolution depending on sampling and interpolation, and are smoothed both forward and backward in time (Leben and Born 1993; Sturges and Leben 2000, Leben et al. 2002). The CCAR altimeter product is based on a quick-look analysis technique that references data to an independent mean surface described in Leben et al. (2002). In addition to the gridded data, the alongtrack data for each satellite were obtained from the CCAR data archive, so that crossings of the LCFEs could be identified more precisely. These data were scaled for ease of interpretation and superimposed on GOES SST composites for the period of this study. An example of the gridded product superimposed on GOES SST is shown in Figure 5 (upper panel). An example of the alongtrack data obtained on the same day as the GOES SST composite is shown in Figure 5 (lower panel). The alongtrack altimeter data provides detail on the structure of the LCFEs as the data has a 1-Hz alongtrack sampling rate equivalent to approximately 6-7 km.
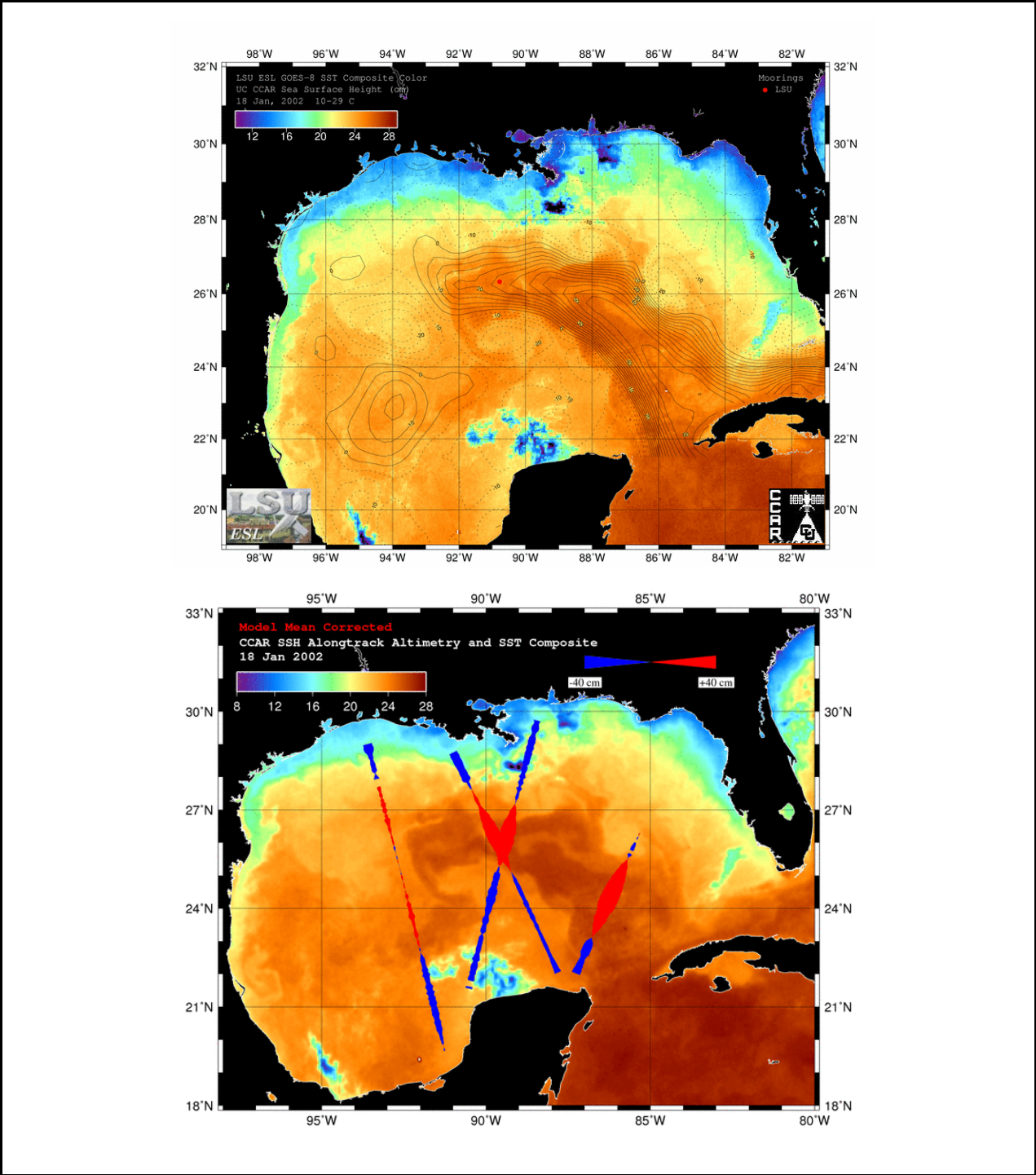
Figure 5. Merged SST and SSH products developed for this study including (upper panel) interpolated and gridded SSH data product for January 18, 2002, superimposed on the GOES SST night-time composite for January 18, 2002, and (lower panel) Alongtrack SSH measured on January 18, 2002, superimposed on the GOES SST night-time composite for January 18, 2002.

2.3 Drifter Measurements

The Far Horizon Drifting buoy (FHD) is a low cost, air-deployable drifting buoy that was designed and first deployed in 1985 by Horizon Marine Inc. The FHD works well for its designed purpose of tracking mesoscale ocean features as part of Horizon Marine Inc.'s Eddy Watch[sm] program. A weekly Eddy Watch summary for the period, including January 18, 2002, is shown in Figure 6. From 1985 to 2002, standard ARGOS positioning was used to track these drifters. In 2002, the FHD transmitters were upgraded and GPS receivers were installed. The buoy hull is cylindrical, and measures 96.5 cm by 12.4 cm in diameter. The parachute drogue has an effective drag area of 1.28 m^2 and is connected to the buoy with a 45 m nylon tether (Figure 7).

Since the first two FHDs were deployed in Fast Eddy (May 1985), they have successfully tracked the location and current velocities in 42 anticyclonic eddies. The buoys have also been valuable in defining the northern extent and strength of the Loop Current and in tracking eddies and monitoring the currents associated with them as they migrate across the entire Gulf of Mexico. In addition, "barrier buoys," buoys that are not circulating in strong ocean features, provide valuable information in the "benign" zones.

Following deployment by either aircraft or ship, the buoy's transmitter broadcasts a platform identification code (PTT number) to the Argos system aboard NOAA polar orbiting satellites. The broadcasts occur at intervals of 90 seconds. A Doppler shift technique applied over a series of buoy-satellite "hits" produces a real-time buoy position fix accurate to better than 500 m. Satellites pass within range about 10 times per day providing buoy locations. When a sufficient number of buoy positions is compiled and plotted, their trajectories are then analyzed. Analyses of drifters circulating within an eddy yield information on configuration, current velocities, orientation of major and minor ellipsoid axes, angular rotation, and migration speed and direction. When eddies of interest form, drifters are placed in their centers and along the fronts that threaten offshore operators. As eddies migrate, additional buoys are deployed in them to maintain sufficient data density to observe their structure and frontal locations.

This project utilized the Eddy Watch reports to select drifters of interest for further analysis in combination with the SST and SSH information. Horizon Marine's quality controlled drifter data was used and when possible the GPS buoys were chosen for analyses.
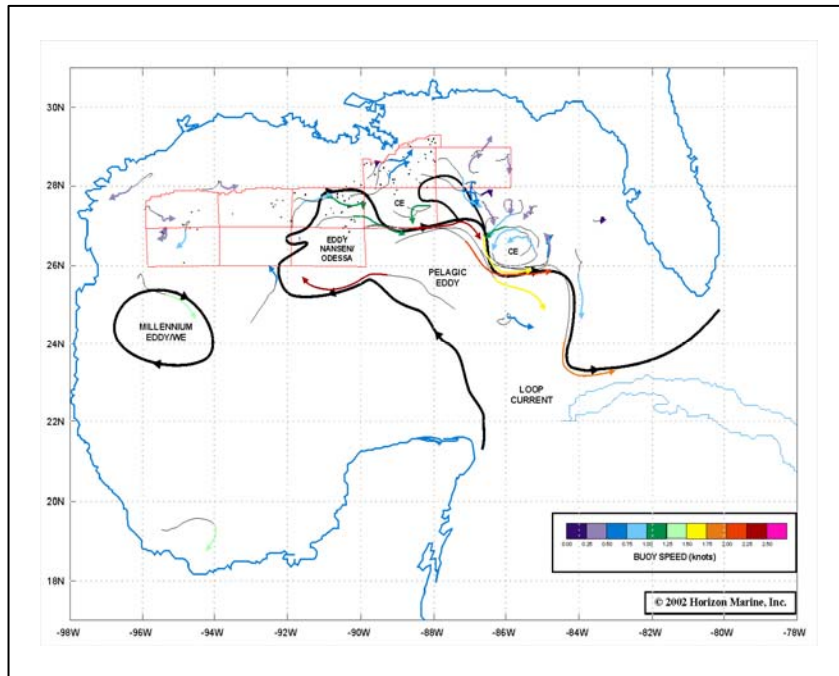
Figure 6. Eddy Watch Report for week including January 18, 2002, to match with satellite products shown in Figure 5.

Buoy Cylinder

96.5cm x 12.4 cm DIA
7.82 kg out of water

45 meter Tether

0.476cm solid braid nylon
in water: 0.112 kg per 100m

Parachute - Drogue

0.034 kg in water
Effective Drag Area=1.26 m²
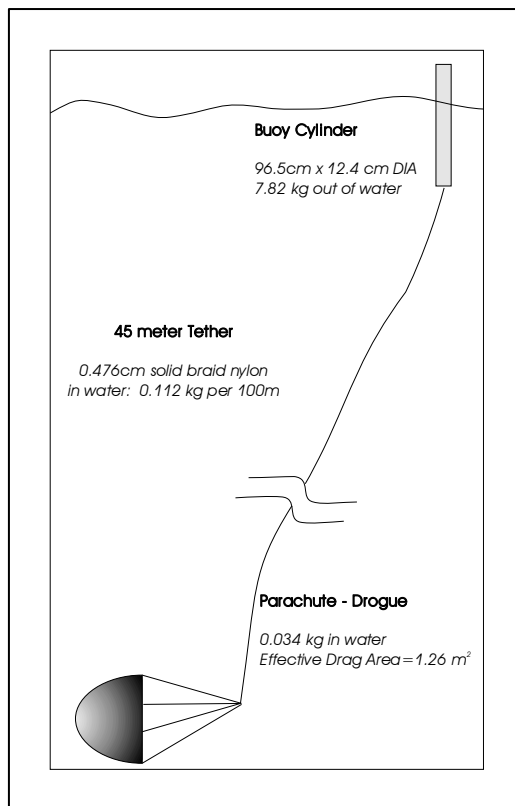
Figure 7. Schematic of the Far Horizon Drifter.

2.4 Web Page Products

During the first six months of the project, a web page was developed where real-time GOES SST imagery and integrated SST/SSH products were posted and updated daily. Eight unique products are displayed, including color and black/white SST images of the GoM and zoomed views of the central GoM. The central GoM view focused on the Sigsbee Escarpment region and western part of the LC, where current meter moorings were deployed from 2000 to 2004. The locations of these moorings are shown on the imagery to aid researchers in data interpretation. The image products included the same GOES SST images with gridded SSH data superimposed upon them. Animation software was also developed for these products. The time sequence available on this page starts in January 2000. The internet link for this project page is http://www.esl.lsu.edu/research/CMI-GOES.

2.5 Development of New Techniques for Tracking LCFEs

The first objective of this project was to develop new techniques to track the LCFEs more effectively. During a meeting of the three main project participants (Walker, Leben, Anderson) in Boulder 2004, an attempt was made to use time/distance Hovmoller graphs employing SST as the environmental variable to track LCFE motion along the western side of the LC. A program was written in MATLAB to extract SST information along a specified line, trending SSE to NNW approximately 50 km west of the western margin of the LC. The location of this line was based on the observed motion of LCFEs in May 1999 with endpoints of 21ºN, 86ºW and 28º N, 90ºW (Figure 8).

The initial result was created by interpolating the gridded thermal data to the line with a latitude resolution of 0.01. This was actually finer than the GOES data which has a spatial resolution of 4 x 4 km. The median value from the nearest four grid points was calculated after selecting only the points greater than 10º C and less than 32º C, to exclude obvious cloudy data. Data between April 1, 2001, and October 31, 2004, was analyzed and the resulting graph for January through October 2004 is shown in Figure 9. During this time period, LCFE motion was best resolved. Hovmoller diagrams provide an effective technique for providing phase velocity information for traveling waves (Hovmoller, 1949). In our case, linear features trending from lower left to upper right indicate LCFEs moving NNW along the western margin of the LC. The initial success with tracking the LCFEs using this technique encouraged the group to attempt tracking LCFEs around the entire perimeter of the LC. It was decided to experiment with a technique which employed the 17 cm contour obtained from the gridded SSH database as a best-guess reference line for the LC. Leben (2005) found this contour to represent the margin of the LC well and used it as a basis for computing metrics on the LC and eddy shedding. At LSU, a procedure was developed using mainly UTC software to extract SST values along a line tangent to the 17 cm SSH contour at a distance of 50 km. Experimentation was performed with other distances, but 50 km gave the most realistic results. This technique enabled tracking the LCFEs around the entire margin of the LC, rather than along the western margin only.
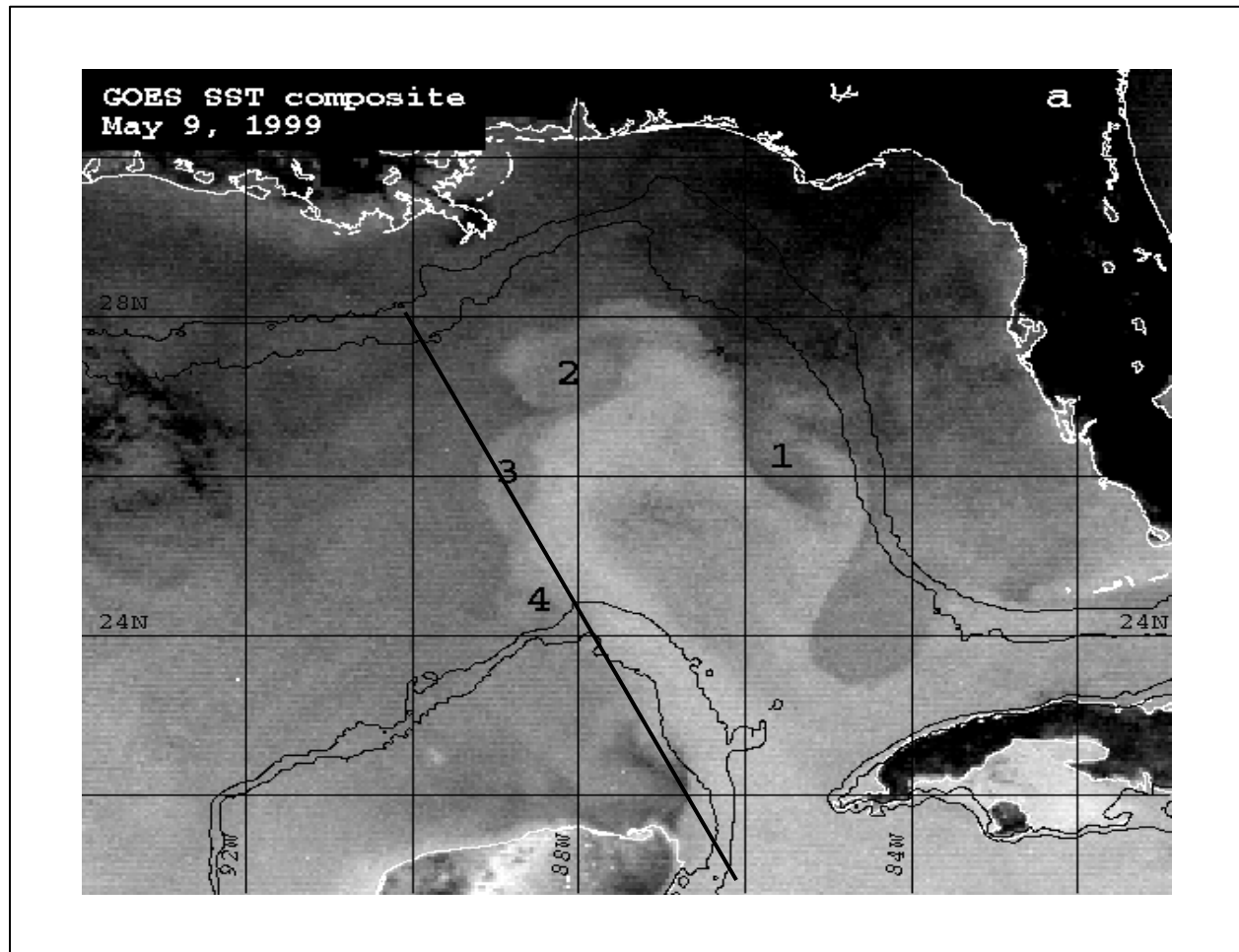
Figure 8.   GOES SST night-time composite for May 9, 1999, depicting the line along which channel 2 brightness temperatures were extracted to construct first Hovmoller diagram.

After program development and experimentation, Hovmoller diagrams were produced for October-December 2001, January-May 2002, October-December 2002, January-May 2003, October-December 2003, January-May 2004 using optimal and sometimes variable SST gray shade enhancements for individual diagrams. The January to May 2004 Hovmoller diagram is shown in Figure 10, for comparison with Figure 9. Although the mid-IR channel can resolve surface temperature gradients in summer in high humidity conditions, surface temperatures across the GoM are very close to isothermal with gradients often less than 1º C. In these conditions, LCFEs may be detectable but tracking them was not effective using the Hovmoller techniques we developed. Thus, our analysis was confined to October through May of three years. Our observations did reveal an interesting phenomenon during mid-summer, generally June-July. Somewhere during that time period, the ambient GoM surface waters become warmer than LC surface waters. Thus, the SST gradient between the LC and surrounding waters reverses! This also inhibits the tracking of LCFEs. This reversal in surface temperature structure is usually observed by early July but the timing is variable.

16
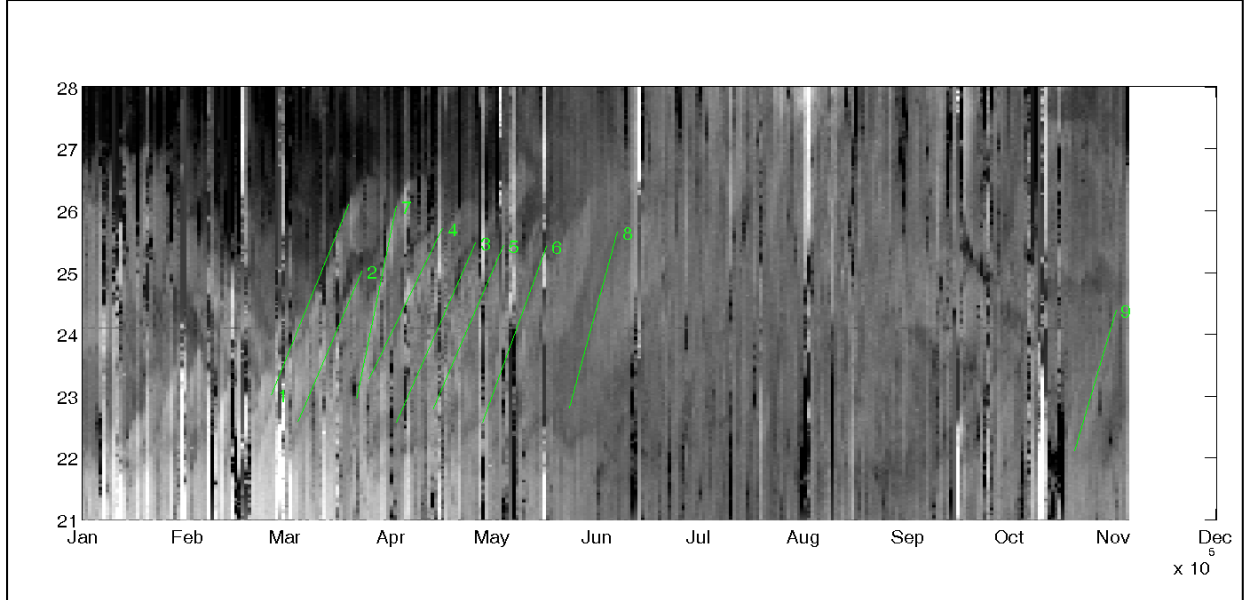
Figure 9. Time/latitude Hovmoller diagram based on GOES SST composites for January through October 2004. Green lines are drawn to show the movement of LCFEs along the western margin of the LC. Phase speed was calculated for selected events and will be discussed in the results section.

The Hovmoller diagrams have yielded a wealth of information about the movement and growth of the LCFEs. Phase velocity can be extracted directly from the diagrams by measuring distance along the y-axis and dividing by the corresponding time value along the x-axis for time periods when linear features are clearly revealed for several days. However, as the LC undergoes substantial changes both in length and width, the y-axes on the Hovmoller graphs change substantially over time. In Figure 10, as an example, the LC perimeter increases from ~1100 to ~1700 km. Through initial testing, we found that the phase velocities measured beyond 400 km on the diagrams were not sufficiently accurate and a decision was made to measure manually along the northern and eastern flanks of the LC (beyond 400 km). An interactive web-based analysis package was developed at LSU for this purpose. It enables the user to track features and to obtain mean velocities between selected pixels (latitude/longitude) when features are clearly apparent in the imagery. Outputs from this program are used extensively in the Results Section.

17
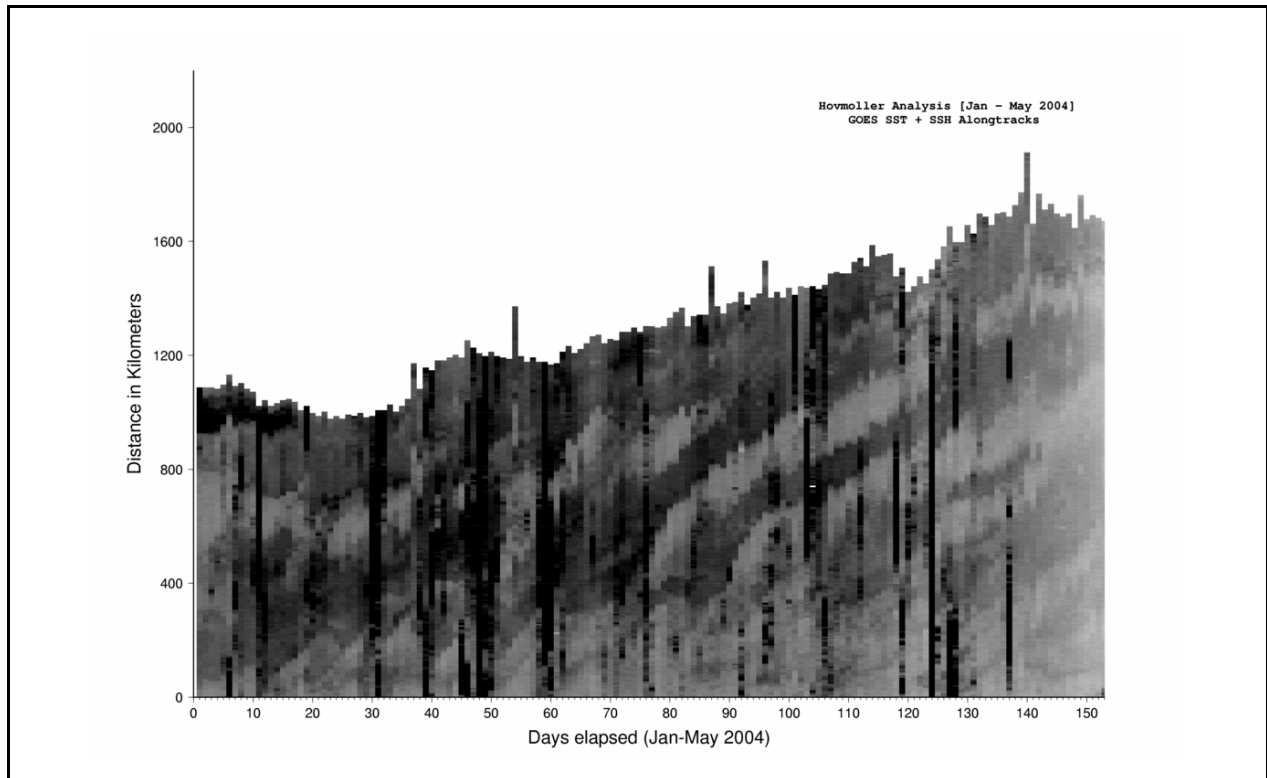
Figure 10. Time/distance Hovmoller diagram showing SST extracted along a line tangent to the 17 cm SSH contour, at a 50 km distance, for each nighttime composite image from January 1 through May 30, 2004. Linear features apparent in the graph depict the motion of LCFEs and their associated meanders, located adjacent and downstream. Lighter (darker) shades of gray depict warmer (cooler) temperatures. Black depicts clouds or cold water. The time axis starts at 00h00 UTC on January 1, 2004, and the x-axis numerals indicate Julian days.

3.0 RESULTS

This chapter of the report is divided into several sections to discuss circulation events of interest as well as statistical information. Section 3.1 presents a case study of LCFE circulation in January 2000 when AXBT data, obtained across a developing LCFE cyclone, revealed the sub-surface structure and vigorous upwelling. Drifter data were fortuitously available to study the time history of near-surface currents associated with two LCFES along the northern margin. Section 3.2 presents an analysis of a northward intrusion of the LC and intense cyclonic circulations in February 2001 which resulted in a "full water column" event and abnormally strong currents at an LSU mooring near the Sigsbee Escarpment. Section 3.3 introduces the use of Hovmoller diagrams for tracking LCFEs along the periphery of the LC from September 2001 through May 2004. A statistical analysis of LCFE motion along the western margin of the LC where it interacts with the CB is presented. Section 3.4 discusses the motion and structure of the LC and LCFEs during January-May 2002, when the LC exhibited a most unusual intrusion into the western GoM. Section 3.5 reviews the details of LCFE motion and structure in January-May 2004, a more typical LC circulation period when it remained in the eastern GoM and south of 27º N. Section 3.6 presents new information on cyclonic eddy motion away from the LC proper based on Eddy Watch observations using drifter data. Some of these cyclones are associated with WCEs and the LC at some stage in their lifecycle. Section 3.7 summarizes results of research concerning observed air-sea interactions and hurricane intensity changes associated with two LCFEs during Hurricane Ivan's transit of the GoM in September 2004. The full peer-reviewed paper is provided in Appendix A.

3.1 Mixed Layer Circulation and Sub-Surface LCFE Structure: January 2000

Surface circulation associated with LCFEs was investigated for a case study event in January 2000. Within this month, clear sky imagery, drifter data and AXBT data were available to investigate the circulation associated with two LCFEs along the LC's northwestern and northeastern margin. Figure 11 depicts the motion and growth of four LCFEs using clear-sky imagery from January 3, 11, 18, and 22. Features are numbered 1-4 for ease of interpretation. The location of the AXBT transect obtained from Gilligan and Blaha (2003) is shown in Figure 11d. The data collected along this line is provided in Figure 12.

The SST patterns of January 11 clearly show the LCFEs around the LC margin; two on the northwest margin, one on the northeast and one on the east. Clear evidence of cyclonic circulation is shown by the warm LC water which was advected away from the outer margin and counter-clockwise around the cyclone centers. Each of the cyclones was located upstream from a distinct meander or bend in the LC. By January 18, the 2 meanders along the northeast margin had merged and so had LCFE 1 and LCFE 2, resulting in a substantially larger LCFE, which is labeled LCFE 1. This feature continued to grow and by January 22 LCFE 1 had become elongated north to south with the eastern margin along the Florida escarpment between 26 and 28º N (Figure 11d). LCFE 3 and its associated meander grew rapidly northwards. On January 11, the northern edge of the meander was near 26º N but by January 22 it had reached 27.5º N. It is possible but not conclusive from the image data that LCFE 4 merged with LCFE 3. A vertical section of temperature was obtained across LCFE 3 on January 22 (Figure 12). It shows
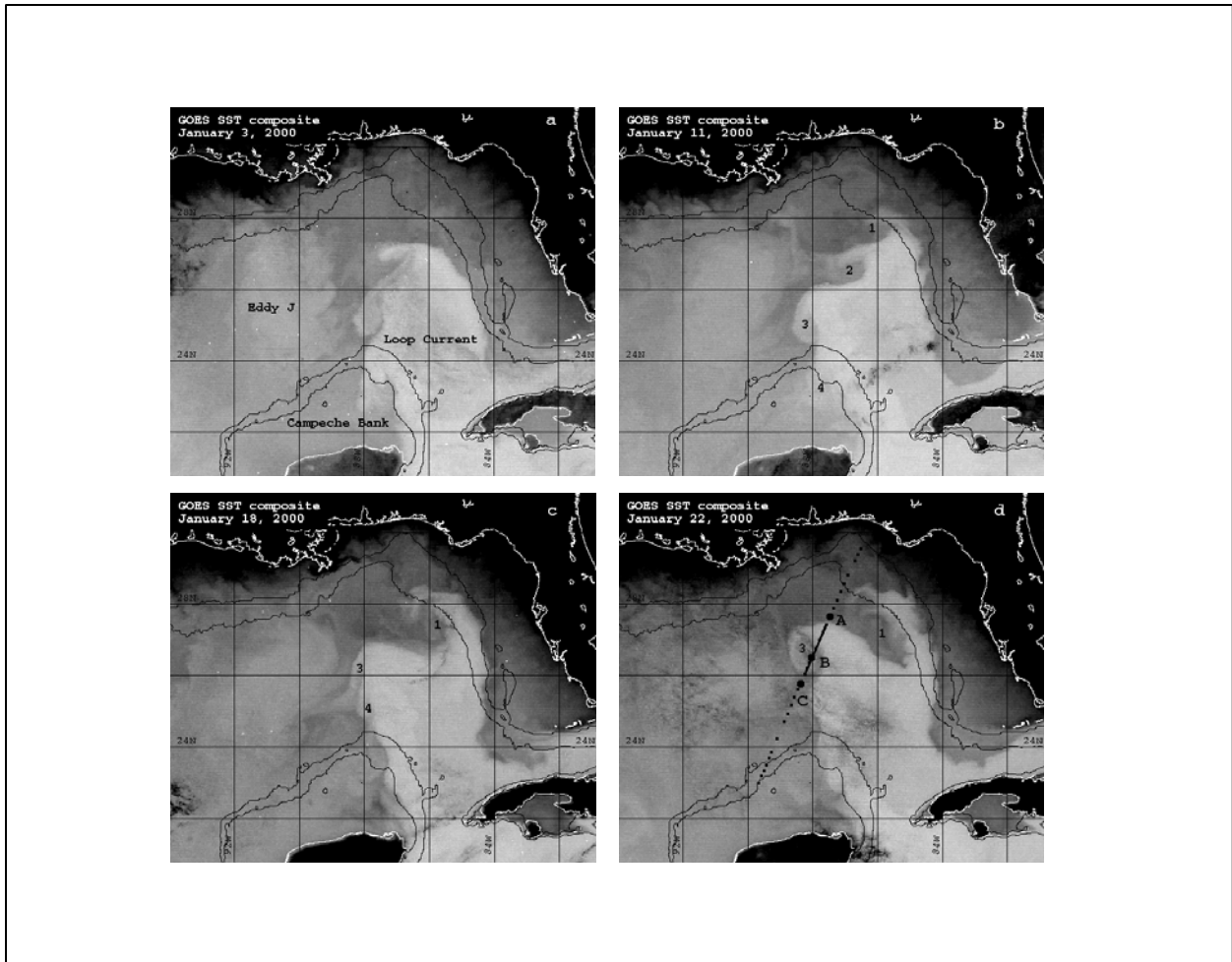
Figure 11. GOES night-time SST composites for (a) January 3 (b) January 11 (c) January 18, and (d) January 22, 2000. The relatively warm LC is shown in the lightest shades of gray. The LCFEs are labeled starting in (b). The AXBT transect is superimposed on the January 22 image, the date of collection by Gilligan and Blaha (2003). The labels (A,B,C) along the transect are used for reference in Figure 12. Two degree latitude/longitude grids are provided on the imagery.
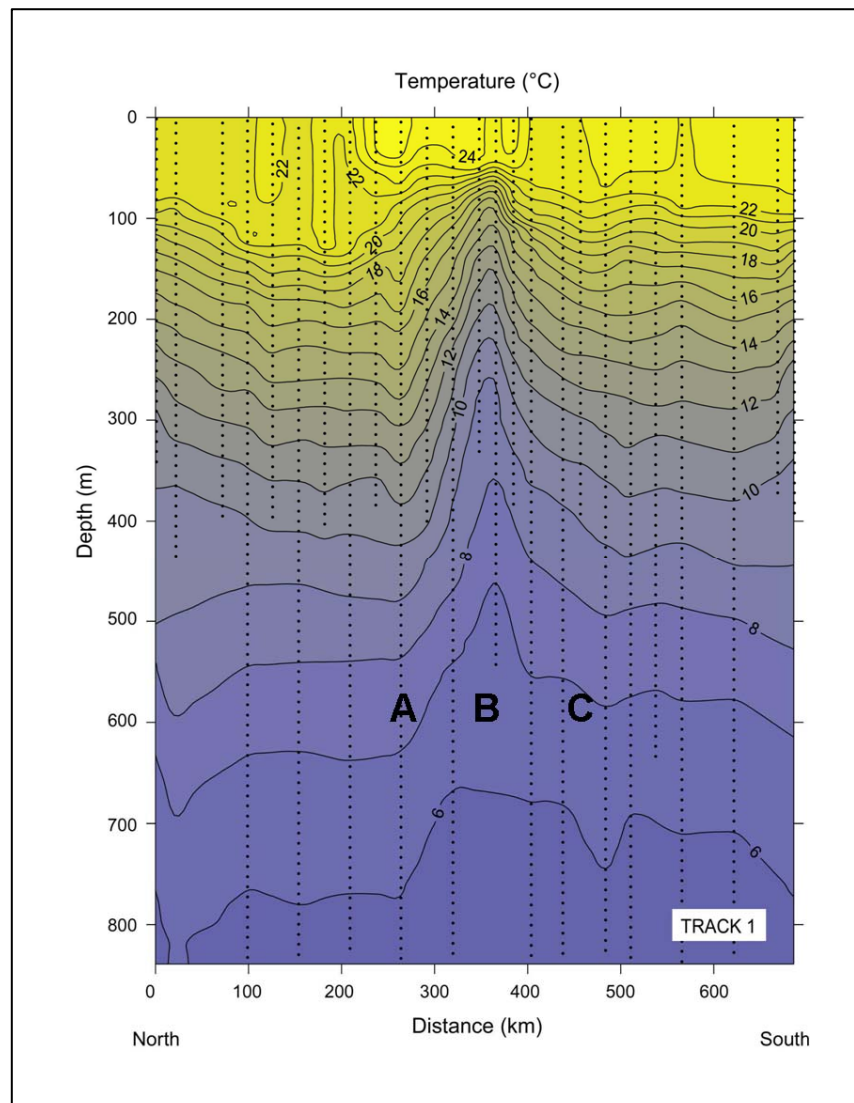
Figure 12. AXBT temperature section from January 22, 2000 (from Gilligan and Blaha 2003). Locations A,B, and C are shown on Figure 11. Location B depicts the center of LCFE 3 on January 22 (Figure 11d). Upwelling of water is apparent between ~50 m to 800 m. Cool waters are blue; warm waters are yellow.

vigorous upwelling within LCFE 3 from ~ 50 m to 800 m (Location B in Figures 11 and 12) in contrast to the surrounding waters. The surface mixed layer extended to 50 m water depth within LCFE 3 whereas it extended to 100 m or more outside of LCFE 3 in both directions. The dimensions of LCFE 3 along this track are estimated at ~150-175 km based on the temperature gradients. It is apparent from close inspection of these data that the northeast (downstream) side of the cyclone exhibited significant downwelling in comparison to the southwest (upstream) side.

Several FHDs were available to investigate circulation associated with LCFE 1 and LCFE 3 (Figure 13). Drifter positions of FHD 590 (drogued at 50 m) are shown for the time period January 1-29, 2000, along with the time series of drifter speed in m/s. The distinct acceleration (to 1.25 m/s or 124 cm/s) occurred on January 9-10 as the drifter moved along the margin of the LC in close proximity to LCFE 2. It experienced another major acceleration on January 25-27 within LCFE 1. See January 23 image in Figure 14 for track of FHD 590 in LCFE 1.
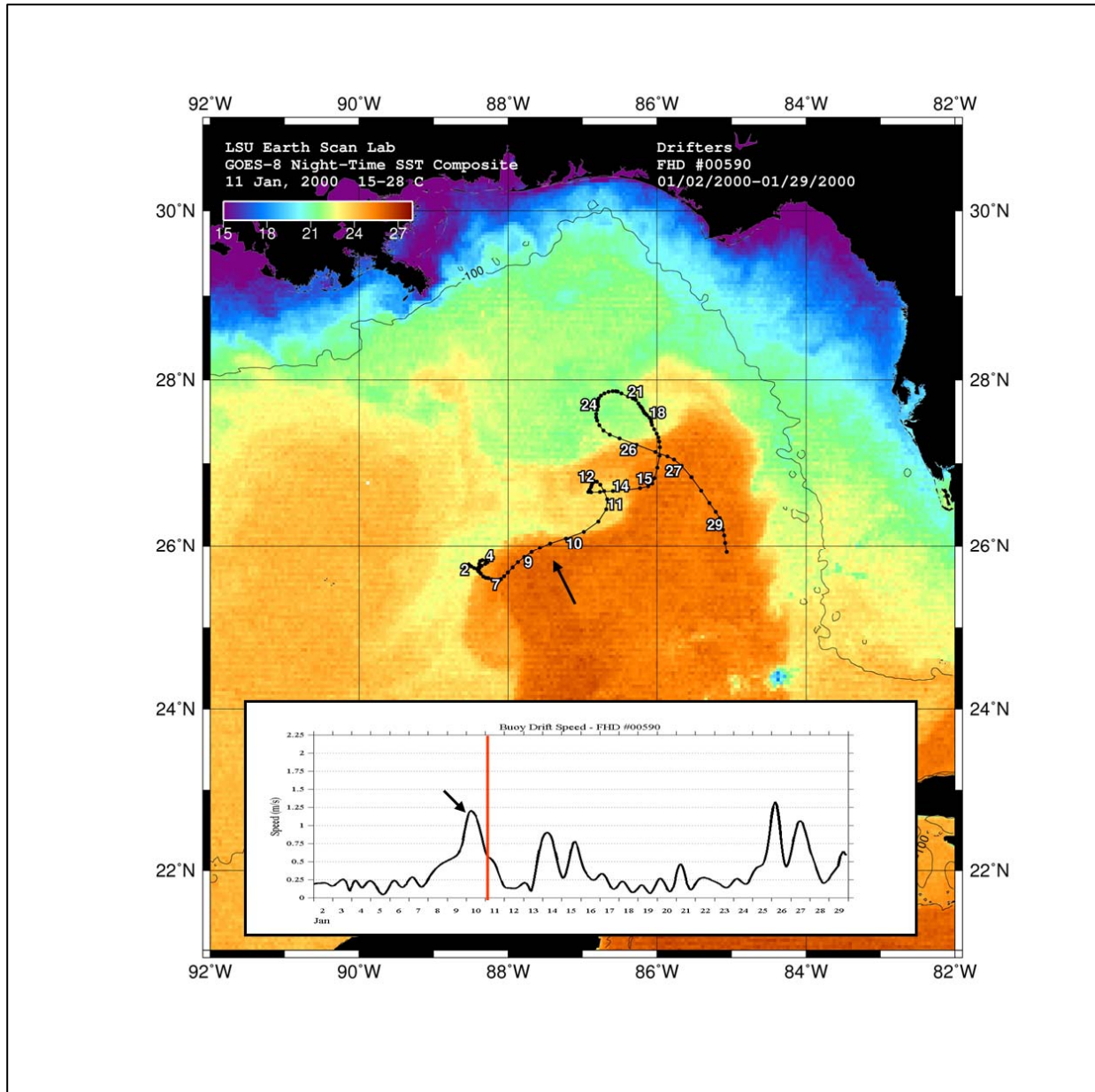
Figure 13. Color-enhanced GOES night-time SST composite image from January 11, 2000, superimposed with tracks of FHD 590 labeled with dates along track. Bottom panel shows current speeds of this drifter from January 1-29, 2000, in m/s. The red line on speed graph depicts the day of image acquisition. Arrows indicate the approximate location and time of current speed maxima.

Figure 14 shows GOES SST distributions for January 23, 2000, with tracks of FHD 590 and FHD 612 superimposed. Speeds exhibited by FHD 612 are shown for the January 16-March 12, 2000, time period in the time series graph. The tracks confirm the location of LCFEs 1 and 3. Note that FHD 590 accelerations on 25-27 January (shown in Figure 13) better match the frontal configuration on January 23, revealing that the observed high velocities of 1.25 m/s (125 cm/s) occurred in the interaction zone between LCFE 1 and the meander east of LCFE 3. As for FHD 612, highest speeds for the period shown in Figure 14 (January 16-29) occurred on January 16-18 when the drifter moved 0.75-1.0 m/s (75-100 cm/s) southeastward towards the western margin of LCFE 3 and also when the drifter moved into the region of interaction between the LC and LCFE 3 where velocities reached 1.25 m/s (125 cm/s) for a short time period (Figure 14 bottom panel, see arrows).
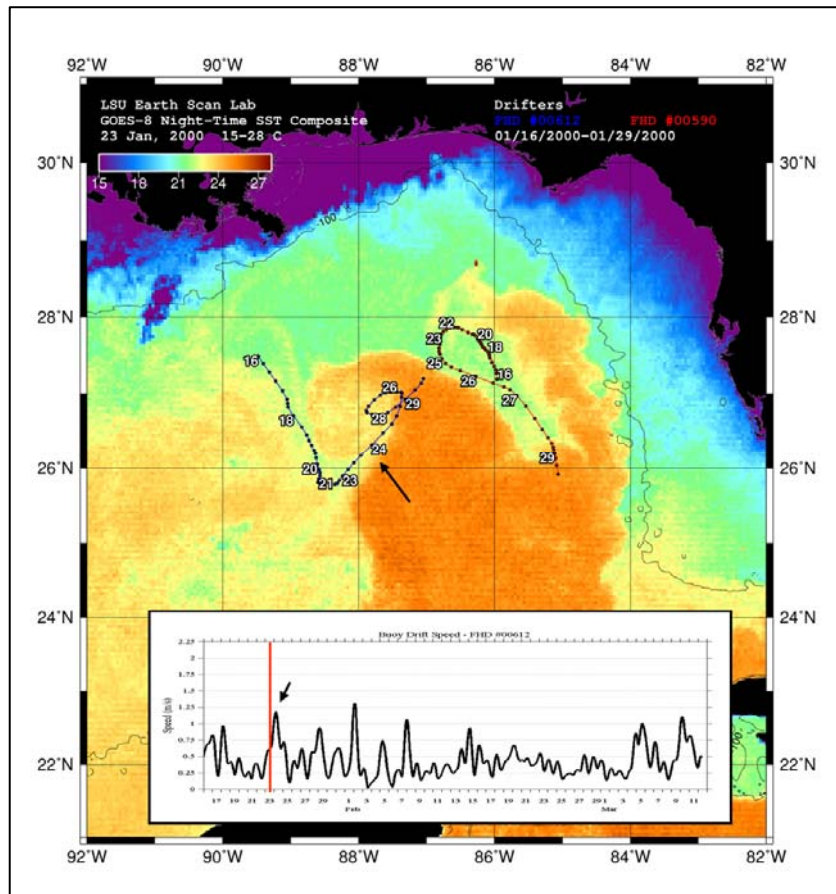
Figure 14. Color-enhanced GOES night-time SST composite image from January 23, 2000, superimposed with tracks of FHD 590 (in eastern LCFE 1) and FHD 612 (in western LCFE 3) labeled with dates along track. Bottom panel shows current speeds of this drifter (m/s) from January 1-29, 2000. A red line is used to indicate time of image acquisition. Arrows indicate the approximate location and time of current speed maxima of FHD 612.

3.2 Near Surface Circulation and Linkages to Deep Water Flow Accelerations along the Sigsbee Escarpment: February 2001

The LC was deeply intruded into the northern GoM in late February 2001 as can be seen in the SST image of February 27, 2001 (Figure 15). From late February to early March, an abnormal flow event was observed especially between 400 and 2250 m at an LSU mooring on the plateau in 2300 m water depth near 26º N, 92º W (McKone et al. 2007). This was the only "full water column" high velocity flow event at this LSU mooring during the March 2000 - April 2001 deployment. Three additional "full water column" events were measured in subsequent deployments which were located in deeper water (~3000 m) seaward and close to the Sigsbee Escarpment, in 2002-2004 (McKone et al. 2007). Drifter data revealed very strong currents at the surface, especially where the LC interacted with cyclonic circulations. FHD drifter 821
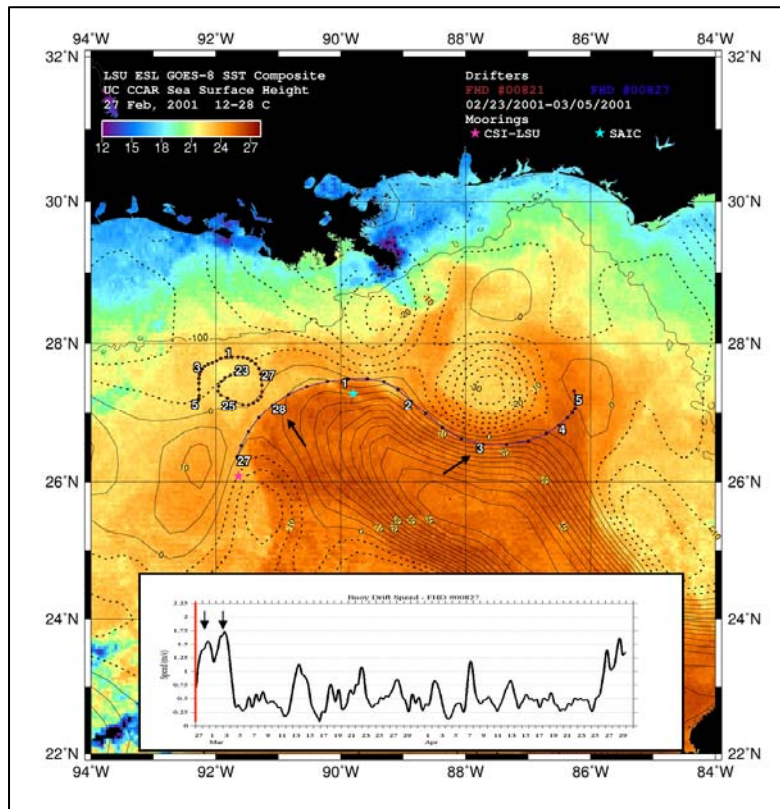
Figure 15. GOES night-time SST composite superimposed with gridded SSH data (positive SSH are solid lines) and tracks of FHD drifters 821 (western) and 827 (eastern) from February 23 - March 5, 2001, and February 27 - March 5, 2001, respectively. The graph shows the track of drifter 827. The red line on the speed graph shows the time of image acquisition. Arrows show the location and time of current speed maxima along the track of 827. The LSU mooring was northwest of LC and shown with a pink star.
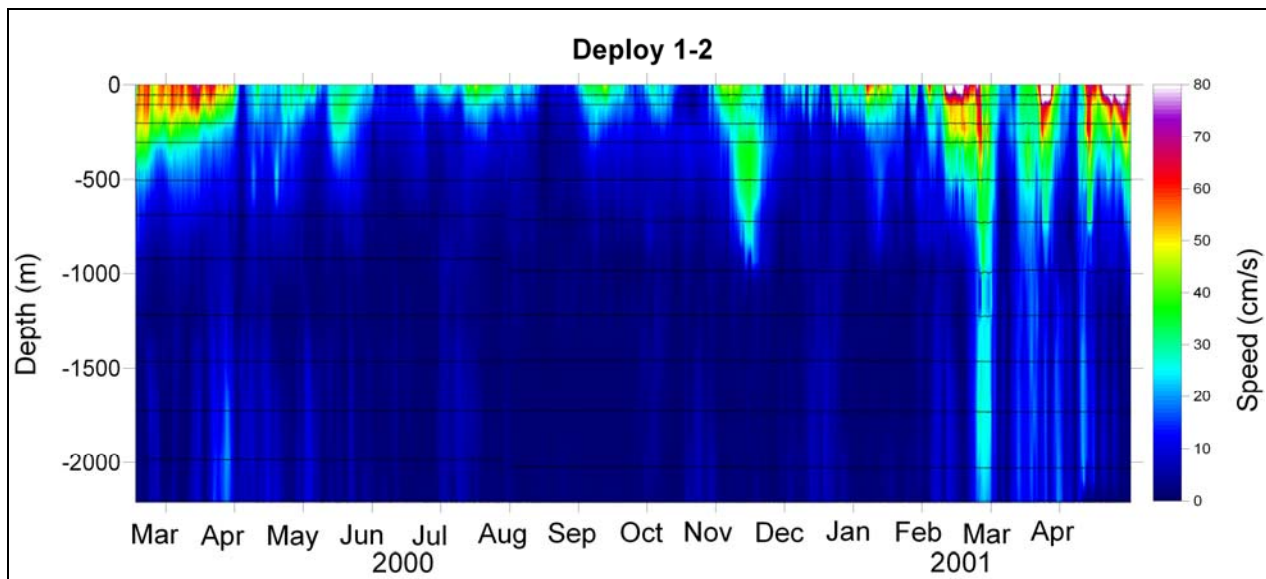
Figure 16. Full water column current speeds for Deployment 1-2, in 2300 m of water on the plateau landward of the Sigsbee Escarpment, 26.0862º N, 91.6392º W. Current measurements were obtained using RDI ADCPs and Aanderaa below 675 m. Modified from Figure 76 in McKone et al (2007). The "full water column" event is observed at the end of February when current speeds exceeded 20 cm/s within the mid and lower water column.

revealed the position of a small cyclone, northwest of the main LC meander. Drifter 827 moved along the outer margin of the LC where it interacted with this small cyclone as well as a well-formed LCFE (SSH of -30 cm) northeast of the LC. The time series for 827 (Figure 15, bottom panel) reveals current speed maxima of 1.5-1.75 m/s (150-175 cm/s) between February 28 and March 3. Maximum speeds occurred where the LC interacted closely with the small and large cyclones.

A time sequence of four SST images superimposed with gridded SSH data reveal that the LC intruded northwestwards at a rapid rate between February 15 and February 28 (Figure 17). Between February 24 and 28, the leading front advanced at 29 cm/s. The leading margin of the LC approached and collided with the Sigsbee Escarpment east of the mooring site near the initiation of strong flow on February 24. Currents at or below 2000 m exceeded 20 cm/s from February 24 to March 1. The SST data revealed that a LCFE (southwest of the main LC meander) grew rapidly at the surface (extending out from the LC ~150 km) and moved over the LSU mooring site during this LC intrusion. Gridded SSH data (Figure 17) and alongtrack SSH data (Figure 18) revealed the presence of weak cyclonic circulation in that area prior to the intrusion. The SSH data gave no evidence that this LCFE strengthened until March 6 when the alongtrack data transected this feature showing SSH of -20 cm (Figure 18). Although gaps in SSH coverage do occur due to the 10-30 day repeat coverage, the available data do not yield any evidence that this LCFE was an energetic feature, initially, even though the surface SST indicates that it covered a large area. In contrast, the cyclonic circulations along the north and northeast margins of the LC were relatively intense (see Figure 18, February 28). The drifter data

gave evidence that these cyclones enhanced near-surface circulation where they interacted with the LC. Although the cyclone northwest of the LC was not revealed in either SST or SSH data, the LCFE northeast of the LC, near 28º N, 88º W intensified from -25 to -30 cm between February 21 and 24 (Figure 17). Based on the available data, it appears that the strong bottom currents at the LSU mooring my have resulted from the interaction of the LC with the shoaling topography along the Sigsbee Escarpment or alternatively from strong vertical motion associated with interaction of the LCFEs and cyclones with the LC meander. In either case, it is possible that topographic Rossby waves were generated that propagated westward along the Sigsbee Escarpment, affecting currents at the LSU mooring.
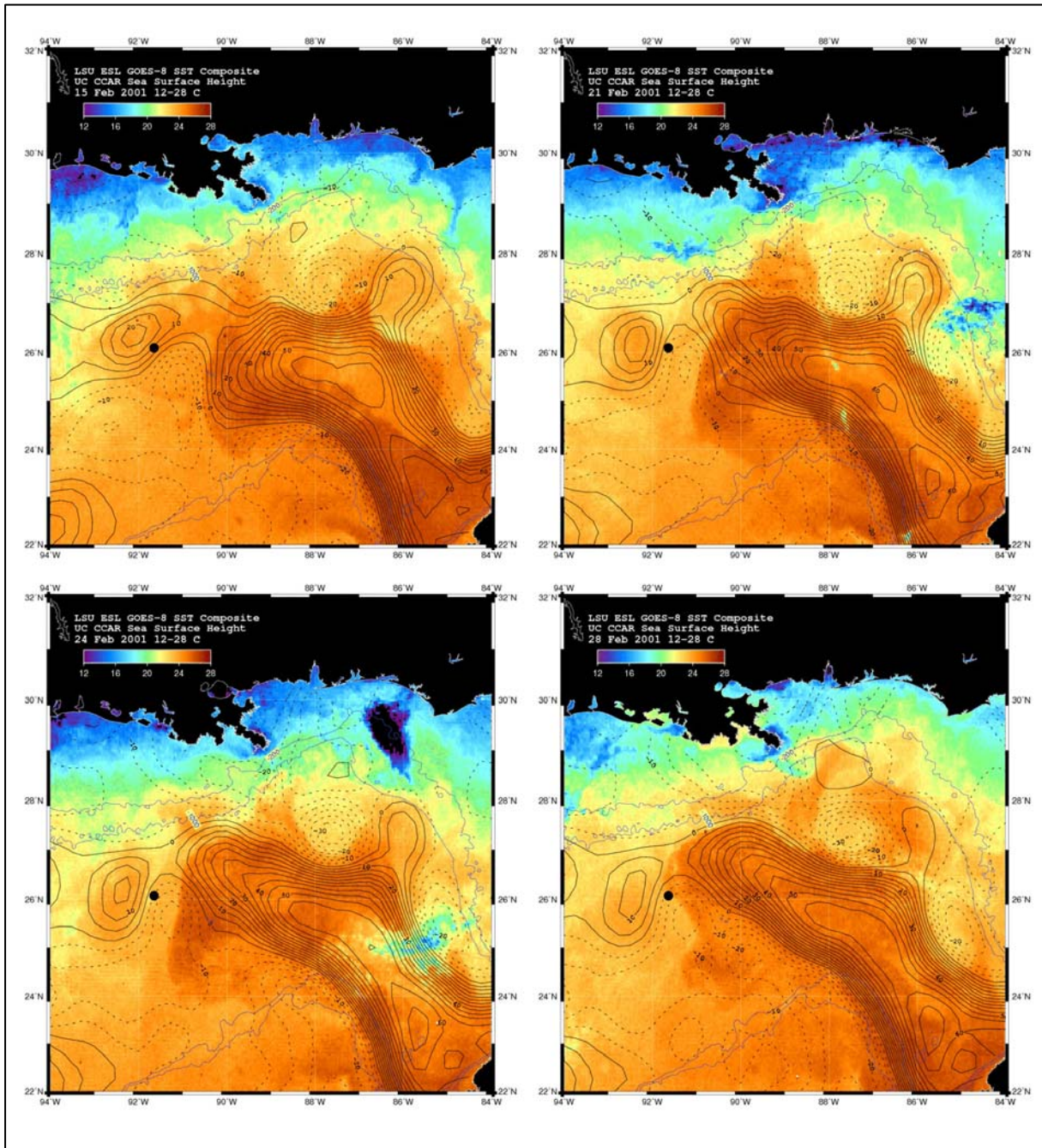
Figure 17. Color-enhanced GOES night-time SST composite image on February 15, 21, 24, and 28, 2001, superimposed with gridded SSH data for same dates. The mooring location is shown with a solid dot near 26º N, 92º W. Positive SSH are depicted with solid lines and negative with dotted lines.
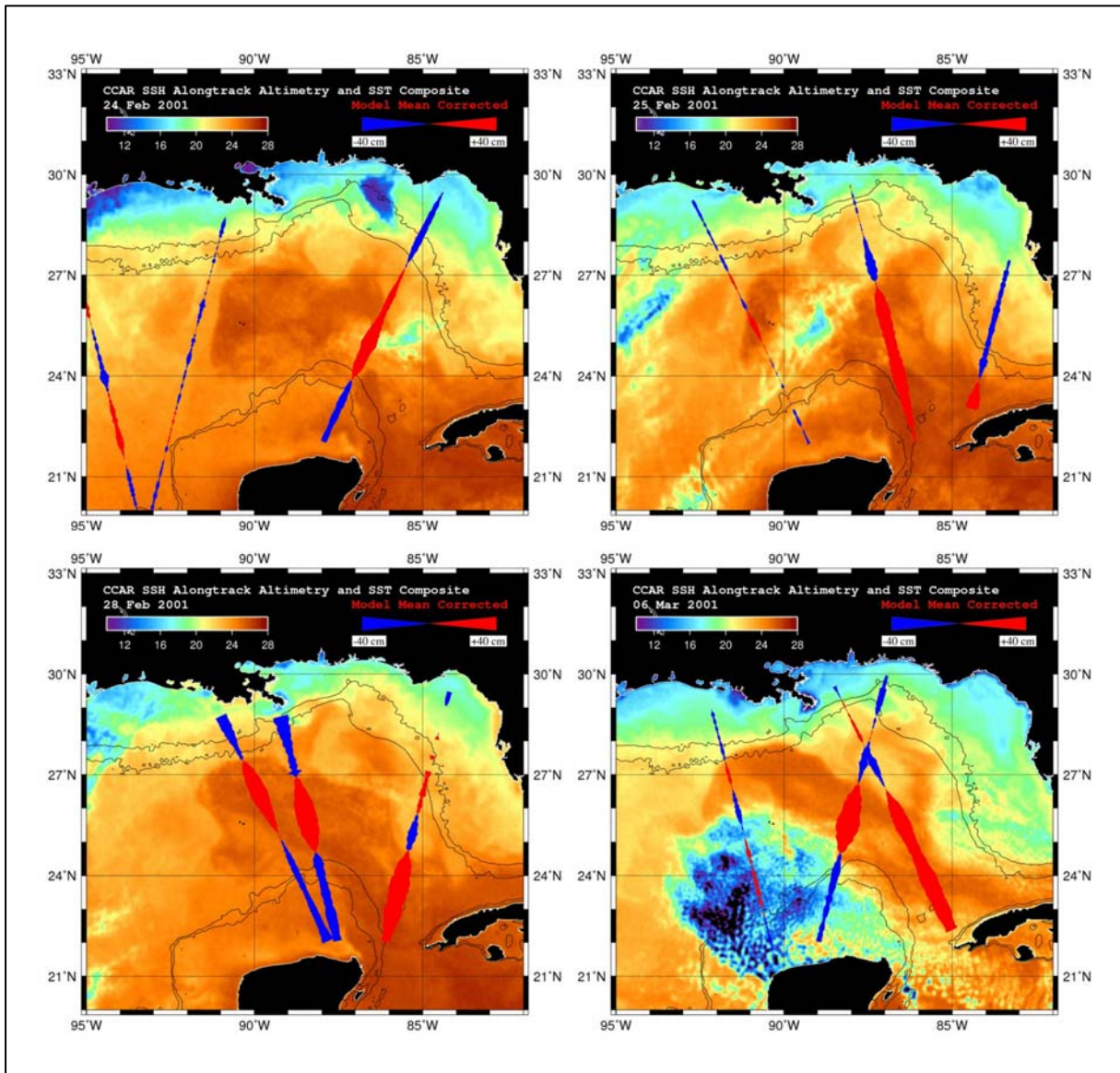
Figure 18. Color-enhanced GOES night-time SST composite images on February 24, 25, 28, and March 6, 2001, superimposed with alongtrack SSH data for same dates. Positive SSH is red and negative is blue ranging from 40 to -40 cm. SST legends are shown on individual panels.

3.3 LCFE Motion from Hovmoller Diagrams: September 2001-May 2004

The Hovmoller diagrams were produced for six time periods: September-December 2001; January-May 2002; September-December 2002; January-May 2003; September-December 2003; January-May 2004. These diagrams are shown in Figures 19-24. The diagrams were created by extracting GOES night-time SST composite data at 4km resolution along a line drawn parallel and 50 km away from the 17cm SSH line (See Section 2 for more detailed information). This technique is useful as a method for tracking the motion of moving features along the margin of the LC. Linear features, trending from bottom left to top right on these diagrams, show motion of LCFEs and associated meanders along the margin of the LC. In black and white figures, such as these, the LC and its meanders are depicted in lighter shades of grey while the LCFE cyclone centers are relatively dark grey. Clouds are black and white indicates missing data.

Inspection of these graphs reveals that each period was distinctly unique. The perimeter of the LC varied from 600 km to 2400 km during the time periods under review. The longest perimeter occurred in February 2002 before the separation of Eddy P (Figure 20). During the September-December 2003 period, the LC spent over 60 days with a perimeter less than 600 km, following the initial separation of Eddy T (Figure 23). After a ~ 2 month period of separation, the LC recaptured this eddy for about 1 month. Eddy T separated finally on December 31, 2003.

As the LC surges northward, the perimeter of the LC increases and the distance axis increases. Due to these changes in the distance axis, velocities are only accurate within a relatively short distance of the starting point at 21.5º N. Comparisons between feature motion determined from the Hovmoller graphs and those based on manual feature tracking revealed that the currents were most accurate (within 10%) for distances from 0 to 400 km from the starting point. Thus, we present in this section the motion characteristics of LCFEs from 21.5º to near 25º N. In later sections, LCFE motion beyond 400 km will be determined and discussed.

LCFE motion along the western LC margin where it interacts with the CB escarpment are summarized by time periods and depicted in Table 1. The measurements include mean, maximum, and minimum speed, number of LCFEs tracked, frequency/month, and frequency/day. Statistics were computed for each 4-5 month time period. Mean speeds ranged from 20-28 km/day. Maximum speeds ranged from 27 to 53 km/day and the highest speed occurred in Jan-May 2003. Minimum speeds ranged from 9-12 km/day. A seasonal signal was not readily apparent in these data. The frequency for LCFE formation along the western margin ranged from 3-4.4/ month. These results demonstrated a larger range of speeds than did Walker et al. (2003) most likely due to the larger sample size.

Table 1

LCFE Characteristics: Western Margin 0-400 km from YC (21.5-25º N)

Time Period	Mean Speed cm/s	Max Speed cm/s	Min Speed cm/s	No. LCFEs tracked	Freq/Mo	Freq/day
Sep-Dec 2001	26.6	41.6	17.4	7	3.5/mo	1 in 8.6
Sep-Dec 2002	23.1	31.2	10.4	11	4.4/mo	1 in 6.8
Sep-Dec 2003	None trackable					
Jan-May 2002	32.4	40.5	23.1	3	3/mo	1 in 10
Jan-May 2003	31.2	61.3	13.9	12	3/mo	1 in 10
Jan-May 2004	31.2	38.2	16.2	15	3/mo	1 in 10
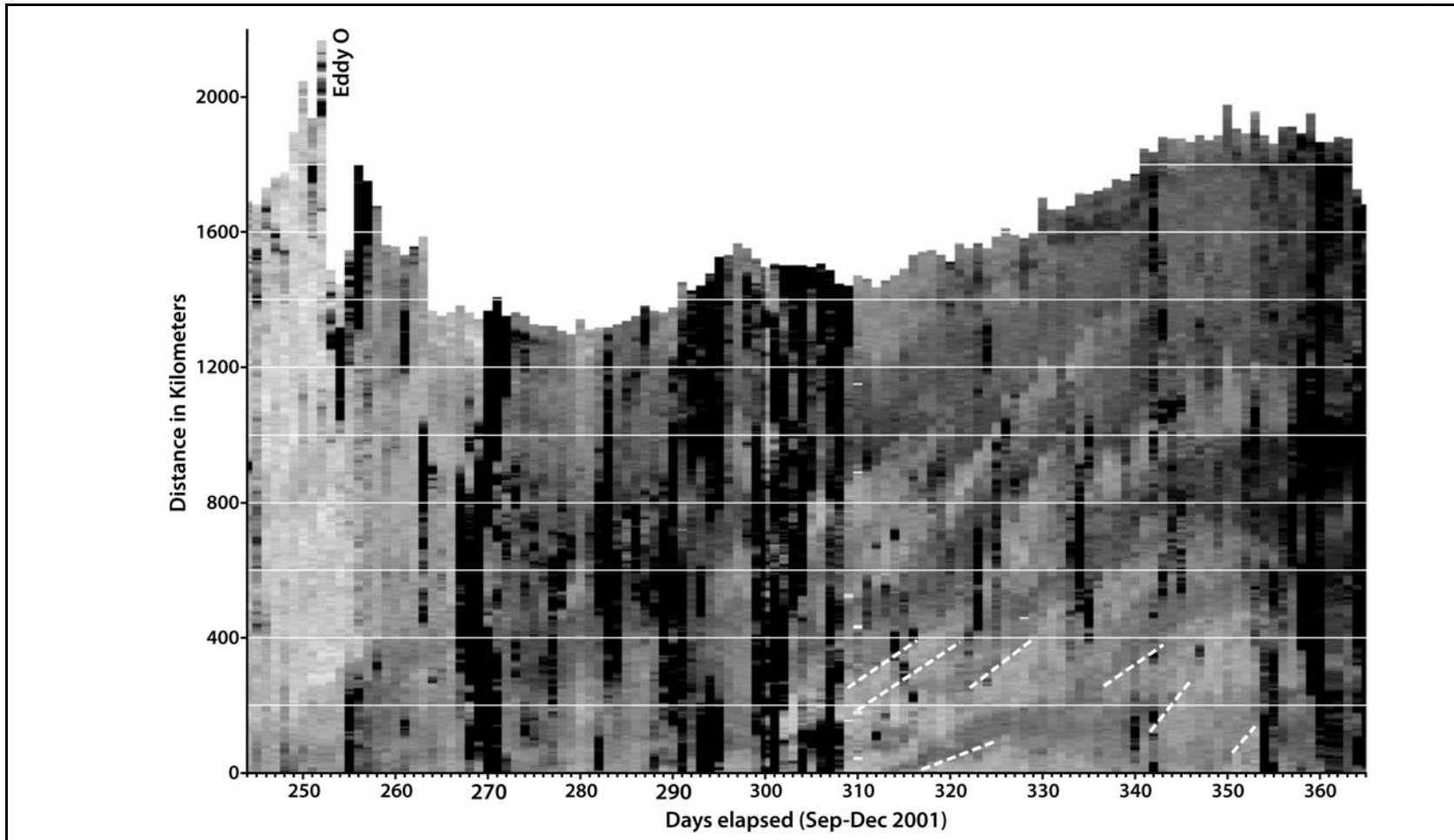
Figure 19. Time/distance Hovmoller diagram constructed by extracting GOES SST along the 17 cm SSH contour for each julian day from September through December 2001. Lighter shades of gray depict warmer waters such as the LC. Cyclones are dark and clouds are black. Linear features show motion of meanders and LCFE's around the margin of the LC. Lengthening and shortening of the perimeter of the LC is reflected on the y axis. Eddy separation resulted in a rapid decrease in the LC perimeter; see Eddy O separation during September 2001. The dashed white lines indicate the LCFEs tracked and summarized in Table1.
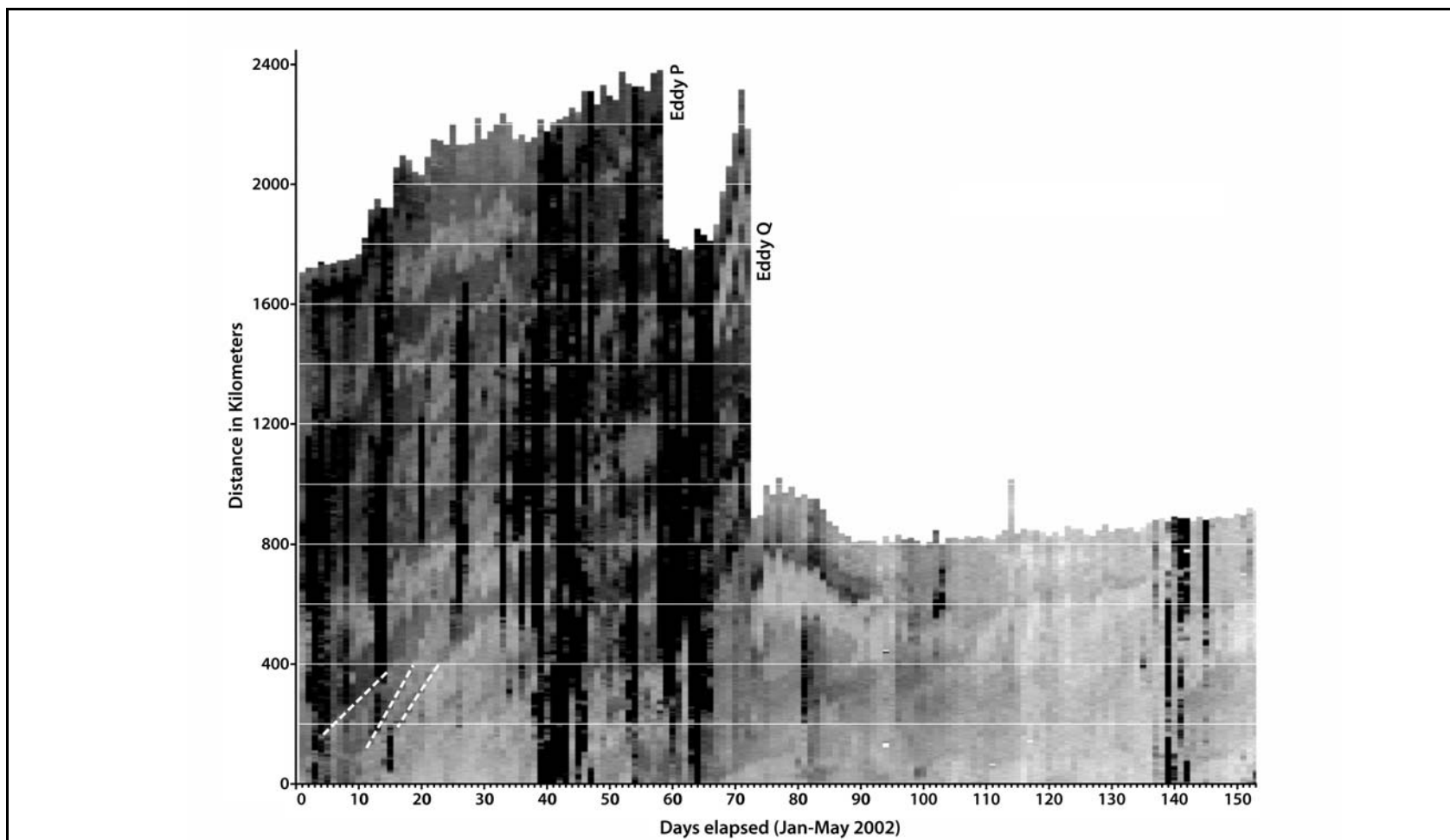
Figure 20. Time/distance Hovmoller diagram constructed by extracting GOES SST along the 17 cm SSH contour for each julian day from January through May 2002. Lighter shades of gray depict warmer waters such as the LC. Cyclones are dark and clouds are black. Linear features show motion of meanders and LCFE's around the LC. Eddy separation results in a rapid decrease in the LC perimeter as is shown when Eddy P and Q separated during February and March 2002. Thereafter, the LC remained in a retracted state with a perimeter less than 900 km. The dashed white lines indicate the LCFEs tracked and summarized in Table1.
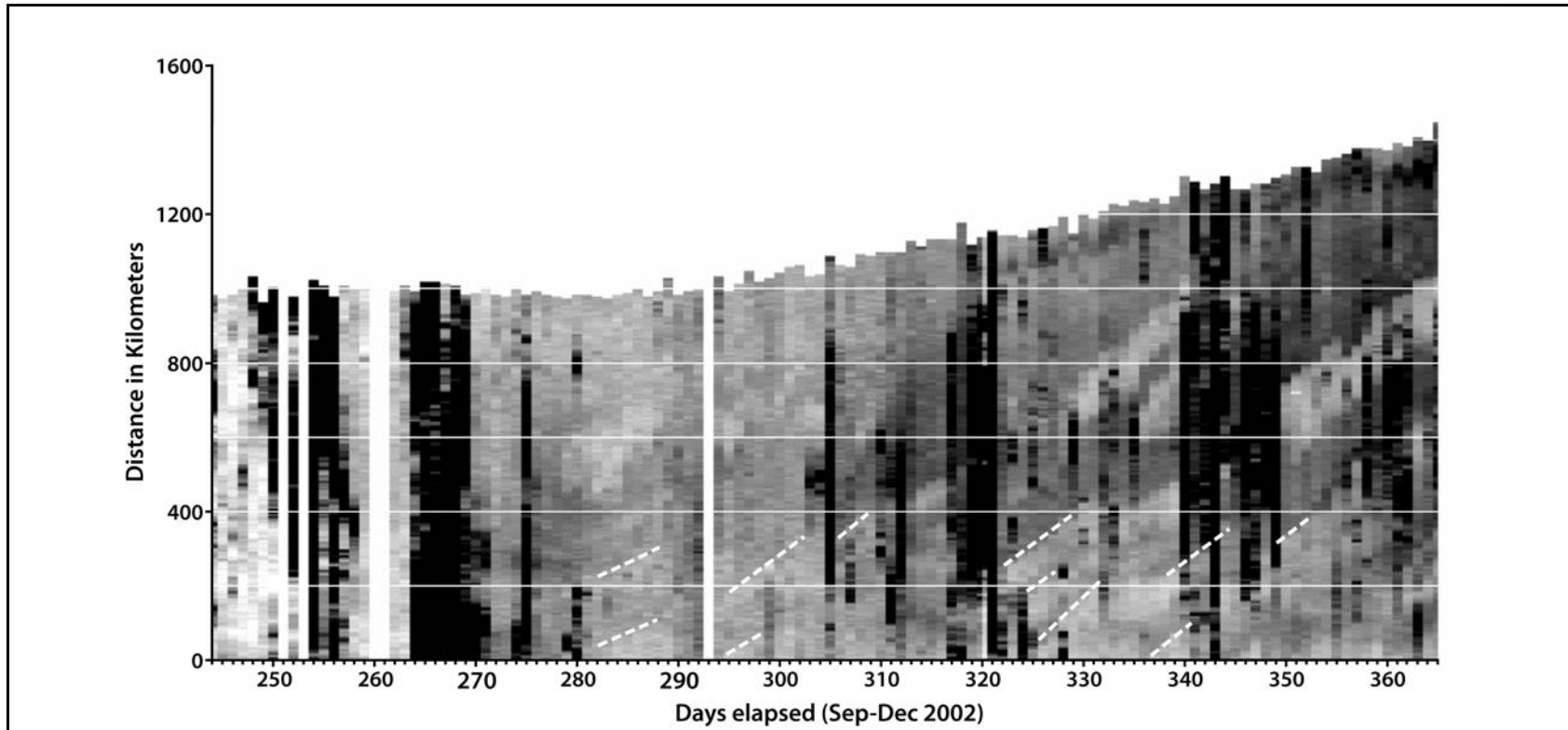
Figure 21. Time/distance Hovmoller diagram constructed by extracting GOES SST along the 17 cm contour for each julian day from September through December 2002. Lighter shades of gray depict warmer waters such as the LC. Cyclones are dark and clouds are black. Linear features show motion of meanders and LCFE's around the margin of the LC. Lengthening and shortening of the perimeter of the LC is reflected on the y axis. White areas indicate missing GOES SST data. LC separation events were not observed during this time period. The dashed white lines indicate the LCFEs tracked and summarized in Table1.
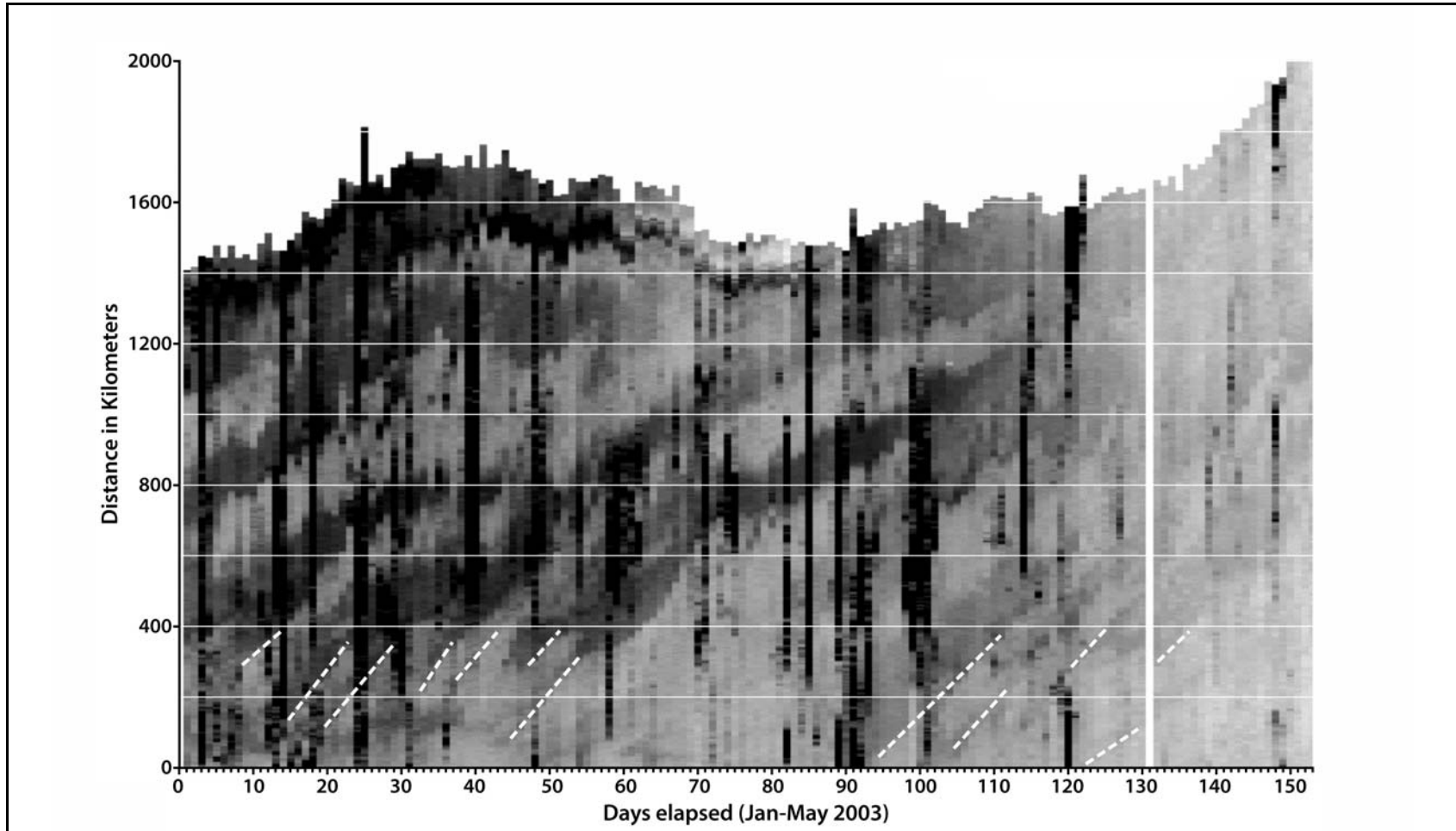
Figure 22. Time/distance Hovmoller diagram constructed by extracting SST from the 17 cm SSH contour for each julian day from January through May 2003. Lighter shades of gray depict warmer waters such as the LC and its meanders. Cyclones are dark and clouds are black. Linear features show motion of meanders and LCFE's around the margin of the LC. Lengthening and shortening of the perimeter of the LC are reflected by the y axis. White indicates missing GOES SST data. The dashed white lines indicate the LCFEs tracked and summarized in Table1.
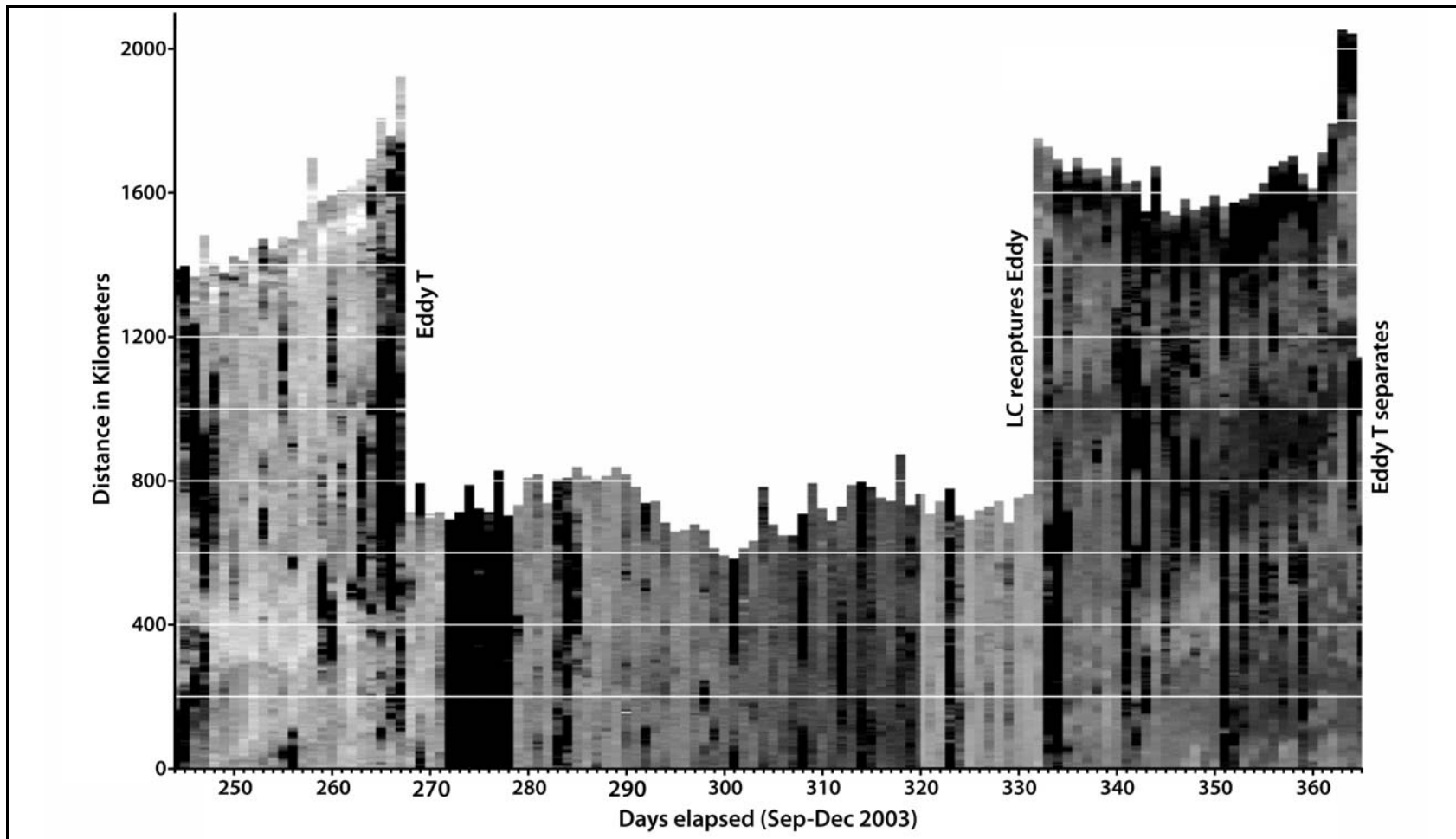
Figure 23. Time/distance Hovmoller diagram constructed by extracting GOES SST data along the 17 cm SSH line for each julian day from September through December 2003. Lighter shades of gray depict warmer waters such as the LC and its meanders. Cyclones are dark and clouds are black. Linear features show motion of meanders and LCFE's around the margin of the LC. Lengthening and shortening of the perimeter of the LC are reflected on the y axis. Eddy separation results in a rapid decrease in the LC perimeter as is shown when Eddy T separated in September and again in December 2003.
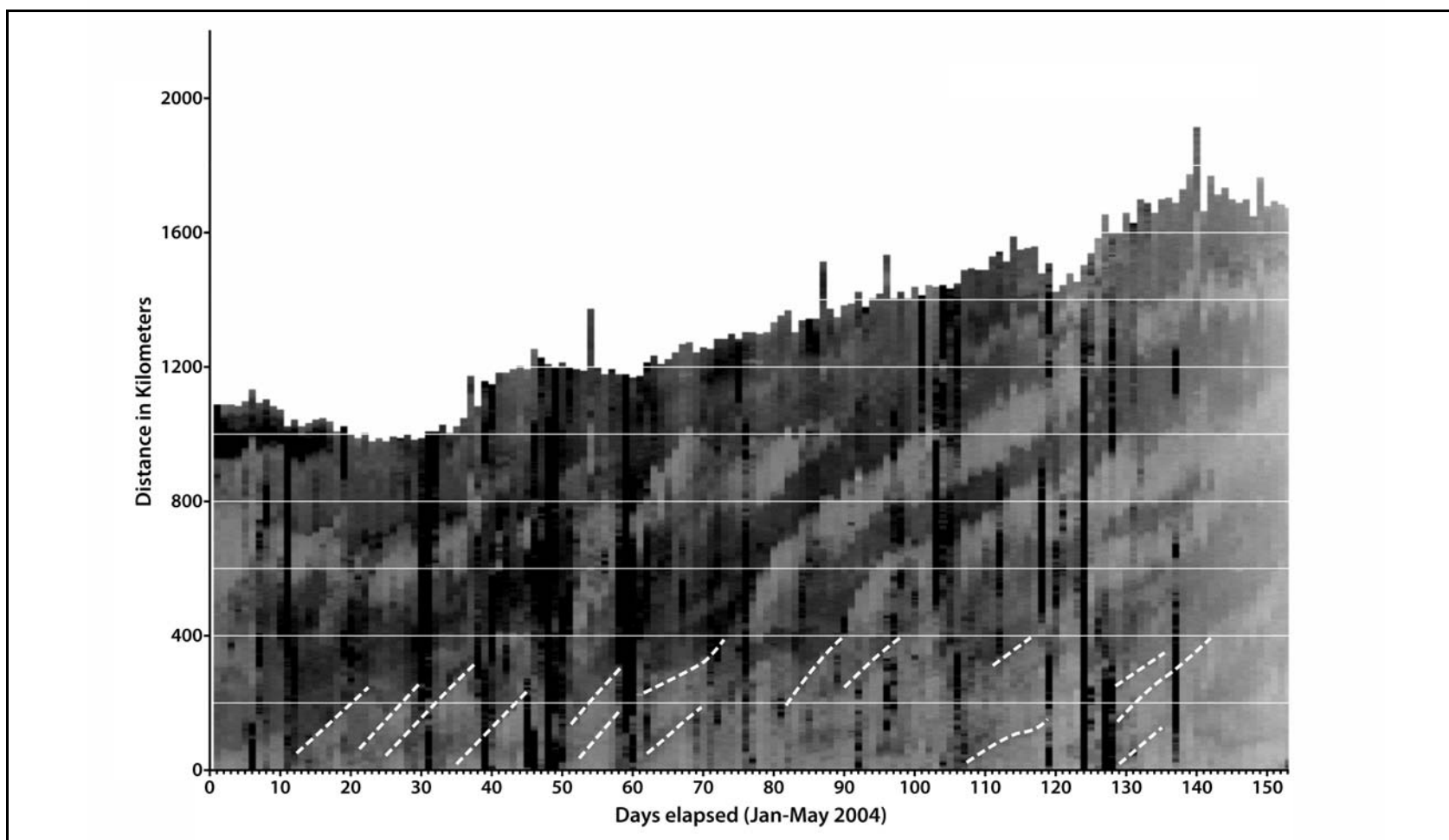
Figure 24. Time/distance Hovmoller diagram constructed by extracting GOES SST data along the 17 cm SSH line for each julian day from January through May 2004. Lighter shades of gray depict warmer waters such as the LC and its meanders. Cyclones are dark and clouds are black. Linear features show motion of meanders and LCFE's around the margin of the LC. Lengthening and shortening of the perimeter of the LC are reflected by the y axis. The dashed white lines indicate the LCFEs tracked and summarized in Table 1.

3.4 LCFE Motion and Structure: January-May 2002

This time period included a most unusual westward intrusion of the LC into the northwestern GoM which led to the separation of Eddy P on ~ 28 February and Eddy Q on ~13 March 2002 (Leben, 2005). These separation events are readily apparent and annotated on the January-May 2002 Hovmoller diagram (Figure 20). The event began with a northwestward surge of the LC on January 10 leading to the lengthening of its perimeter from ~1700 km to ~ 2400 km by day 50 (Figure 20). The word "perimeter" is used to refer to the length scale on Hovmoller diagrams, which is larger than the actual perimeter of the LC based on 17 cm SSH contour. Separation of Eddy P caused the LC perimeter to decrease from ~ 2400 km to 1800 km on day 58 and below 900 km on day 72. A few weeks after separation of Eddy Q, the LC perimeter was only about 800 km. This fascinating sequence of events is discussed using Hovmoller diagrams, SST and SSH information for the time period from January 9 through March 16 (Figures 25-30).

Figure 25 shows the location of circulation features on January 9. At that time, LC water was evident to 92W. SST patterns indicated a large LCFE cyclone southeast of the leading edge of the LC, a situation which is analogous to the circulation observed in mid to late February 2001 (See section 3.2). SSH data captured the eastern part of this LCFE on January 9 showing SSH of -27 and -30, in 2 crossings. Altimeter crossings of this LCFE on January 22 revealed SSH values of -20 cm along both lines, and a width, normal to the LC, of 150-170 km (Figure 26). SSH data indicated that this LCFE had become more intense by February 1 (Figure 27). Cyclonic circulation associated with this LCFE enhanced the westward intrusion of the LC. The SST imagery for February 9 revealed that LC water extended past 96º W into the extreme western GoM (Figure 28). A warm core eddy was in the formative stages near 26-27º N, 93º W. By February 9, two large LCFE cyclones were evident south of the LC, the westernmost feature measured -40 cm and the feature approximately 200 km upstream (to the east) measured -30 cm (Figure 28). The larger LCFE cyclone extended 140 km south from the LC and the other extended 110 km south from the LC. These and other SSH crossings indicated a persistence of low SSH over a broad region south of the LCFEs and across the CB throughout the intrusion event. These observations clearly demonstrated that well developed cyclones south of the LC are effective at entraining LC water into the western GoM.

Warm LC water continued to stream into the western GoM and by February 24 a large pool of water between 93º and 97º W was clearly apparent in SST imagery (Figure 29). This mass of water lay to the west of Eddy P which was now well formed and nearly circular in shape. SSH data for February 24 and 25 clearly crossed a well-formed LCFE cyclone south of the separation region between the westernmost part of the LC and Eddy P (Figure 29). The two LCFEs appear to have merged into one large cyclone by February 24. An LSU mooring in ~ 3000 m of water along the Sigsbee Escarpment (not shown) was directly affected by LCFE intensification and acceleration of currents from surface to bottom were experienced in late February in association with the separation of Eddy P from the LC. The LSU mooring was located at ~ 26º N, 91.6º W and directly impacted by the LCFE which came between the LC and Eddy P.

The alongtrack altimeter data for February 24 also exhibited very low SSH values indicating intense cyclonic circulation north of the YC (between 22º and 23º N) where SSH values of ~ -40 cm were measured over 130 km (Figure 29). Separation of Eddy Q occurred soon after this

LCFE cyclone appeared as it moved eastward, separating the LC from the large mass of warm water that formed Eddy Q. Extremely low SSH (~ -40 cm) was also noted north of the LC over a large region from the Mississippi delta southwards (Figure 29).

By March 3, separation of Eddy Q from the LC appeared eminent near 24 N (Figure 30). Two prominent LCFE cyclones were observed east and west of the region of impending separation (~ 24º N, 86º W). SSH data from 20-24 February revealed that both LCFEs exhibited SSH minima near -40 cm. Both LCFE cyclones had a length scale of about 130 km based on the along track SSH data. The western cyclone was detected at 22-23º N, 86-87º W in a location usually occupied by the LC just east of the CB. This cyclone may have played the most critical role in separating Eddy Q from the LC as it effectively blocked the flow of LC water into the Gulf. On March 3, the LC was clearly separated from Eddy Q and the LCFE was still in evidence, although the SSH data showed some weakening since February 24. Separation of Eddy Q occurred on about 13 March (Figure 31) and the LC remained far south at least until the end of May as is clearly revealed in the Hovmoller diagrams.

It is instructive to track the motion of LCFE activity during this abnormal episode. On January 18 (Figure 32), seven LCFEs of various sizes were evident along the entire margin of the LC. These were observable by the alternating light and dark shading on the Hovmoller diagram. Four of the seven LCFEs were trackable using the GOES SST imagery starting 18 January. LCFEs 1 and 2 were tracked by following their approximate centers of circulation. LCFE 1 was trackable from January 18 - March 3. LCFE 2 was tracked from January 18 to February 19. LCFEs 3 and 4 were tracked by detecting the relatively warm leading edge of the meander ahead of the cyclone. LCFE 3 was tracked from January 18 to 23 and LCFE 4 was tracked from January 18 to February 9. The LCFEs along the southern margin of the LC traveled at a much faster rate than those on the northern margin (See Table 2 for speed summary). LCFE 3 exhibited a mean phase speed of 74 cm/s over the 5 days (Figure 32), exhibiting a range of 63-87 cm/s. This cyclone appeared to have merged with the pre-existing LCFE between 91º and 92º W by January 23 (Figure 32). LCFE 4 was tracked from January 18 to February 9 revealing a mean speed of 30 cm/s with a range of 10-59 cm/s. LCFE 4 grew to become the 2nd large LCFE south of the LC near 90º W, which on February 9 measured -30 cm and extended south from the LC a distance of 110 km. Between February 9 and 19, the leading margin of the LC grew in areal extent forming Eddy P, a nearly circular feature, whose western margin was close to 94º W on February 19. At that same time, LCFE 4 was located between 90º and 91º W where it deformed the LC, possibly leading to the separation of Eddy P on 28 February. Compared with the LCFEs on the southern side of the LC, those on the northern margin moved slowly. LCFE 2 was tracked between January 23 and February 19 with a mean propagation speed of 11 cm/s with a range of 3 to 28 cm/s. LCFE 1 exhibited a mean speed of 9.7 cm/s with a range of 3.5 to 21.2 cm/s. The statistics on current speeds for the four LCFEs are summarized in Table 2.
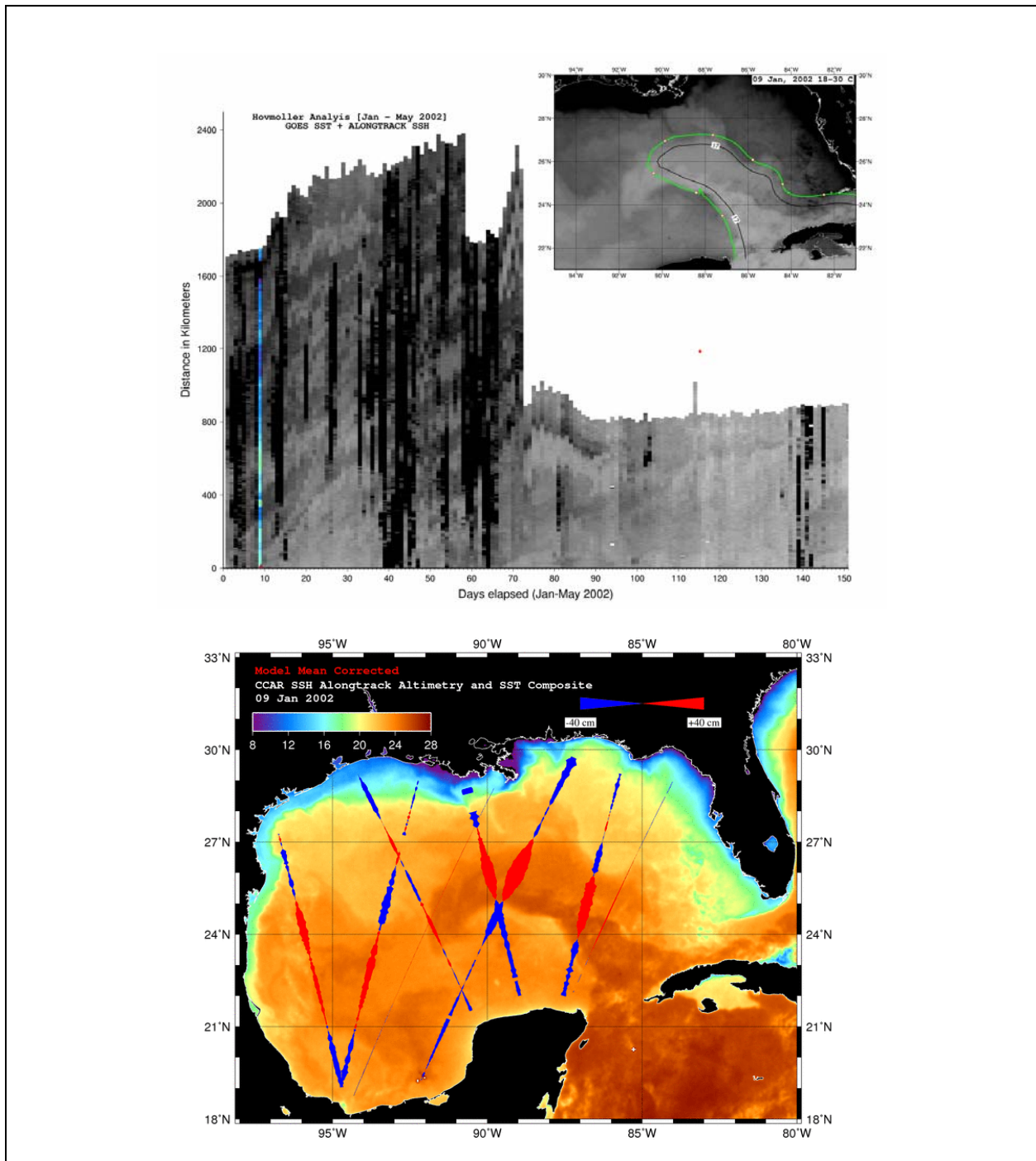
Figure 25. (top) GOES black/white SST image with 17 cm SSH contour showing the LC and LCFEs on January 9, 2002. Hovmoller diagram for January-May 2002 is shown with a color line depicting the time of SST image acquisition. (bottom) Alongtrack SSH data for January 8 and 12 superimposed on GOES color SST image from January 9, 2002. Blue indicates negative SSH and cyclonic circulation.
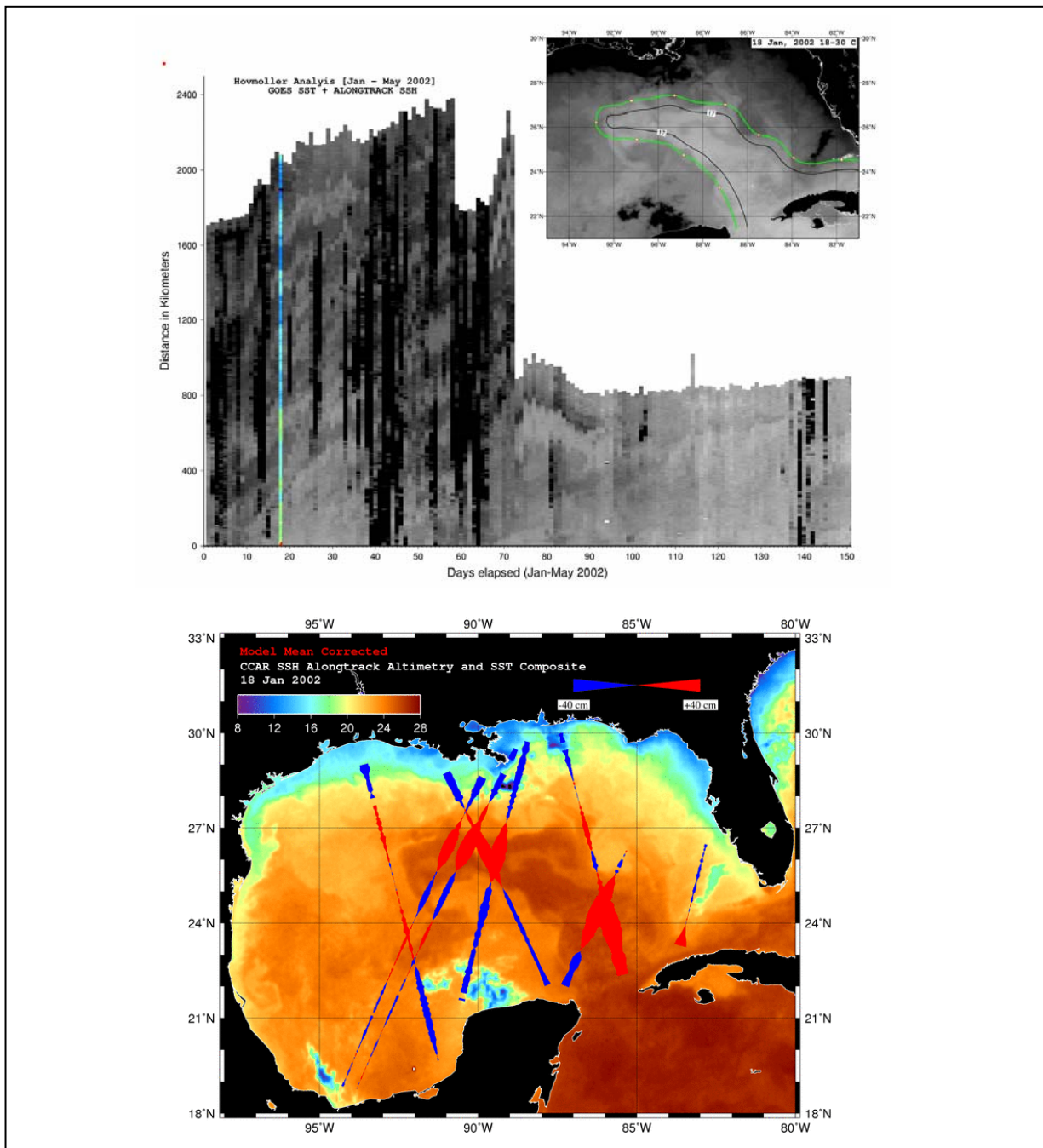
Figure 26. (top) GOES black/white SST image with 17 cm SSH contour showing the LC and LCFEs on January 18, 2002. Hovmoller diagram for January-May 2002 is shown with a color line depicting the time of SST image acquisition. (bottom) Alongtrack SSH data for January 18 and 22 are superimposed on GOES color SST image from January 18, 2002. Blue indicates negative SSH and cyclonic circulation.

40
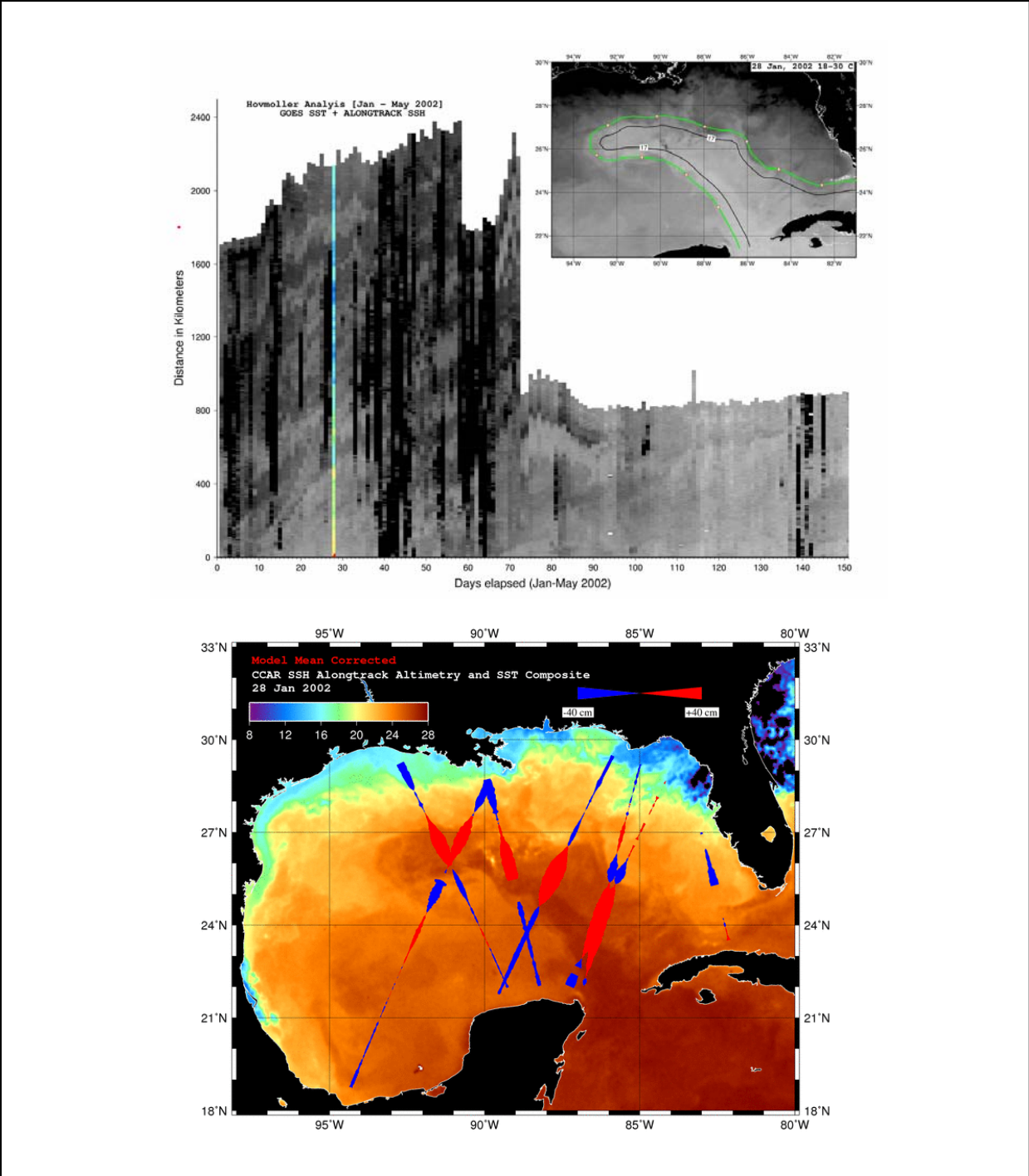
Figure 27. (top) GOES black/white SST image with 17 cm SSH contour showing the LC and LCFEs on January 28, 2002. Hovmoller diagram for January-May 2002 is shown with a color line depicting the time of SST image acquisition. (bottom) Alongtrack SSH data for January 28 and February 1 are superimposed on GOES color SST image from January 28, 2002. Blue indicates negative SSH and cyclonic circulation.
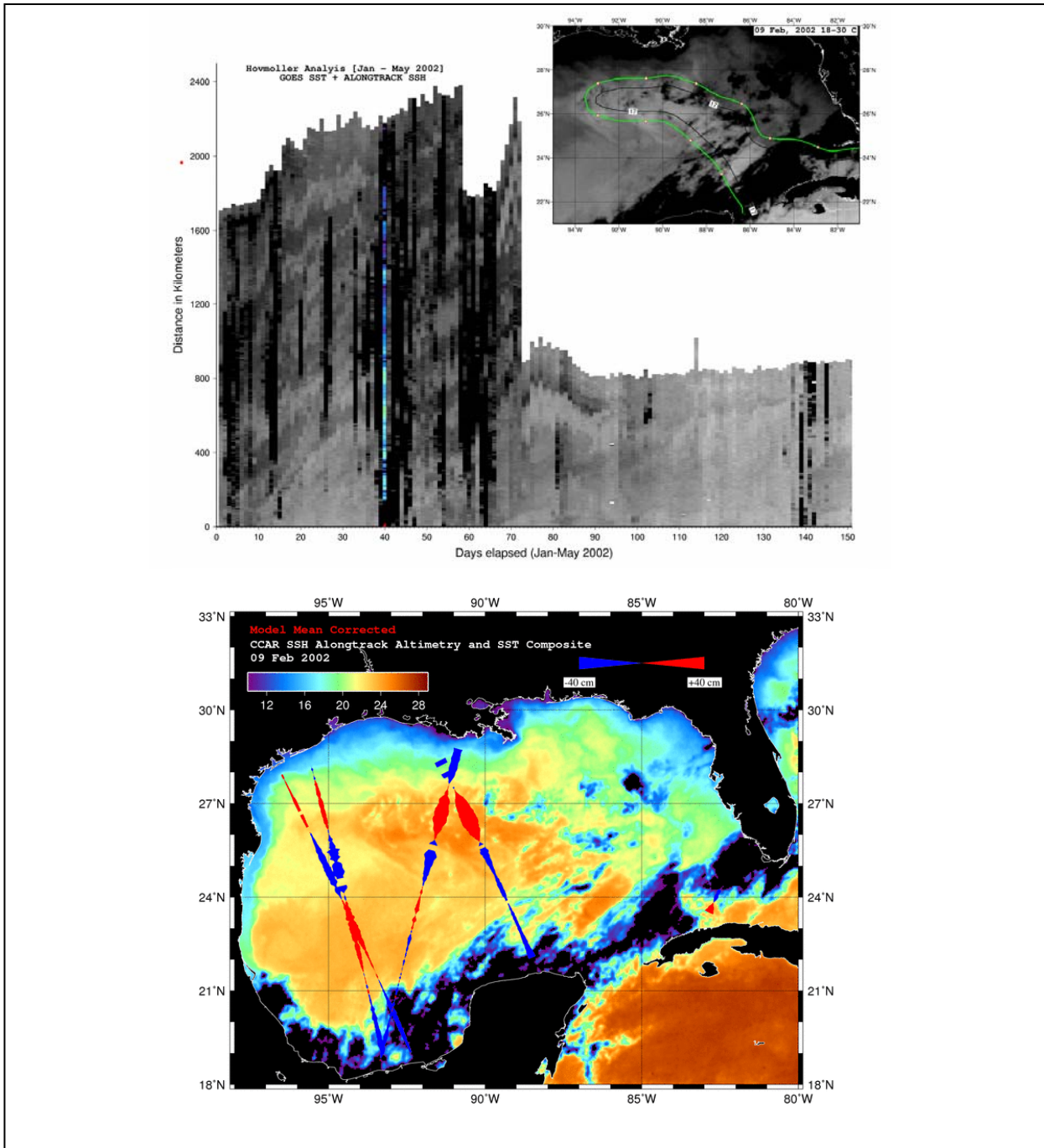
Figure 28. (top) GOES black/white SST image with 17 cm SSH contour showing the LC and LCFEs on February 9, 2002. Hovmoller diagram for January-May 2002 is shown with a color line depicting the time of SST image acquisition. (bottom) Alongtrack SSH data are superimposed on GOES color SST image from February 9, 2002. Blue indicates negative SSH and cyclonic circulation.
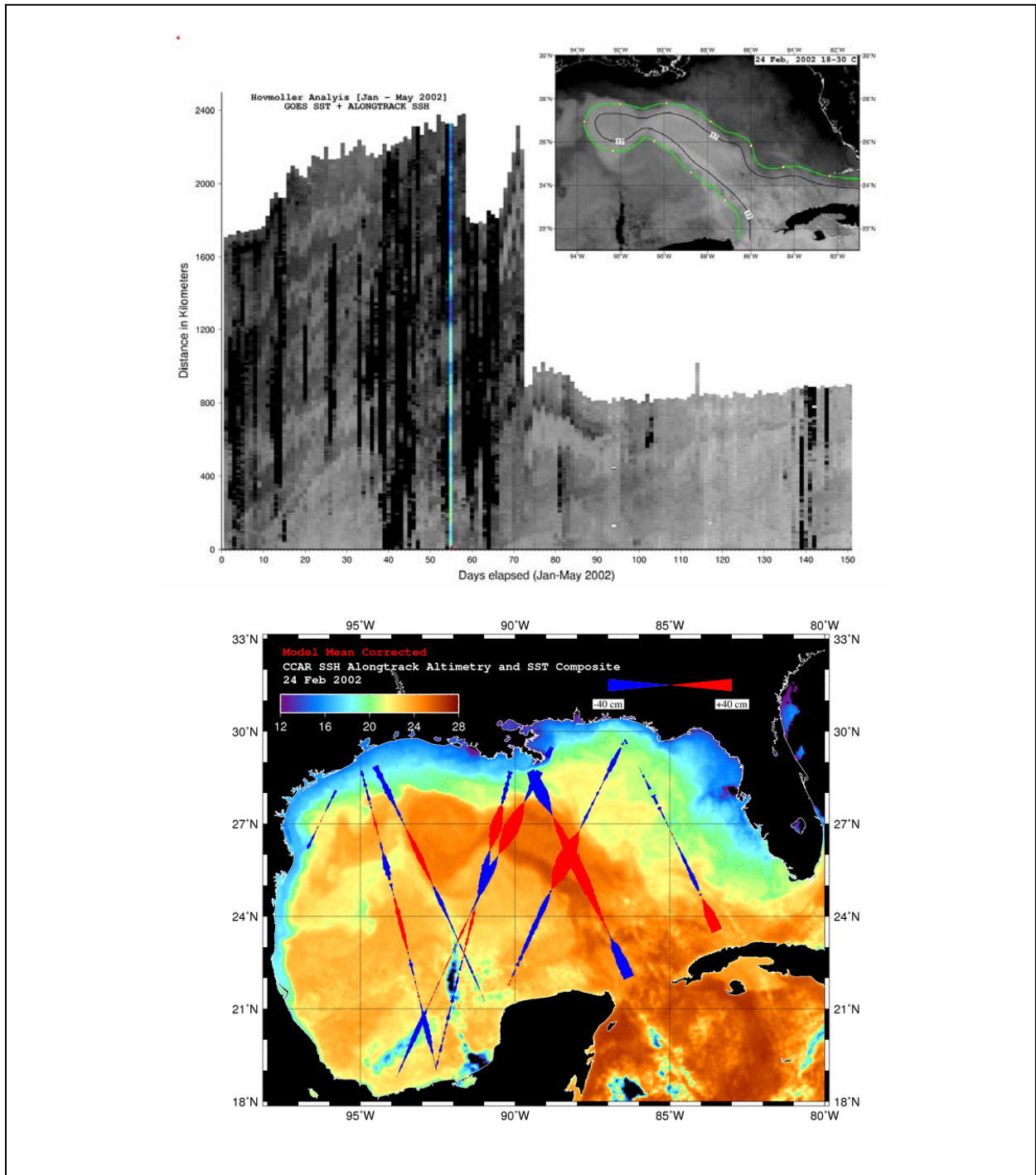
Figure 29. (top) GOES black/white SST image with 17 cm SSH contour showing the LC and LCFEs on February 24, 2002. Hovmoller diagram for January-May 2002 is shown with a color line depicting the time of SST image acquisition. (bottom) Alongtrack SSH data for February 24 and 25 are superimposed on GOES color SST image from February 24, 2002. Blue indicates negative SSH and cyclonic circulation.
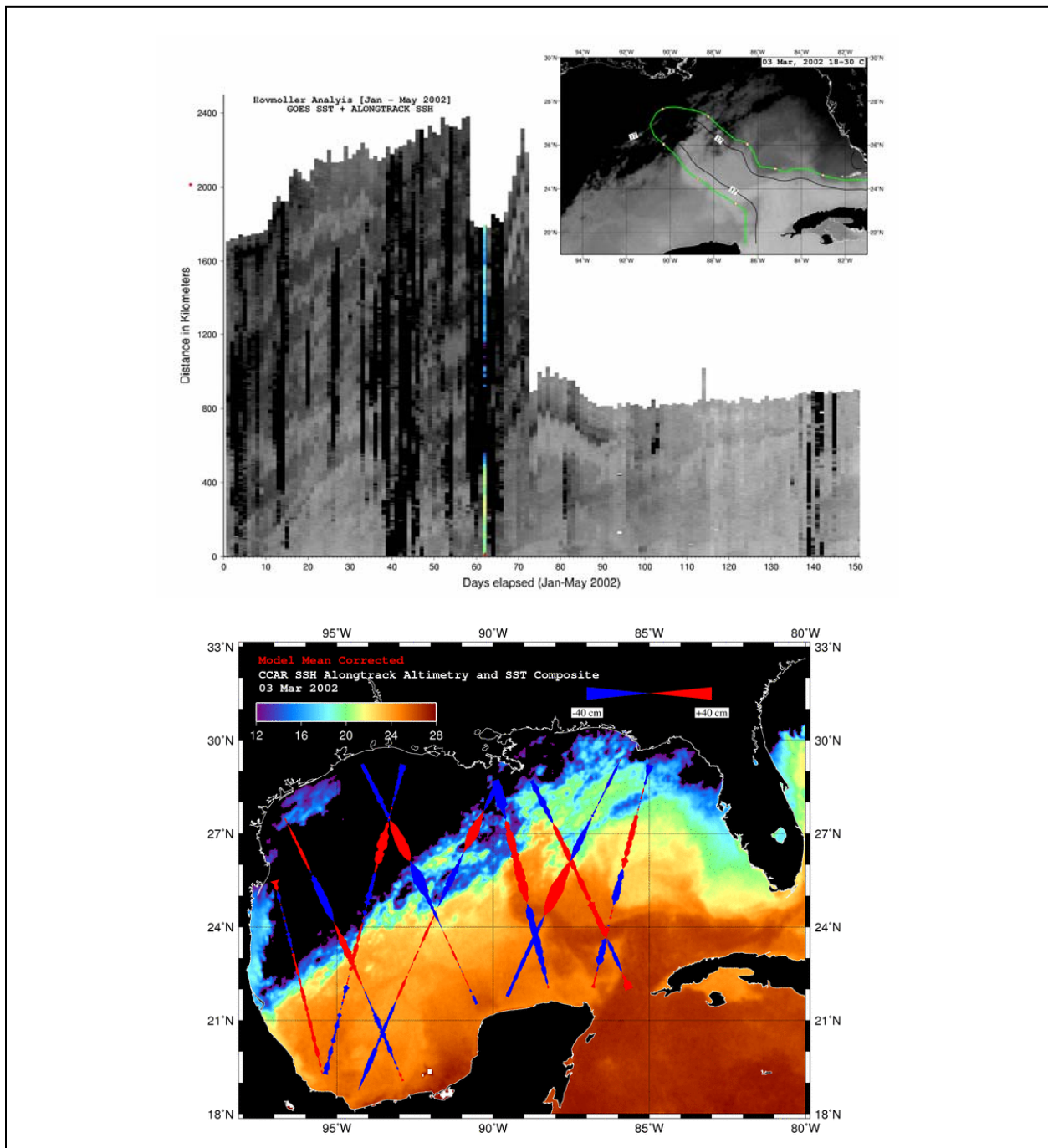
Figure 30. (top) GOES black/white SST image with 17 cm SSH contour showing the LC and LCFEs on March 3, 2002. Hovmoller diagram for January-May 2002 is shown with a color line depicting the time of SST image acquisition. (bottom) Alongtrack SSH data for March 3 and 4 are superimposed on GOES color SST image from March 3, 2002. Blue indicates negative SSH and cyclonic circulation.
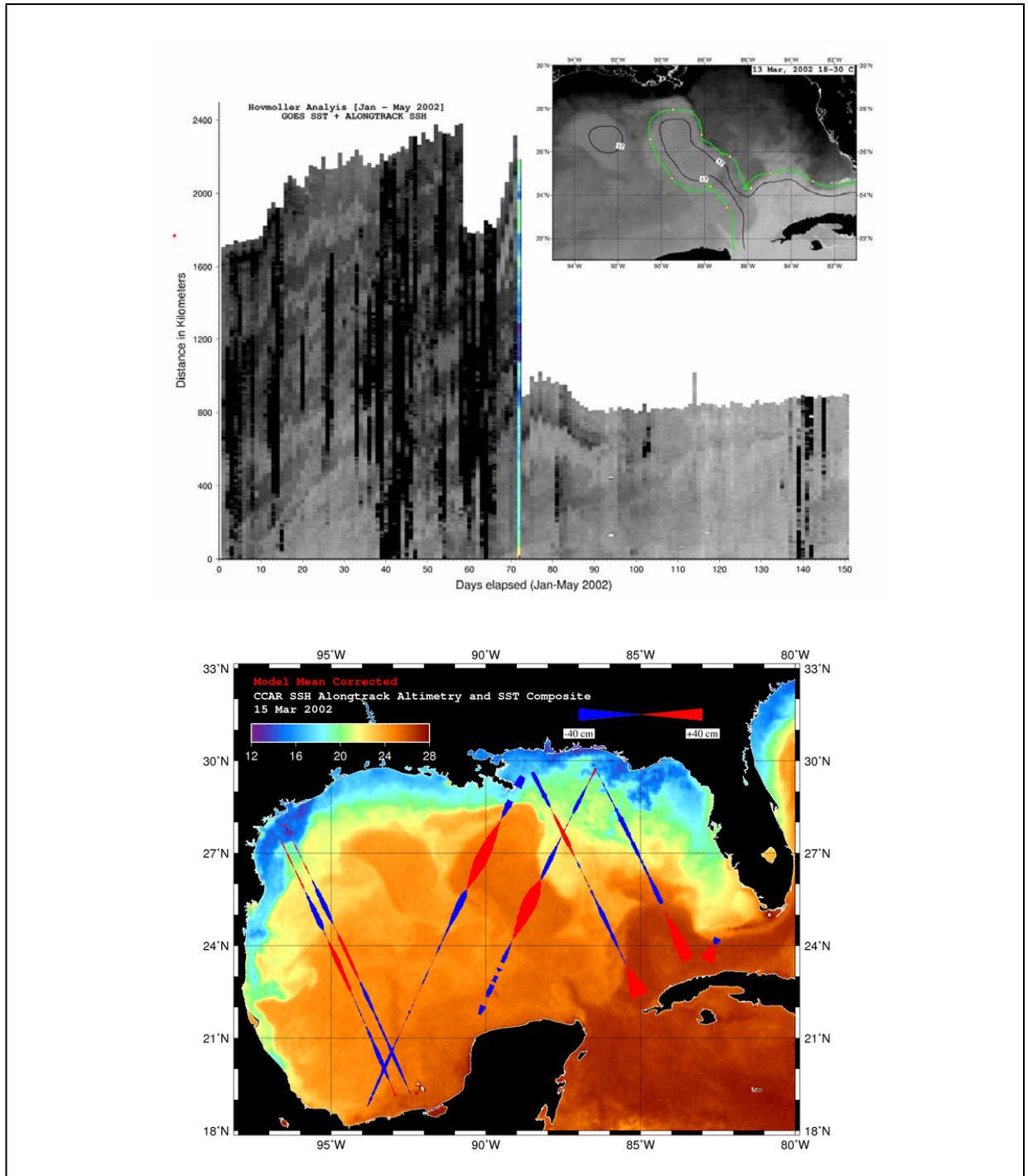
Figure 31. (top) GOES black/white SST image with 17 cm SSH contour showing the LC and LCFEs on March 15, 2002. Hovmoller diagram for January-May 2002 is shown with a color line depicting the time of SST image acquisition. (bottom) Alongtrack SSH data for March 14, 15, and 16 are superimposed on GOES color SST image from March 15, 2002. Blue indicates negative SSH and cyclonic circulation.
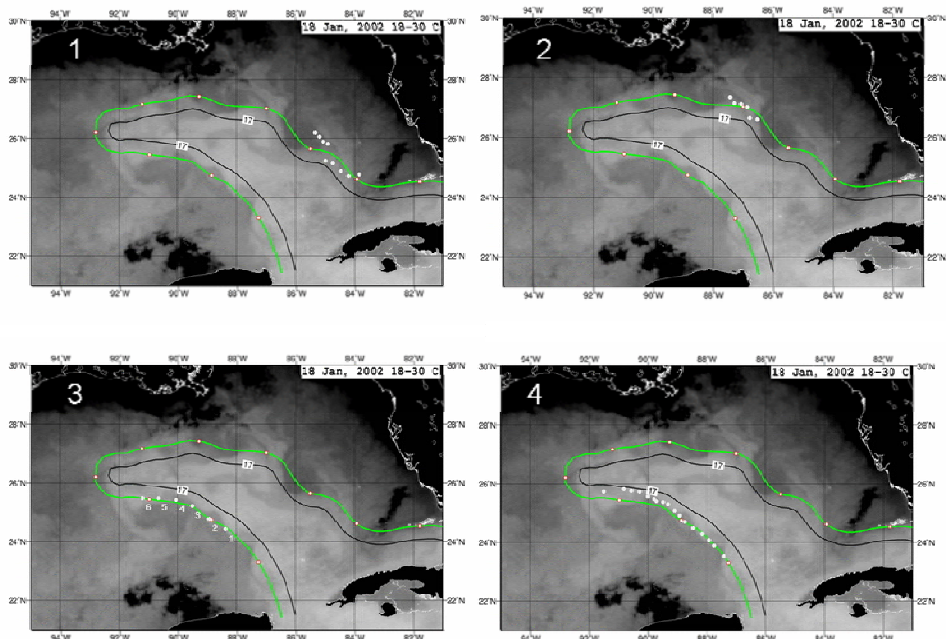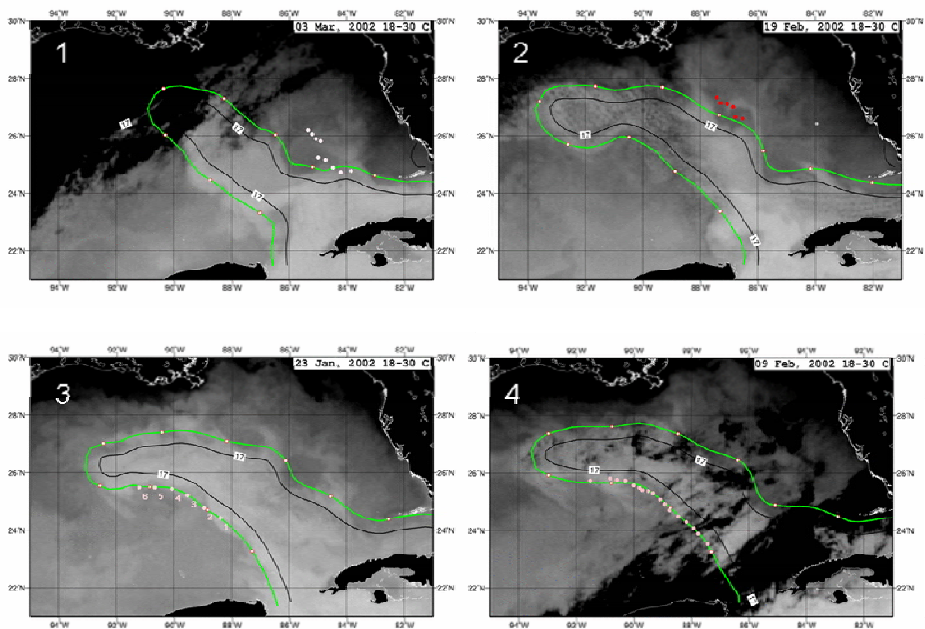
Figure 32. GOES SST panels showing manual tracking of LCFEs 1-4 starting on January 18 (top panel) and ending on the dates shown in upper right hand corner. Positions used for tabulating current speed statistics are shown with white or colored dots. The green line indicates 17 cm SSH contour. Summary of feature speeds are given in Table 2.

Table 2
Propagation Speeds (cm/s) of Four LCFEs Starting January 18, 2002

	LCFE 1	LCFE 2	LCFE 3	LCFE 4
N	8	5	5	16
Mean	9.7	11.2	73.8	30.3
St dev	5.6	10.6	9.9	13.4
Min	3.5	2.5	62.8	9.5
Max	21.2	28.4	87.3	59.4
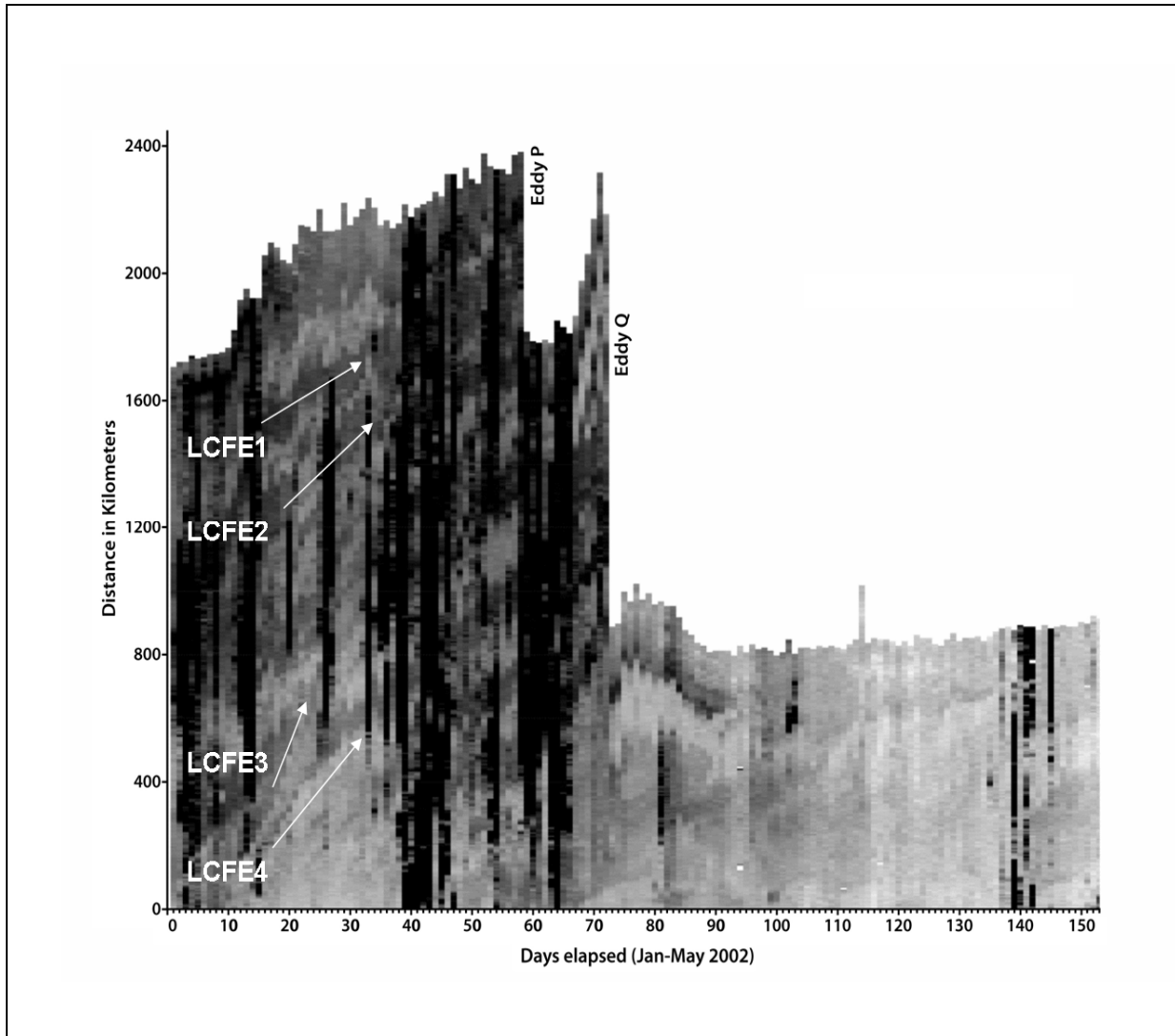
Figure 33. Hovmoller diagram for January-May 2002 annotated with general motions of LCFEs 1 through 4 whose speed statistics are given in Table 2. LCFEs 1 and 2 were tracked using cyclone centers, whereas LCFEs 3 and 4 were tracked using leading edges of meanders ahead of cyclone centers. Meanders appear as lighter shades of gray and cyclones appear as darker shades of gray. LCFE 3 exhibited the fastest motion with an average speed of 73.8 cm/s.

3.5 LCFE Motion and Structure: January-May 2004

During this time period, the LC exhibited more typical behavior than during January-May 2002, remained confined to the eastern GoM and did not intruding north of 27º N. At the beginning of January 2004, the northern margin of the LC was located near 26º N and relatively far east with Eddy T positioned to the west of the LC (Figure 34-top). As Eddy T moved northwestward, the LC resumed a more normal position as is shown in the image obtained on January 25, 2004 (Figure 34-bottom). During January, a progression of LCFEs formed along the western margin of the LC, with the appearance of "shingles" as described by Schmidt et al. (2005). The Hovmoller diagrams also revealed a progression of meanders moving along the northern margin of the LC (Figure 34). Most of these features moved rapidly around the perimeter without growing appreciably. However, during March and April two LCFEs developed into large cyclonic features northwest and north of the LC. These features were unique in that they were first clearly detected along the west side of the LC near 24º N as warm water bulges which rapidly developed into larger LCFEs. Interactive software was used to track these features and to obtain estimates of propagation speeds over time. Alongtrack SSH data was used to study their sea surface height characteristics, as a proxy for intensity.

LCFE 1 was first detected in the SST image of March 10 (Figure 35). This image and three others (Figures 36-38) are used to depict temporal and spatial changes in LCFE 1 as it moved downcurrent along the outer LC margin. Its tracked positions are superimposed on each of the four panels. The SSH crossings of LCFE 1 are shown as the bottom panels to these figures. SSH crossings on March 11 and 12 revealing values of -10 to -20 cm within this cyclone, while it was still west of the LC (Figure 35). The SSH track of March 12 also revealed low SSH farther south along the LC margin (22-23º N) with minimum SSH of -27 cm. Some of the variability in the SSH measurements along track occur as the tracks rarely cross cyclone centers.

The next image panel is March 19 (Figure 36) and it shows rapid development of LCFE 1 along the northwest margin of the LC. Inspection of the Hovmoller clearly reveals that the feature exhibited most rapid movement between days 76 to 81. The maximum propagation speed occurred between March 17 and 18 and was estimated at 63.6 cm/s. The SSH data for March 19 revealed the presence of an intense LCFE downstream from LCFE 1 with an SSH value of -40 cm (Figure 36 bottom panel). An SSH track came close to crossing LCFE 1 but missed the low SSH in the center. By April 3, LCFE 1 was positioned on the northeast margin of the LC and exhibited SSH of -35 cm and dimensions of 175 x 117 km (based on the SST patterns). The SSH data confirmed the minor axis of 117 km. Its center was near 27º N, 86.5º W. Two SSH crossings were made of a LCFE east of the LC (25º N, 85º W) revealing similar SSH values of -35 cm.

The final panel of this series depicts the last date of tracking on May 2 (Figure 37). After this, the LC became deformed and it was difficult to track motion accurately. At this time, LCFE 1 was positioned on the eastern margin of the LC (see red dot, Figure 37). A large meander was positioned downstream of LCFE 1 and another cyclone was positioned west of the entrance to the FS. At this time, LCFE 2 was positioned north-northeast of the LC (See red dot 9, Figure 37). An SSH track crossed near the center of LCFE 1 showing a minimum SSH value of -27 cm. (Figure 37-bottom).
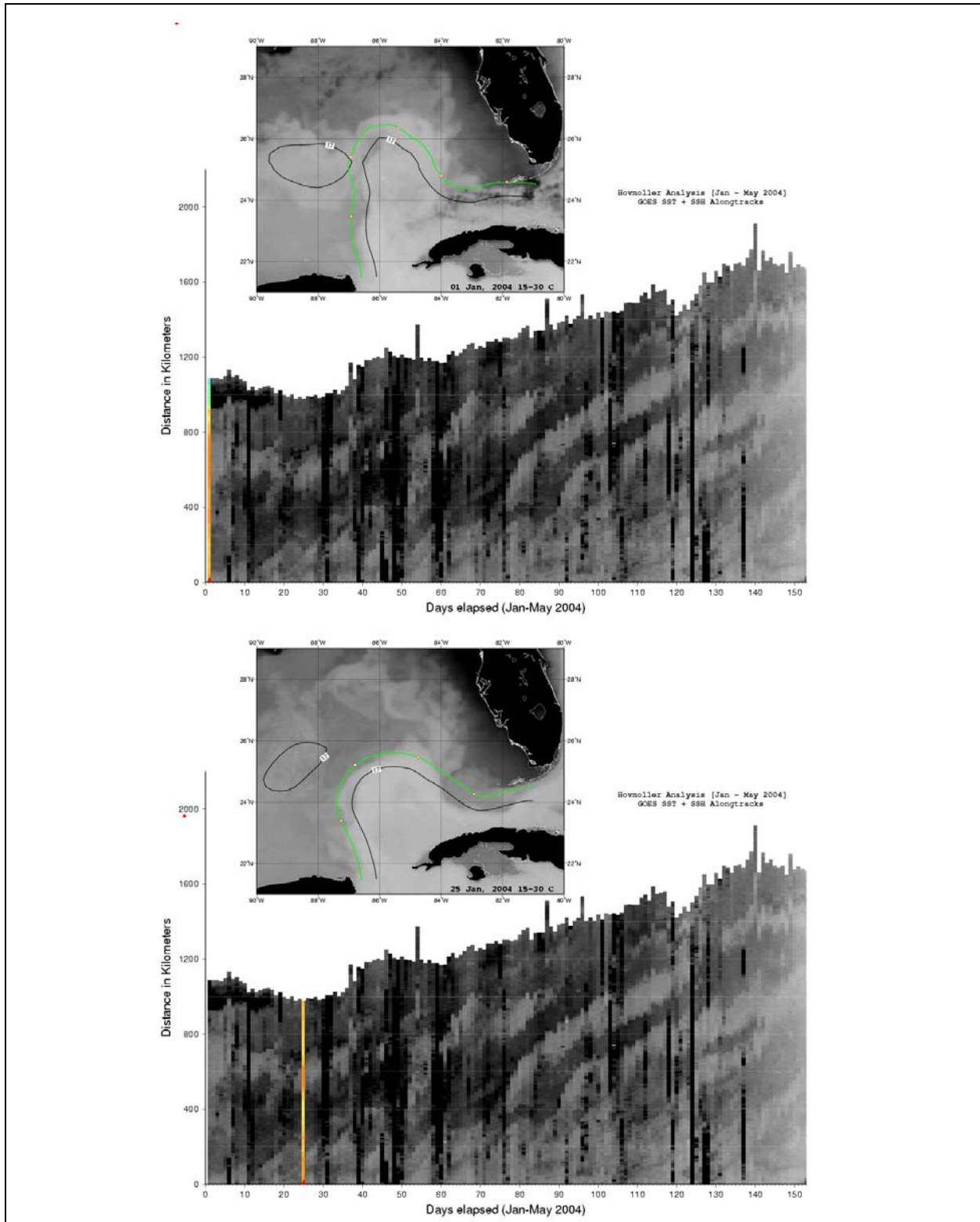
Figure 34. SST images of January 1 and 25, 2004, showing position of LC and Eddy T to the west. The orange line depicts time of image panel displayed on Hovmoller diagram.
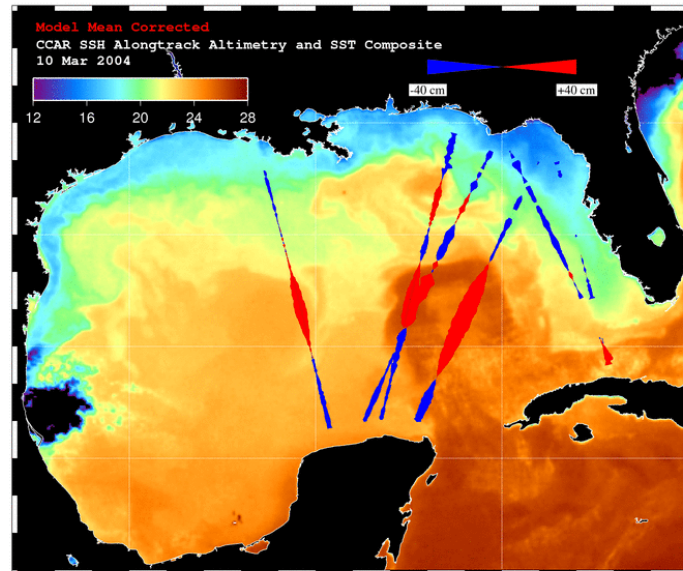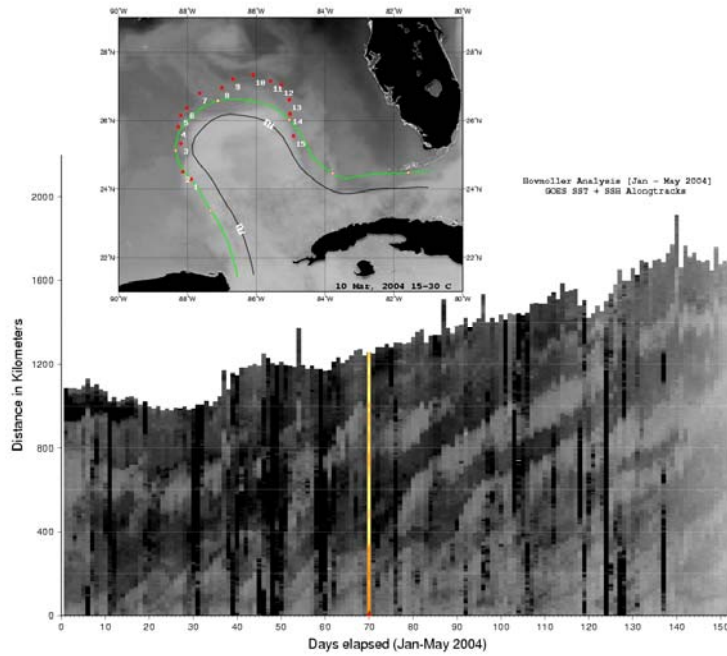
Figure 35. (top) GOES black/white SST image with 17 cm SSH contour showing the LC and LCFE 1 on March 10, 2004. Red dots show the location of the cyclone center on selected clear sky images. Hovmoller diagram for January-May 2004 is shown with a color line depicting the time of SST image acquisition. (bottom) Alongtrack SSH data for March 11 and 12 superimposed on GOES color SST image from March 10, 2004. Blue indicates negative SSH and cyclonic circulation.
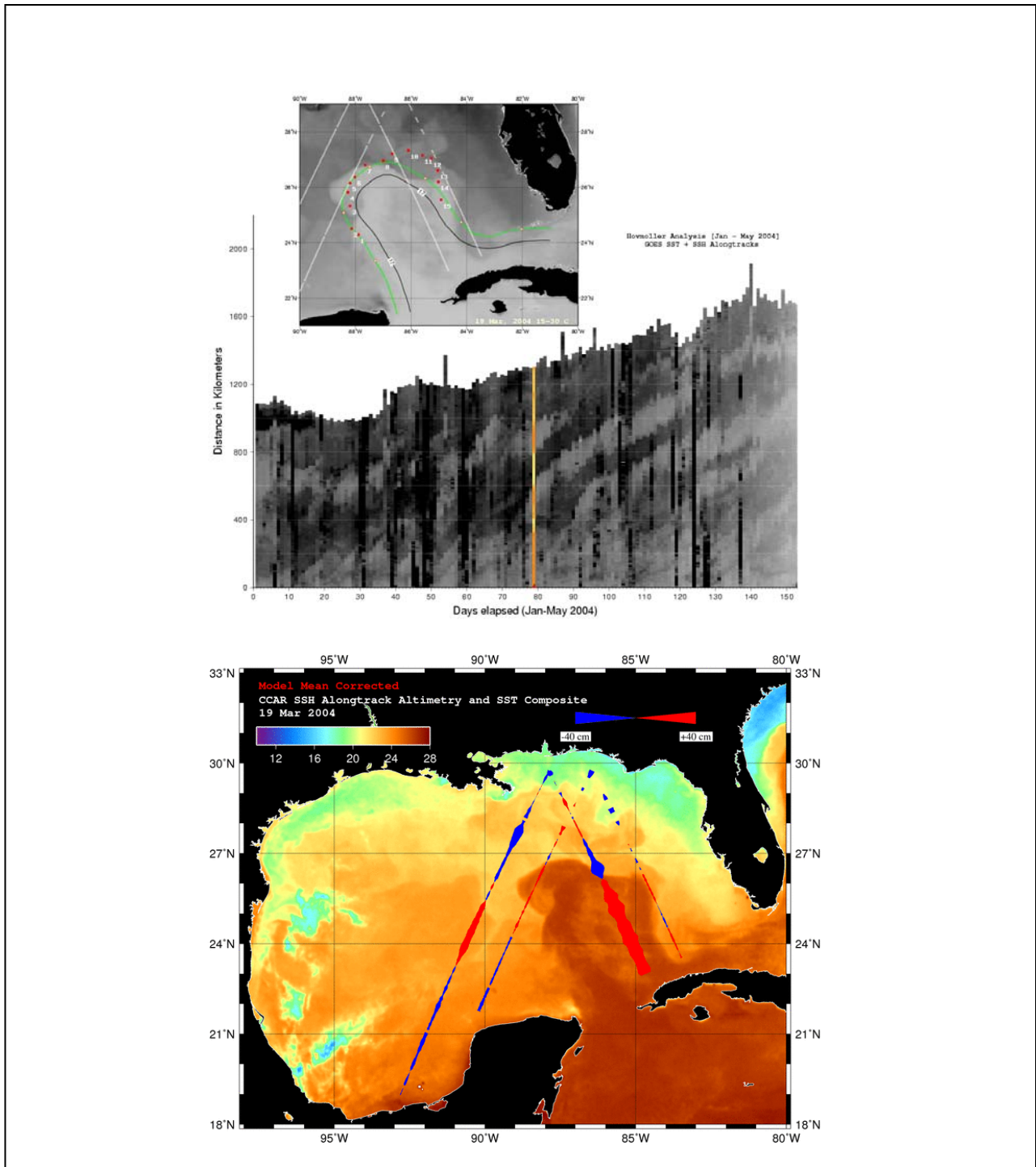
Figure 36. (top) GOES black/white SST image with 17 cm SSH contour showing the LC and LCFE 1 on March 19, 2004. Red dots depict the location of the cyclone center for selected dates. SSH tracks for March 19 are shown. Hovmoller diagram for January-May 2004 is shown with a color line depicting the time of SST image acquisition. (bottom) Alongtrack SSH data for March 19 are superimposed on GOES color SST image from March 19, 2004. Blue indicates negative SSH and cyclonic circulation.
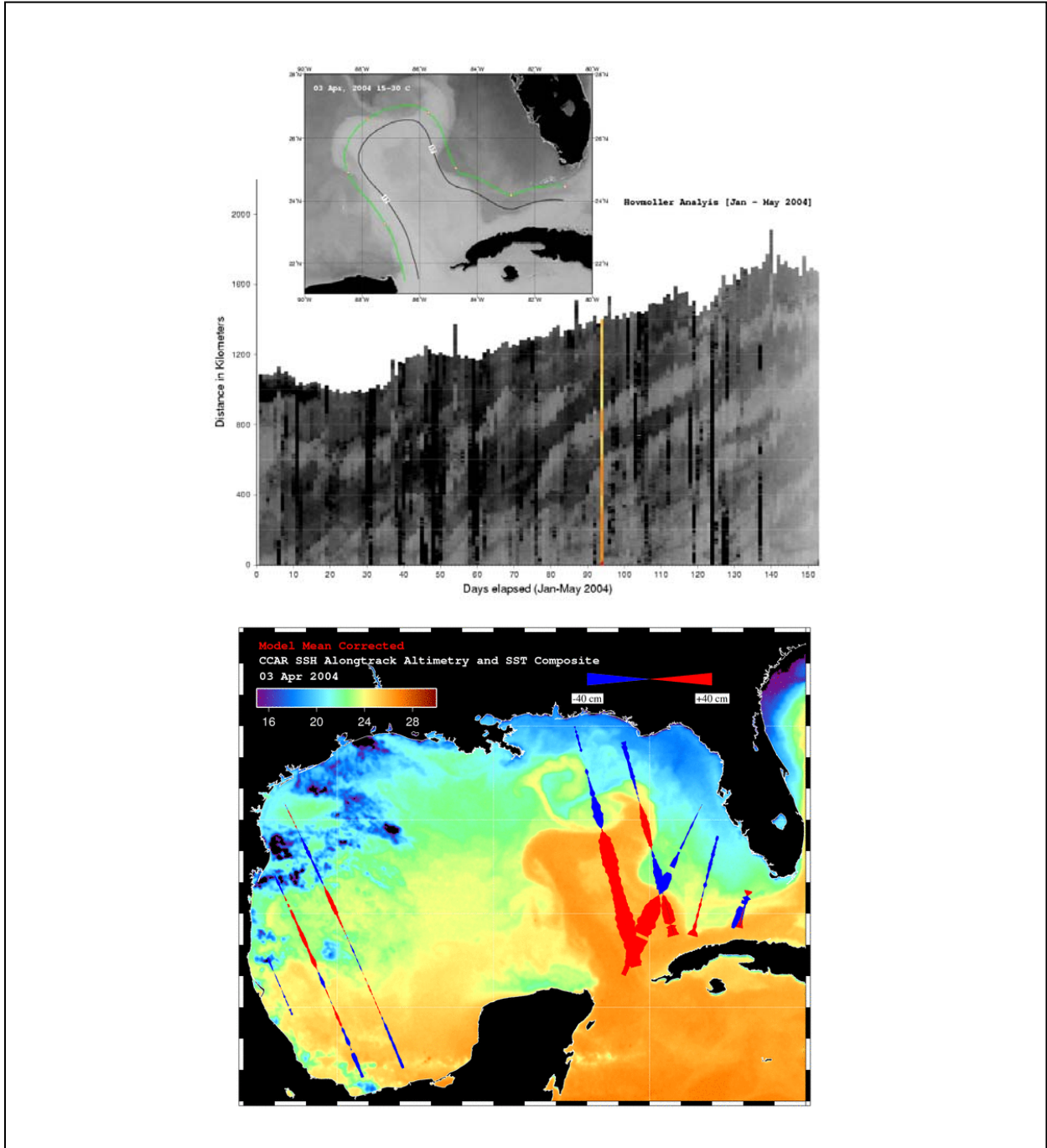
Figure 37. (top) GOES black/white SST image with 17 cm SSH contour showing the LC and LCFE 1 on April 3, 2004. SSH tracks for April 3 are shown. Hovmoller diagram for January-May 2004 is shown with a color line depicting the time of SST image acquisition. (bottom) Alongtrack SSH data for April 3 and 6 are superimposed on GOES color SST image from April 3, 2004. Blue indicates negative SSH and cyclonic circulation.
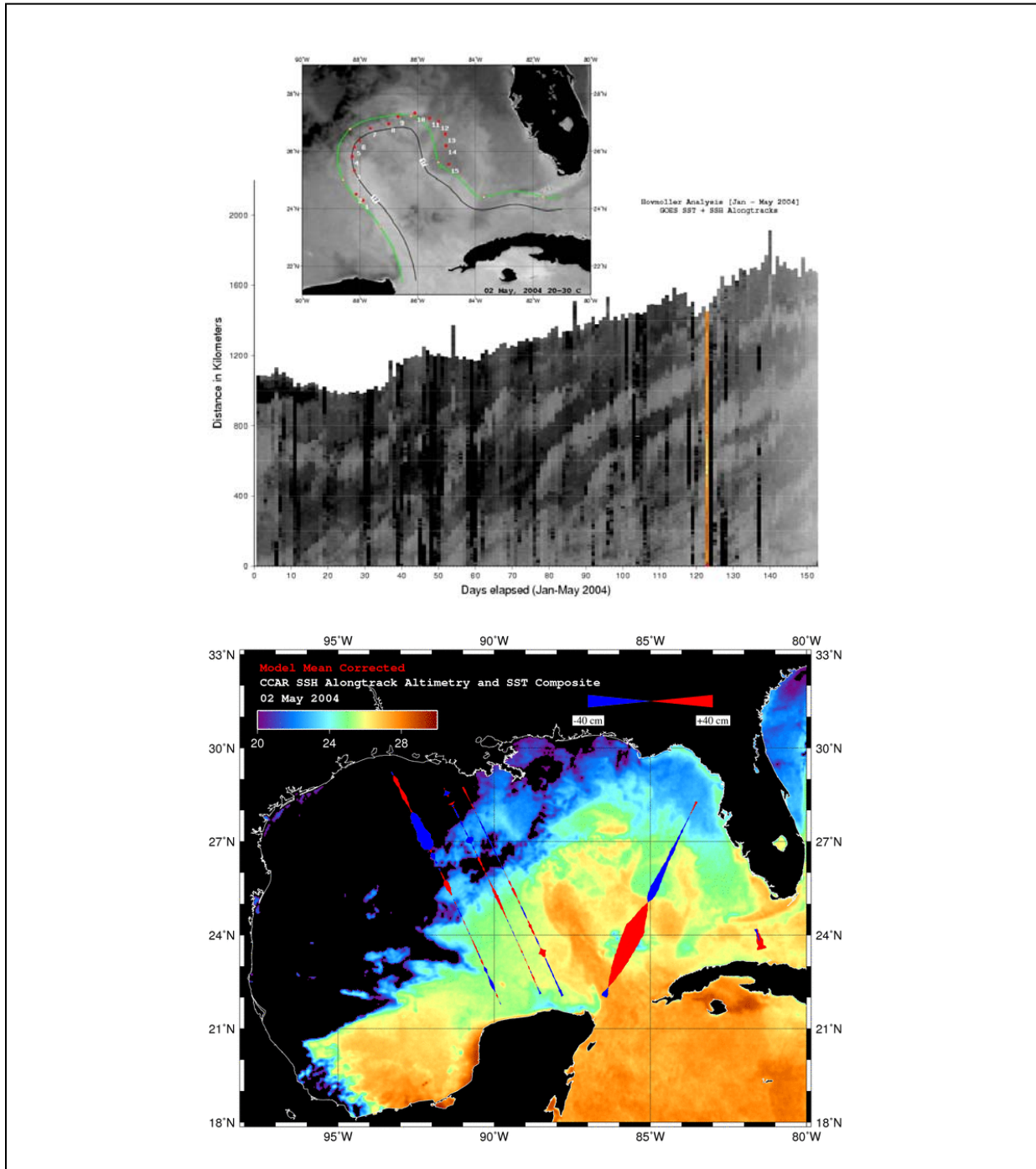
Figure 38. (top) GOES black/white SST image with 17 cm SSH contour showing the LC and LCFE 1 on May 2, 2004. Red dots show the location of cyclone center for selected dates. Hovmoller diagram for January-May 2004 is shown with a color line depicting the time of SST image acquisition. (bottom) Alongtrack SSH data for May 2 are superimposed on GOES color SST image from May 2, 2004. Blue indicates negative SSH and cyclonic circulation.

The motion of LCFE 1 is summarized in Table 3 and its motion is depicted schematically on Figure 39. It exhibited a mean speed of 22.3 cm/s between March 10 and May 2, 2004. Speeds ranged from 6.2 to 63.6 cm/s, producing a very large standard deviation. LCFE 2 followed closely behind and exhibited similar motion characteristics. Its mean speed was higher averaging 29.8 cm/s, but the range was similar spanning 6.0-52.1 cm/s. LCFE 2 was tracked between March 27 and April 22, 2004. The time periods over which these two eddies were tracked are depicted in Figure 39 with white and green lines.

Table 3
Propagation Speeds (cm/s) of LCFEs 1 and 2 Starting March 10 and March 27, 2004, Respectively.

	LCFE 1	LCFE 2
N	14	10
Mean	22.3	29.8
St dev	15.2	15.6
Min	6.2	6.0
Max	63.6	52.1
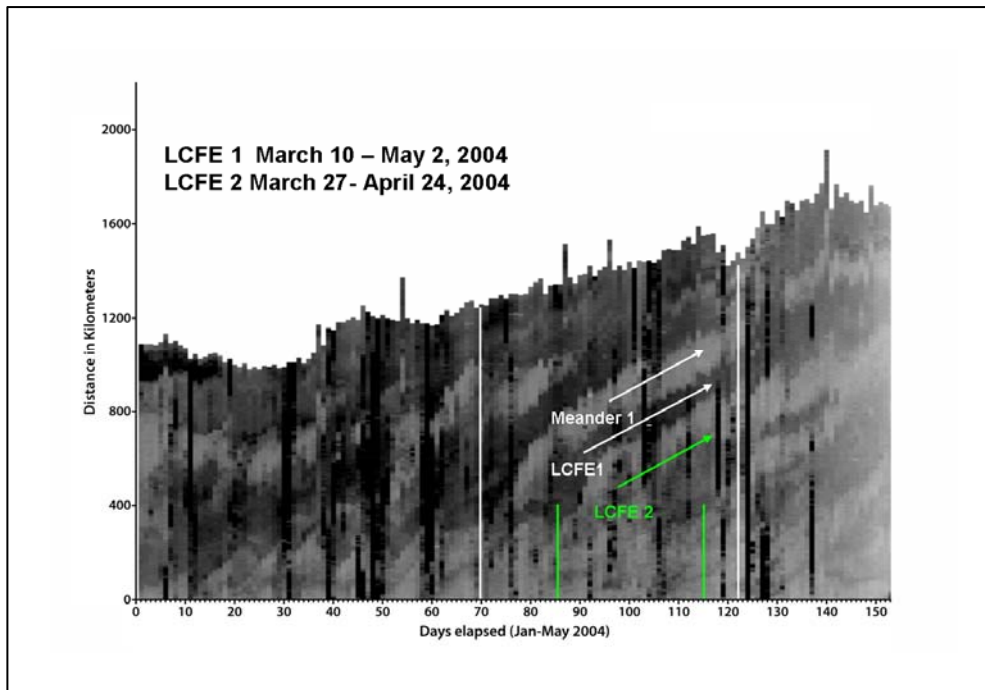
Figure 39. Hovmoller diagram for January through May 2004 showing motion of LCFE 1 and LCFE 2, as well as time periods for which statistics were reported in Table 3. Meanders appear as lighter shades of gray and cyclones appear as darker shades of gray. The meander down current from LCFE 1 is annotated. Both LCFEs moved fastest along the margin between 400 and 800 km from the YC, which placed them northwest and north of the LC at this time.

To further investigate LCFE cyclone intensity characteristics around the margin of the LC, estimates of LCFE SSH values were extracted from the SSH alongtrack data. The alongtrack data was superimposed on GOES SST data to confirm cyclone location (as shown in the bottom panels of Figures 35-38). The minimum SSH values were determined for each crossing of a LCFE within the January through May 2004 period. In addition, where deemed accurate, a size measurement was also obtained along the track. This was sometimes difficult along the western side of the LC as low sea surface height was often observed on the CB. The assumption was made that the cyclone could not be fully formed in water shallower than 200m, thus measurements were stopped at the 200m bathymetric contour. Summary statistics for intensity and size are listed in Table 4 and Table 5, respectively.

The LC margin was divided into five sections for this analysis- west (W), northwest (NW), north-northeast (N-NE), east-southeast (E-SE), and the Florida Straits (FS). SSH values were found to be lowest on the NW, N-NE, and E-SE sections, where mean values ranged from -27.3 to -29.8 cm. SSH values on the W margin and in the FS were -21.1 and -21, respectively. Minimum values were similar (-14 to -15 cm) for all locations except the E-SE section which were lower (-20 cm). Maximum values were considerably lower (almost 2 times) in the NW, N-NE and E-SE sections, ranging from -50 to -45 cm. Maximum values in the W and FS sections were -30 cm and -27 cm, respectively. In terms of size, LCFEs on the northern sections exhibited largest sizes. Mean length scales ranged from 120-125 km in the northern sections. Length scales in the E-SE section were somewhat lower, averaging 119 km. The W margin of the LC exhibited a mean length scale of 49 km and within the FS the mean length was 63 km. Maximum length scales were observed on NW, N-NE and E-SE sections, with maximum values of 150-175 km. Maximum length scales along the CB was 70 km and in the FS was 80 km. These measurements should be considered as estimates as the SSH tracks rarely crossed the mid-section of LCFEs and note that the standard deviations of the distance data were large.

Table 4
Summary of Statistics for LCFE Intensity from Alongtrack SSH Data
(All SSH values are cm and negative.)

	W	NW	N-NE	E-SE	FS
N	21	13	32	15	8
Mean	21.1	27.3	28	29.8	21
St dev	5.4	11.6	9.7	6.5	5.3
Min	14	15	15	20	14
Max	30	50	49	45	27

Table 5
Summary of Statistics for LCFE Size (in km) from Alongtrack SSH Data

	W	NW	N-NE	E-SE	FS
N	20	12	26	14	5
Mean	49	120	125	119	63
St dev	12.2	33.5	24	17	16
Min	26	70	80	95	40
Max	70	175	150	150	80

3.6 Horizon Marine Cyclonic Eddy Study

This section documents the occurrence and motion of three LCFEs associated with WCEs in the northern GoM. Two of the LCFEs separated from WCEs and became solitary features for some time in the northern GoM. The discussion centers around a selection of Horizon Marine's Eddy Watch charts which depict pertinent features such as WCEs, the LC and CEs. The abbreviation "CE" denotes cyclonic eddies, including LCFEs. Drifter speeds (drogued at 50 m) are reported in knots (multiply by 51.44 to convert to cm/s) and are color coded as shown in lower right corner on charts.

The LCFE in the western GoM was first visible on November 8, 2001 (Figure 40). It formed along the northern front of WCE 'Millenium', centered at approximately 25°48'N 94°00'W. Three Far Horizon Drifters (FHDs) moved along the southern and northern fronts of this LCFE. These buoys reported between 1.5 and 2.0 knots along the front and 0.75 knots closer to the center of the LCFE. Over the next two weeks, Millenium Eddy continued on its migration to the southwest while the LCFE remained more or less in the same location. The drifters remained within the LCFE, reporting 0.75 to 1.25 knots. On November 29, 2001, the LCFE separated from the WCE completely. The three drifters remained in orbit in the LCFE reporting 0.75 knots (Figure 41). The LCFE was last visible on December 20, 2001, centered at approximately 25°27'N 93°15'W.
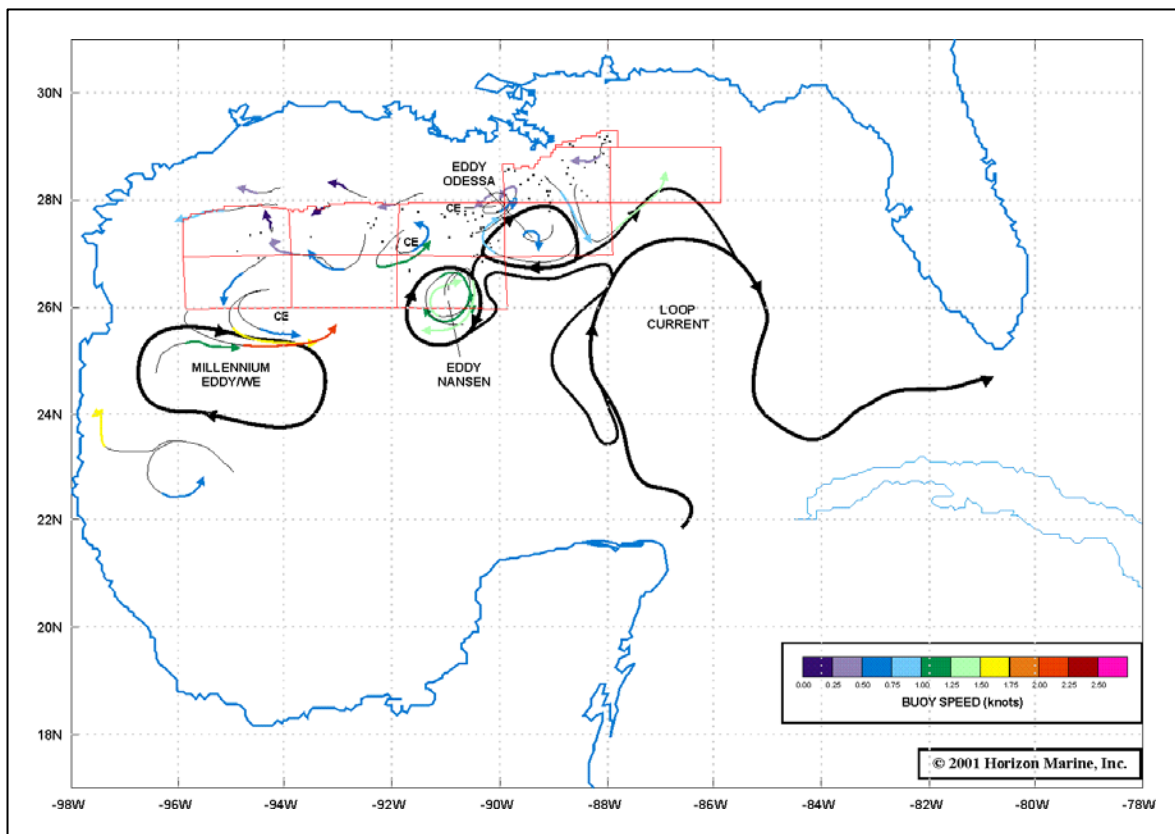
Figure 40. LCFE in western Gulf during week of November 8-15, 2001, when first detected in drifter data.
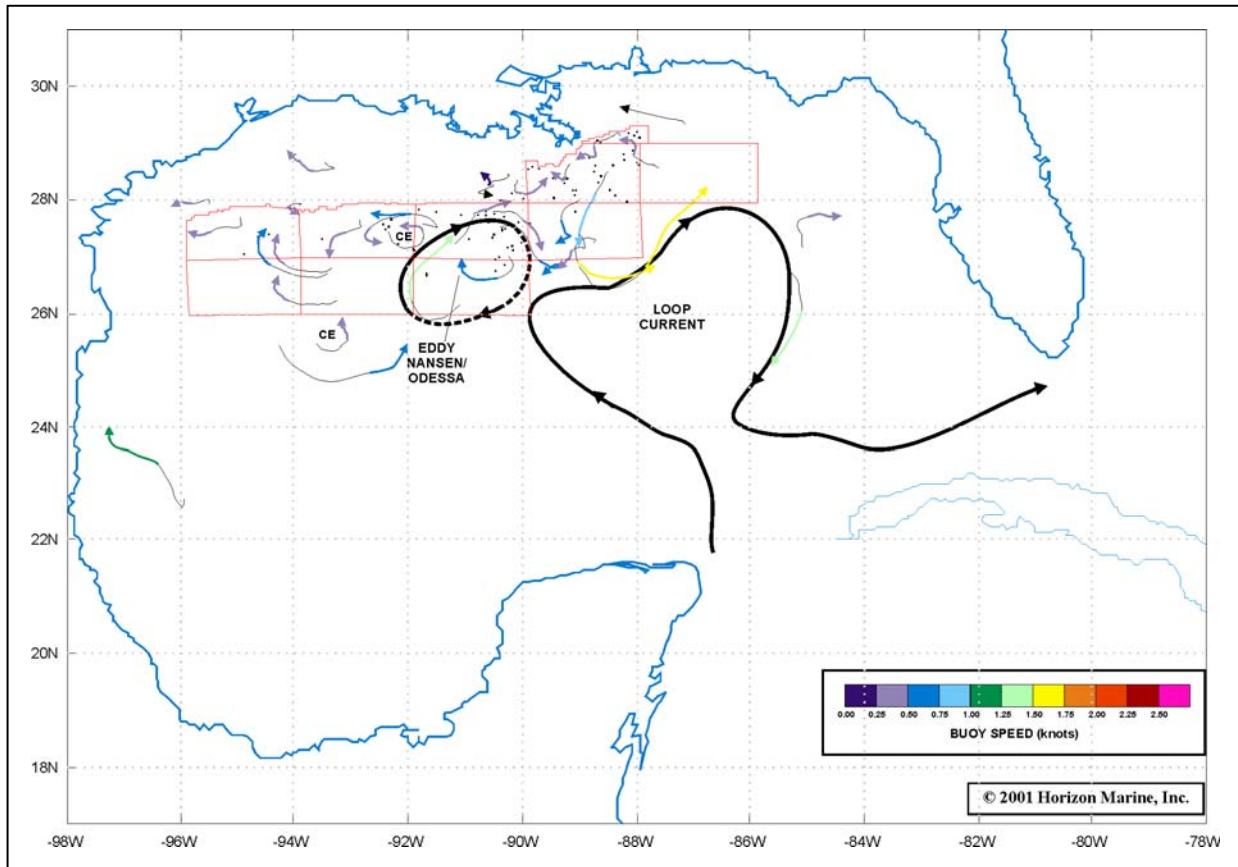
Figure 41. Western Gulf LCFE is still present although Millennium Eddy has collapsed: November 29-December 6, 2001.

A few cyclonic eddies have been observed forming in the Mississippi Canyon when a WCE or the LC impinges close to the shelf edge. Here we discuss two such LCFEs. The first one was observed on August 8, 2002, when it was centered at approximately 28°36'N 88°48'W (Figure 42). It formed along the northern front of WCE 'QE-2' and was much smaller than the western Gulf LCFE discussed previously. This is evident from the track of the FHD orbiting within the LCFE, reporting 1.0 knot. Over the next few weeks, the LCFE migrated southward along with the WCE. Drifters orbiting inside the LCFE continued to report up to 1.25 knots (Figure 43). It was last visible on September 26, 2002, at which time it was centered at 27°09'N 88°24'W. Throughout the lifetime of this LCFE, there wasn't a significant separation from the WCE and it remained a LCFE until its disintegration.
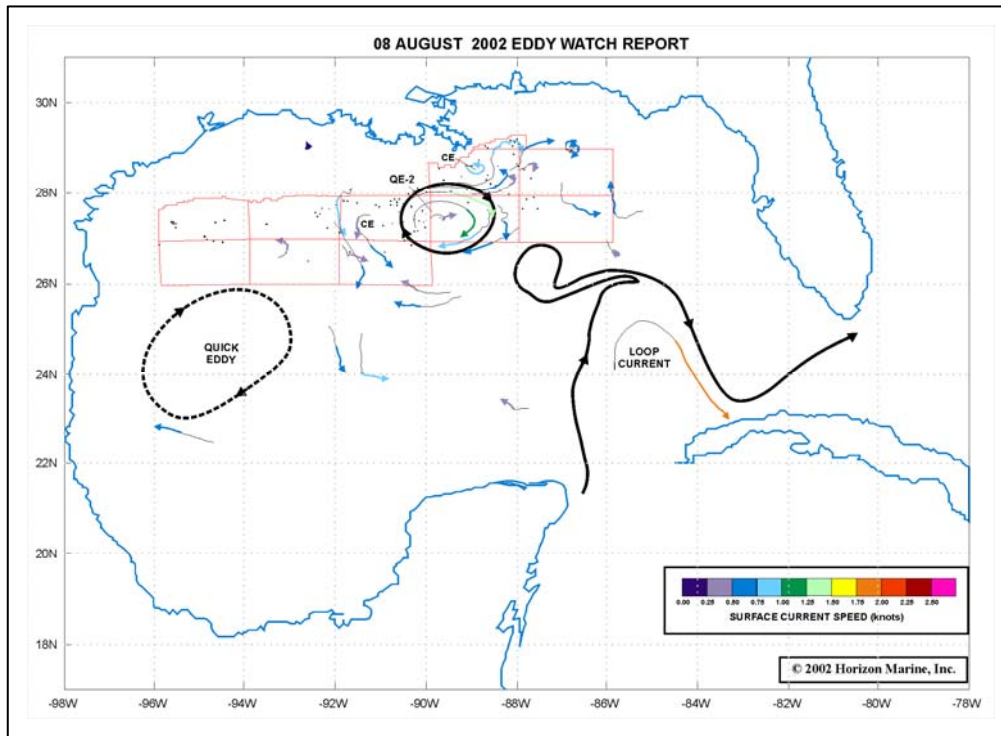
Figure 42. LCFE forming near the Mississippi Canyon: August 8, 2002.
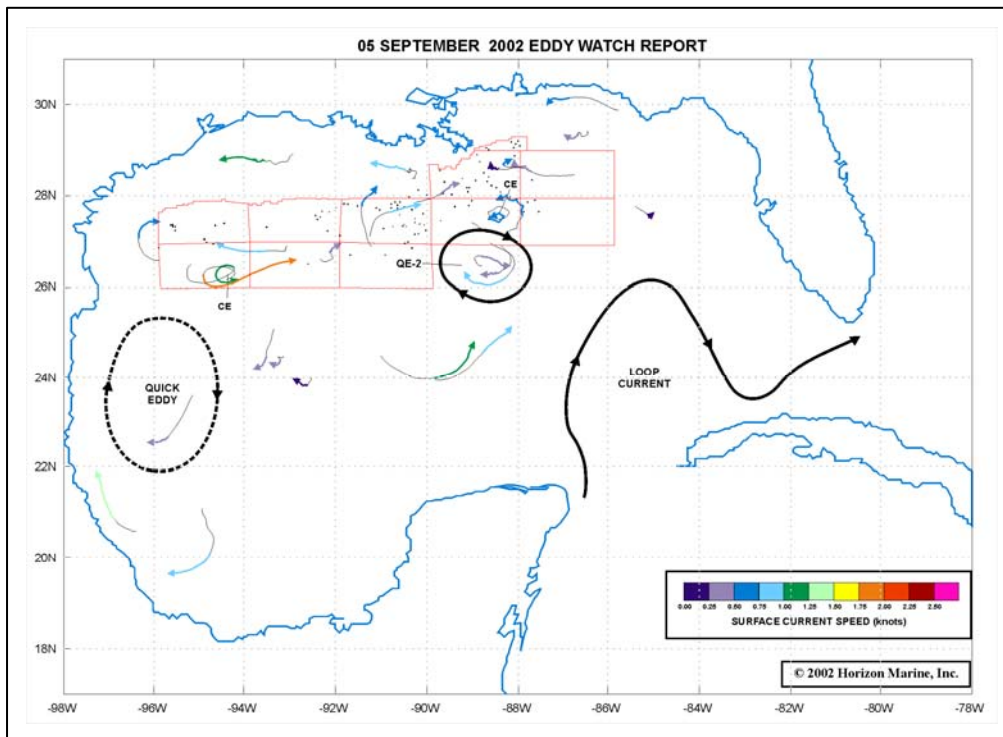
Figure 43. Southward migration of Mississippi Canyon LCFE: September 5, 2002.

Another LCFE was observed forming in the Mississippi Canyon as a frontal cyclone. It was first observed on August 4, 2005, when it was centered at approximately 28°15'N, 88°03'W (Figure 44). Although there were no drifters orbiting the cyclone, it was easily visible as a notch in the northern front of WCE 'Vortex'. Within a week, the LCFE gained strength and a filament from the WCE began wrapping around the cyclone. The filament was no longer visible after a week and the LCFE remained with two FHDs drifting in it. The drifters reported 0.75 to 1.0 knot. The LCFE continued to migrate to the southeast, picking up two more drifters that fell out of WCE Vortex. The first signs of separation from WCE 'Vortex' were observed on September 1, 2005, after Hurricane Katrina crossed this WCE in its approach to the coasts of Louisiana and Mississippi. The LCFE remained centered at 27°48'N 87°54'W while the WCE migrated southwestward. On September 15, 2005, the LC migrated northward and came in contact with the WCE 'Walker' and the LCFE. However, in subsequent weeks, the LC migrated back to the south and the LCFE remained centered at approximately 27°57'N 88°27'W. During November, drifters continued to mark out the position of the LCFE, reporting 0.75 to 1.25 knots (Figure 45). When WCE 'Walker' began forming, the LCFE gained strength along its northern front. FHDs measured 1.5 knots along the northern front of the WCE and the southern front of the LCFE. On November 23, 2005, a drifter reported 2.0 knots as it encountered the combined strengths of the LCFE and WCE 'Walker'. The LCFE was centered at 27°30'N 87°37'W. The LCFE was last observed on December1, 2005, along the northeastern front of WCE 'Walker' and the LC, which had surged north recently.
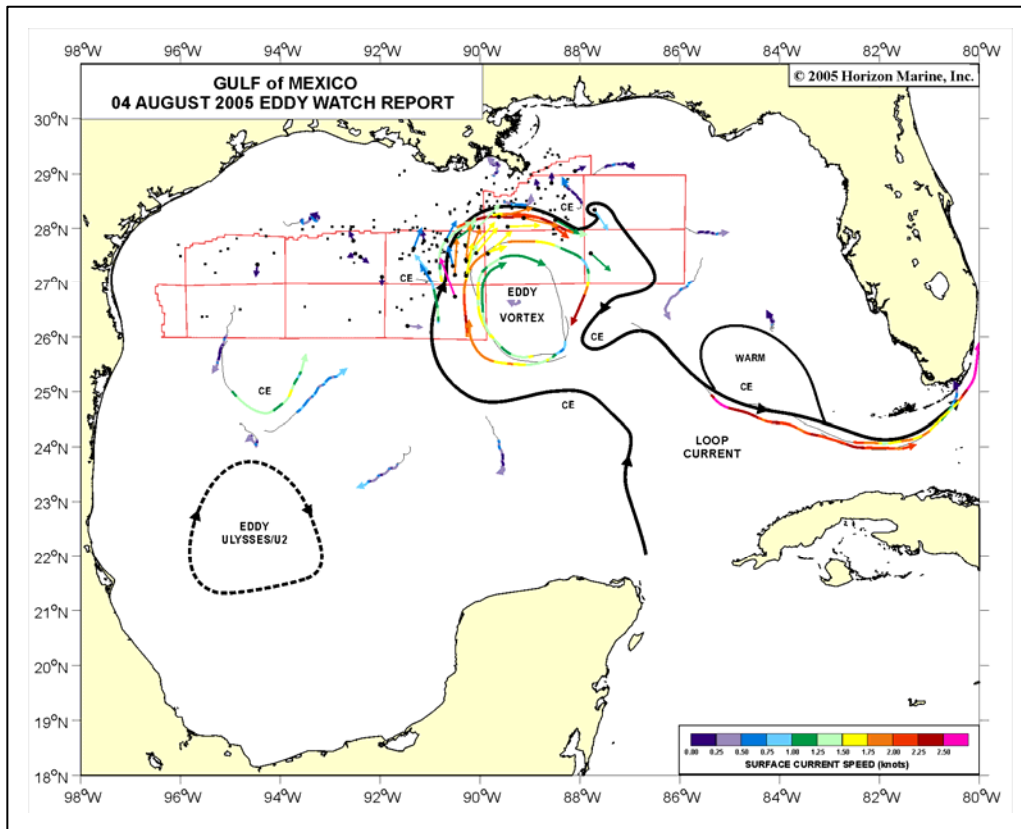
Figure 44. Second Mississippi Canyon LCFE forming along the northern front of Eddy Vortex: August 4, 2005.
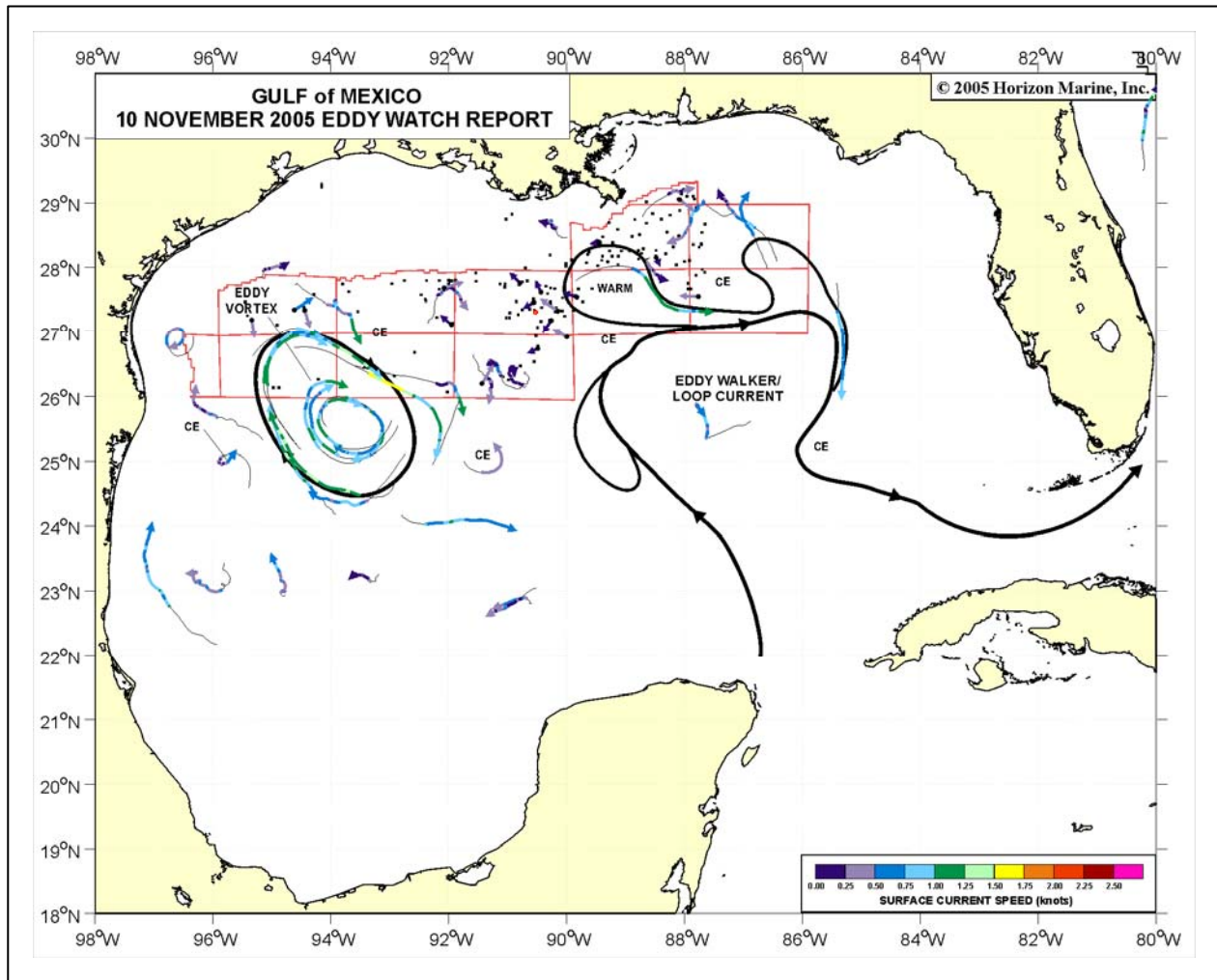
Figure 45. LCFE remained behind when WCE 'Vortex' moved westward and became attached to WCE 'Walker' starting to take shape. The drifters indicate that the LCFE was beginning to lose contact with the front or else the drifters had separated from the LCFE. Conditions during the week of November 10, 2005 are shown.

Figure 46 summarizes the motion of the three LCFEs discussed in this section. All of these were initially observed north of WCEs and exhibited net motion to the southeast. Two were observed to separate from WCEs and one moved from one WCE to another. These observations exhibit the variable nature of cyclonic circulations in the northern GoM. In addition, the Mississippi Canyon is highlighted as a region where LCFEs are generated
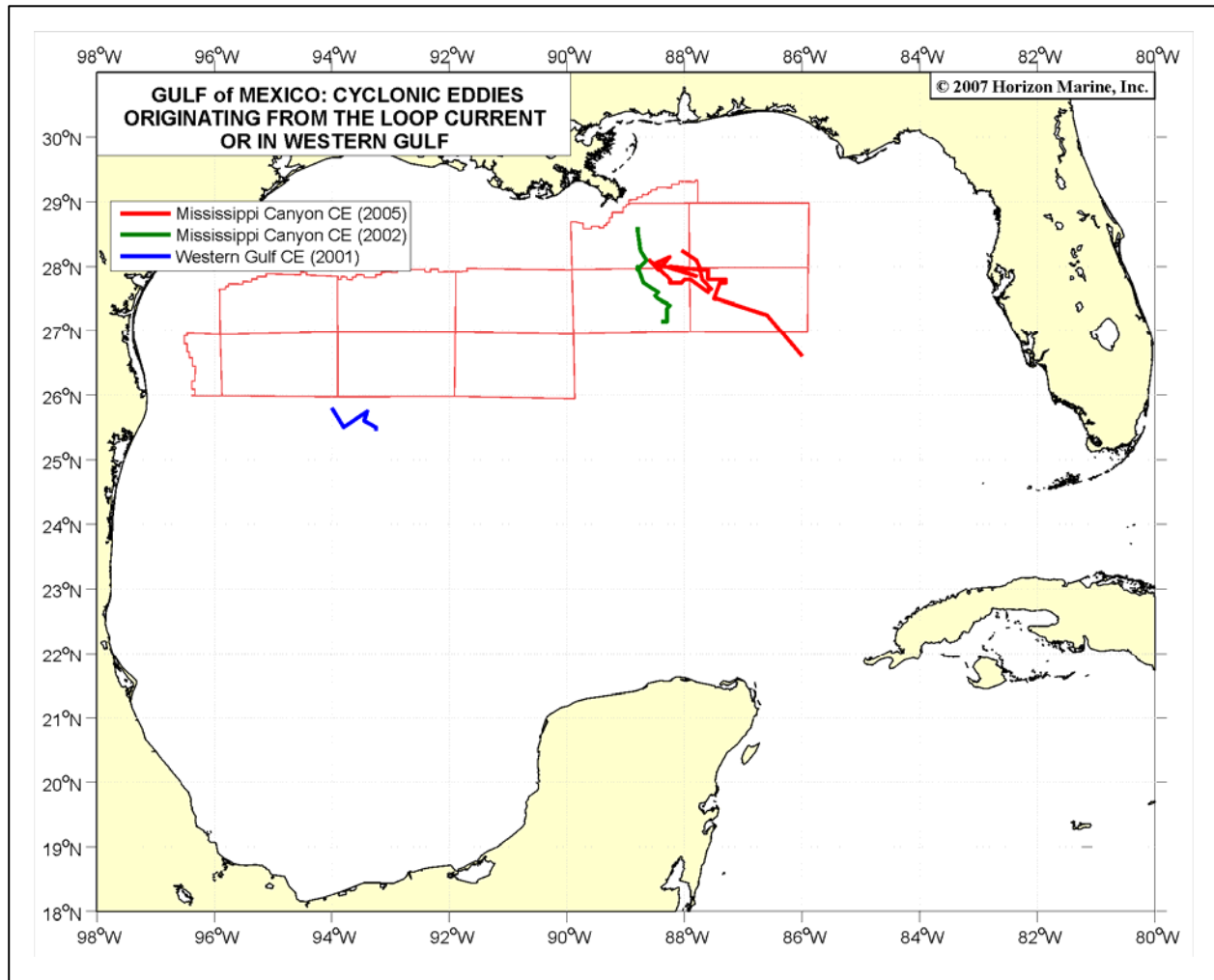
Figure 46. Paths of three LCFEs described in text. Each moved southeast over time.

3.7 Hurricane-Forced Upwelling and Chlorophyll *a* Enhancement within Cold-Core Cyclones in the Gulf of Mexico

A peer reviewed article on cold-core cyclonic eddies in the GoM was published with support from this funded study. This paper is included in its entirety can be found as Appendix A.

Citation: Walker, N.D., R.R. Leben, S. Balasubramanian, Hurricane-forced upwelling and chlorophyll a enhancement within cold-core cyclones in the Gulf of Mexico, *Geophysical Research Letters*, 32, L18610, doi:10.1029/2005GL023716, 2005.

Clear skies, subsequent to Hurricane Ivan's passage across the Gulf of Mexico in September 2004, provided a unique opportunity to investigate upper ocean responses to a major hurricane. Oceanic cyclonic circulation was rapidly intensified by the hurricane's wind field (59-62 m s^{-1}), maximizing upwelling and surface cooling (3-7° C) in two large areas along Ivan's track. Upward isothermal displacements of 50-65 m, computed from wind stress and sea surface height changes, caused rapid ventilation of thermoclines and nutriclines, leading to phytoplankton blooms with peak concentrations 3-4 days later. Wind speed changes along Ivan's track demonstrated that the cool waters (20-26º C) provided immediate negative feedback to the hurricane's intensity. Although our study focused on a relatively small ocean area, it revealed that mesoscale cyclones, in addition to warm anticyclones, may play an important role in producing alongtrack hurricane intensity changes.

4.0 SUMMARY AND CONCLUSIONS

4.1 Answers to Key Questions

(I) How can we most effectively integrate and use the new advanced remote sensing data streams to improve upon the detection, tracking, understanding and prediction of circulation processes of LCFE cyclones that travel rapidly along the margin of the LC?

This project enabled project participants the opportunity to work together over time to develop new techniques for integrating SST, SSH and drifter data to better resolve motion and intensity of the most dynamic features in the GoM, the Loop Current frontal eddy (LCFE) cyclones, features that are always present along the margin of the LC. New products were developed and tested, and many are showcased on the LSU ESL Web page.

A summary of product development funded by this project is listed below.

(1) Animation sequences using GOES SST and Horizon drifter data from April 2001 to November 2004. The SST/drifter animation has been used extensively in research talks and outreach activities to students and was published in the AGU Monograph edited by Sturges and Lugo-Fernandez (2005). Several animation products including the SST/drifter animation are accessible on the Earth Scan Web page (http://www.esl.lsu.edu; "Best of Earth Scan").

(2) A system was developed for ESL staff to access the CCAR gridded SSH by ftp and overlay it on GOES night-time SST composite data. These integrated SST/SSH products are produced using GMT software and are presented in calendar format on the ESL Web page starting in January 2000 and are ongoing (http://www.esl.lsu.edu) (See "Imagery, GOES").

(3) Development of a new automatic technique for tracking LCFEs. The GOES SST data was found to be most useful. We found that the SSH tracks do not update frequently enough to capture the rapid propagation of LCFEs around the LC periphery. The automatic tracking technique is based on detecting temperature changes along a selected transect line through which the frontal eddies are known to move and displaying the temperatures in time and space (Hovmoller) diagrams. Initial results were encouraging as the technique successfully tracked several features only along the western margin of the LC in spring 2004. Along-current translation speeds of 14 to 33 km/day were observed. These values compared well with those obtained by Walker et al. (2003) from manual tracking of features in May 1999.

(4) Subsequent to the encouraging results described in (3), improvements were made to the procedure so that the LCFEs and meanders could be tracked along the entire margin of the LC. This was accomplished by using the CCAR 17 cm SSH contour as a reference for the LC margin. The GOES composite SST data was then extracted along a line 50 km away from this reference line. Hovmoller diagrams and interactive software for manual tracking of features were developed from this initial product. These products have been used extensively in the report. Animations are located on the ESL Web page, under Best of ESL.

(5) The final product was developed mainly at CCAR using GOES SST data and alongtrack SSH data. Although the gridded SSH product is excellent for certain purposes, alongtrack measurements are required to study the LCFEs in detail. The synthesis of SSH and SST in this way enables the user to identify thermal features in the daily cloud-free images that are sampled by the nadir altimeter track. This product provided essential information on the sea surface height structure of LCFEs and surrounding water masses for reference. The presence of negative SSH revealed cyclonic circulation, and the intensity of the cyclones is directly proportional to the SSH value. Image panels and animations have been used extensively in this report.

We expect that these products will continue to provide valuable information for other researchers and expect to continue production of several of these products in support of both research and surveillance activities of the dynamic LC system. Many of the research results are posted on the ESL web page (under Best of Earth Scan).

(II) By using the products developed in (I), can we improve on the available metrics that modelers need to be able to accurately characterize LCFE cyclones as they change in size, intensity, and speed around the margin of the LC?

The new remote sensing products have enabled quantitative estimates of key parameters for LCFEs, such as size, intensity, speed, and frequency information. For the first time, phase speed and frequency information of LCFEs moving northwards along the LC's western margin adjacent to the CB (from 21.5º to 25º N) have been determined using Hovmoller diagrams (See Figures 19-24) over a total of six 4- to 5-month time periods. The metrics are shown in Table 1. The mean speed for the 48 LCFEs tracked between September 2001 and May 2004 was found to be 28.9 cm/s, with a minimum of 10.4 and a maximum of 61.3 cm/s. LCFE formation frequency ranged between 3 per month (1 in 10 days) and 4 per month (1 in 6.8 days). SSH data were used to accurately assess the location of LCFE motion in relation to the bathymetry. These features were located between the 200 and 1000m isobaths.

Although the Hovmoller diagrams were very informative, they were only useful for measuring the LCFE propagation speeds within ~400 km of the intial measuring point, near 21º N. The reason for this was that the length of the LC changed dramatically over time, which affected measurements along the distance scale. A remedy was found by developing a suite of interactive tracking software which displayed the Hovmoller as well as the individual GOES image being sampled. The software enables one to identify and store points of interest on consecutive satellite images (the LCFE centers, for example) and then compute the velocity between those two points. This software was used extensively to generate the speeds for LCFEs around the periphery of the LC.   Detailed motion of LCFEs during January-May 2002 and January-May 2004 are summarized in Tables 2 and 3. During the January-May 2002 time period, a far westward intrusion of the LC occurred. This circulation pattern is atypical when compared with a more typical time period such as January-May 2004 when the LC remained in the eastern GoM. In January-May 2002, four of the seven LCFEs were tracked along the perimeter of the LC which was 2400 km long (Figure 33). During this event, LCFE motion was much more rapid along the southern and southwestern margins where propagation speeds, based on two LCFEs, were 73.8

and 30.3 cm/s. Maxima for these two eddies were 87.3 and 59.4 cm/s, and minima were 62.8 and 9.5 cm/s. The fastest LCFE was tracked for 5 days after which it merged with the large LCFE southwest of the leading edge of the LC. The LCFEs on the northern and northeastern margins of the LC exhibited mean speeds of 9.7 and 11.2 cm/s with maxima of 21.2 and 28.4 cm/s and minima of 3.5 and 2.5 cm/s. Along the southwestern margin, the LCFE cyclones exhibited large spatial scales (100-140 km) and several were observed to collide and coalesce during January and February 2002. The western extension of the LC was clearly associated with the persistence of a large LCFE south of the leading edge of the LC meander and coalescence of new LCFEs with older ones in a large zone where cyclonic vorticity persisted during January and February 2002. Due to the extreme western extension and abrupt curvature of the LC, the LCFEs were not able to move around the entire margin of the LC. Thus, LCFE motion on the northern and eastern margins appeared to be de-coupled from motion of LCFEs on the southwestern margin.

During the January-May 2004 time period, two prominent LCFEs were tracked. These eddies exhibited mean speeds of 22.3 and 29.8 cm/s over 6-week and 4-week periods, respectively. Speed minima were 6.2 and 6.0 cm/s and maximum were 63.6 and 52.1 cm/s (Table 3). Both LCFEs exhibited speed maxima along the NW margin of the LC, between 400 and 800 km from the YS (Figure 39). The maximum speed was associated with explosive growth in size (Figure 36) and it occurred upstream from a large bend/meander of the LC. Measurements of SSH from alongtrack crossings of these LCFEs in combination with SST gradients revealed maximum dimensions of 117 x 175 km. SSH values ranged from -27 to -35 cm when the LCFEs were along the NW and NE sections of the LC.

Results of a detailed analysis of alongtrack SSH data for LCFE crossings during the January-May 2004 time period is presented in Table 4. LCFEs were found to be smaller and less intense (lower SSH) along the western margin of the LC, adjacent to the Campeche Bank where they formed in 200 to 1000m water depth. Many favored the 200-500m depths. The SSH mean value for the CB LCFEs was -21 cm with a mean length scale of 49 km. In contrast, LCFEs along the NW, N-NE and E-SE sections of the LC exhibited lower mean SSH values of -27.3 to -29.8 cm and a doubling of length scales to ~125km. The most intense LCFEs along the CB measured -30 cm, whereas those in the northern regions exhibited eddy core minimums of -45 to -50 cm. LCFEs approaching the Florida Shelf became reduced in size to a mean value of -21 cm and 63 km across. Additional details can be found in Table 4.

(III) Do the new remote sensing tools provide observations that further our understanding of key processes that may lead to better prediction of surface and bottom current accelerations, LC intrusions, detachment of warm-core eddies, or hurricane intensity changes in the GoM?

LCFE Effects on Surface and Bottom Currents

- Our results clearly show that velocities within the surface upper layer (50 m depth) are largest when drifters move in the frontal zone between the LC and a LCFE cyclone. Typical velocities at 50 m water depth ranged from 100 to 175 cm/s.

- LSU mooring data showed that coherent surface to bottom accelerations in current speed were closely associated with LC intrusions and rapid movement and/or growth of LCFEs in close proximity to the Sigsbee Escarpment.

LC Intrusions

- The February 2001 "full water column" current event measured at the LSU mooring in ~ 2250 m water revealed the interaction of LCFEs, detached cyclones and the LC to produce strong currents near the surface (seen in FHD drifters) as well as abnormally strong currents from 400 m to 2250 m. Vertical motion associated with enhancement of upwelling and downwelling along the LC margin or interaction of the LC with the Sigsbee Escarpment provide likely trigger mechanisms for the abnormal current accelerations at depth. Topographic Rossby Waves may have been initiated east of LSU's mooring, propagating westward along the Escarpment.

- The January to May 2002 period showcased an abnormal westward intrusion of the LC to 97°W (Figure 47). This intrusion was associated with large and intense LCFEs on the southwestern margin. SSH data revealed a maximum LCFE dimension of 175 km and SSH of -40 cm.

Detachment of WCEs from the LC

- WCE separations were observed to occur when the Loop Current length scale on the Hovmoller diagram exceeded 2000 km. Examples include Eddy O in September 2001, Eddy P in February 2002, Eddy Q in March 2002 and Eddy T in December 2003. The number of LCFEs along the LC margin during these events ranged from 4 to 7.

- Uncharacteristically large LCFEs along the CB were associated with the WCE separation of Eddy Q. SST/SSH data for February 24, 2002 and March 3, 2002 revealed SSH of -40 cm and length scales of ~ 130 km. This cyclone moved along the northern margin of the LC, further separating Eddy Q from the LC (See Figure 47 for location and SSH data for LCFE on February 24, 2002.)
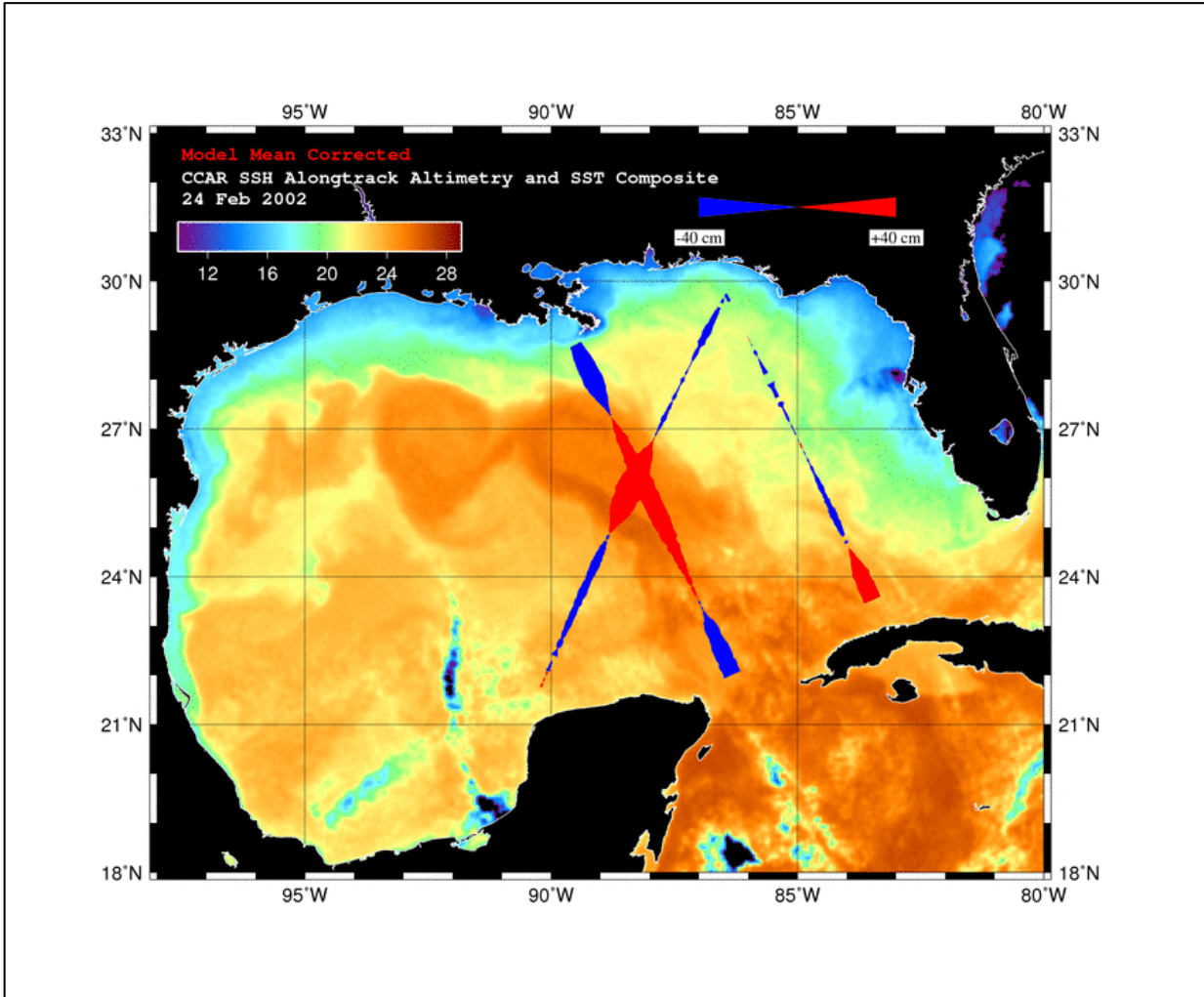
Figure 47. Alongtrack SSH for February 24, 2002 superimposed on GOES color SST image for same day. Blue indicates negative SSH and cyclonic circulation. A relatively large LCFE is apparent between 22º and 23º N near 86º W, as it moves along the northern margin of the LC to separate the LC from Eddy Q.

4.2 Evaluation of Hypotheses

H1. LCFEs form as relatively small (< 50 km across) features and grow in spatial dimension and in intensity as they propagate downstream along the cyclonic shear margin of the LC.

Hypothesis not rejected.

The mean size and SSH intensity of the LCFEs along the CB was found to be 49 km and -21 cm respectively based on a sample size of 20 in the January-May 2004 period. As the LCFEs propagated downstream in a northward direction, the features grew to mean size and intensity of 120 km and -27 cm, based on a sample size of 13. Thus, our measurements do not allow us to reject this hypothesis for most cases. However, a larger and more intense type of LCFE was also observed (such as in Figure 47) that does not fit this general pattern. Also, our observations show that not all LCFEs develop into larger features. They can coalesce and some may leave the margin of the LC. Our observations indicate that LCFE growth is closely related to the behavior of LC meanders upstream and downstream of the eddy.

H2. LCFEs increase in speed as they move downstream along the margin of the LC.

Hypothesis not rejected.

Along the CB, LCFEs exhibited mean speeds of 23-32 cm/s (based on September 2001 through May 2004 data). Minimum speed was 10 cm/s and maximum was 61 cm/s. Along the northern margin of the LC, typical speeds ranged from 22 to 30 cm/s with a minimum of 6 and maximum of 64 cm/s, based on two LCFEs in January-May 2004. The speed of these features is extremely variable. The case study analyses during 2004, however, clearly showed that the features accelerated in speed as the features grew along the northwest margin of the LC. Thus, an increase in speed has been observed, but was not observed for all LCFEs.

H3. When hurricanes move across LCFE cyclones, upwelling is enhanced leading to extreme cooling that may impact hurricane or tropical storm intensity.

Hypothesis not rejected.

The paper by Walker et al. (2005) (see Appendix A) investigated in detail SST changes caused by Hurricane Ivan's wind field. The research clearly showed that the hurricane winds intensified LCFE cyclones and upwelling, both north and south of a developing WCE. In fact, the hurricane may have caused the final separation of this WCE due to its impact on the cyclones. Maximum cooling in the GoM was clearly within the LCFEs where SSTs fell well below the minimum threshold of 26º C and the hurricane experienced decreasing wind speed, despite moving over a WCE. SST cooling in the GoM from Hurricanes Katrina and Rita was greatest within LCFE cyclones and similar negative feedback from the relatively cool SSTs in cyclones may have decreased hurricane intensity before landfall (Walker et al. 2006a; 2006b).

5.0 REFERENCES

Bakun, A. 1996. Patterns in the ocean. California Sea Grant College System. La Jolla, CA., NOAA. 323 pp.

Cochrane, J.D. 1972. Separation of an anticyclone and subsequent development in the Loop Current (1969). In: Capuro, L.R.A. and J.L. Reid, eds. Contributions on the Physical Oceanography of the Gulf of Mexico. Texas A&M University Oceanographic Studies, 2, Gulf Publishing Company, Houston, TX. Pp. 91-106.

Donohue, K., P. Hamilton, K. Leaman, R. Leben, M. Prater, D.R. Watts, and E. Waddell. 2006. Exploratory study of deepwater currents in the Gulf of Mexico. U.S. Dept. of the Interior, Minerals Management Service, Gulf of Mexico OCS Region, New Orleans, LA. OCS Study MMS 2006-074. 399 pp.

Fratantoni, P.S., T.N. Lee, G.P. Podesta, and F. Muller-Karger. 1998. The influence of Loop Current perturbations on the formation and evolution of Tortugas eddies in the southern Straits of Florida. J. Geophys. Res. 103:24,759-24,779.

Gilligan, M.J. and J.Blaha. 2003. Gulf of Mexico airborne survey, January 2000: Dynamic height determination using airborne expendable bathythermographs. Naval Oceanographic Office. Technical Note TN 01-03. 28 pp.

Hamilton, P. and A. Lugo-Fernandez. 2001. Observations of high speed deep currents in the northern Gulf of Mexico, Geophys. Res. Lett. 28:2867-2870.

Hovmoller, E. 1949. The trough-and-ridge diagram. Tellus. 1:62-66.

Huang, J. and Y. Hsueh. 2004. The Loop Current frontal eddies: Observations, generation mechanisms and their movements. EOS Transactions. OS22C-05. Ocean Sciences Meeting, Portland, Oregon, January 2004.

Hurlburt, H.E. 1986. Dynamic transfer of simulated altimeter data into subsurface information by a numerical ocean model. J. Geophys. Res. 91:2372-2400.

Inoue, M., S.E. Welsh, L.J. Rouse, Jr., and E. Weeks. 2008. Deepwater currents in the Eastern Gulf of Mexico: Observations at 25.5^{o}N and 87°W. U.S. Dept. of the Interior, Minerals Management Service, Gulf of Mexico OCS Region, New Orleans, LA. OCS Study MMS 2008-001. 86 pp.

Leben, R. and G. Born. 1993. Tracking Loop Current eddies with satellite altimetry, Advances in Space Research 13:325-333.

Leben, R., G. Born, and B.R. Engebreth. 2002. Operational altimeter data processing for mesoscale monitoring, Marine Geodesy 25:3-18.

Leben, R.R. 2005. Altimeter-derived current metrics. In: Sturges, W. and A. Lugo-Fernandez, eds. Circulation in the Gulf of Mexico: Observations and Models. American Geophysical Union, Washington, DC. Pp. 181-201.

Lee, T.N. and L.P. Atkinson. 1983. Low-frequency current and temperature variability from Gulf Stream frontal eddies and atmospheric forcing along the southeast U.S. outer continental shelf. J. Geophys. Res. 88:4541-4568.

Lee, T.N., J.A. Yoder, and L.P. Atkinson. 1991. Gulf Stream frontal eddy influence on the productivity of the southeast U.S. continental shelf. J. Geophys. Res. 96:22,191-22,205.

Lee, T. N., K. Leaman, and E. Williams. 1995. Florida Current meanders and gyre formation in the southern Straits of Florida. J. Geophys. Res. 100:8607-8620.

Legeckis, R., P.C.T. Zhu, and S. Chen. 1999. Satellite animations reveal ocean surface dynamics for shortest timescales ever. EOS Trans., 80:229, 232-233.

Leipper, D.F., J.D. Cochrane, and J.F. Hewitt. 1972. A detached eddy and subsequent changes In: Contributions on Physical Oceanography of the Gulf of Mexico. Gulf Publishing, Houston, TX. Pp. 107-117.

Maul, G.A. 1974. An evaluation of the use of the earth resources technology satellite for observing ocean current boundaries of the Gulf Stream. NOAA Tech. Report. ERL 335-AOL 18, U.S. Dept. of Commerce, Washington, DC. 125 pp.

Maul, G.A. 1977. The annual cycle of the Gulf Loop Current, 1: Observations during a one-year time series. J. Mar. Res. 35:29-47.

Maul, G.A, F. Williams, M. Roffer, and F.M. Sousa. 1984. Remotely sensed oceanographic patterns and variability of bluefin tuna catch in the Gulf of Mexico. Ocean. Acta. 7:469-479.

May, D.A., J.D. Hawkins, and R.L. Pickett. 1998. Detecting Gulf of Mexico oceanographic features in summer using AVHRR channel 3. J. of Atmos. and Ocean. Tech. 10:64-75.

McKone, K.P., N.D. Walker, and E. Weeks. 2007. Full-water column currents near the Sigsbee Escarpment (91-92 W) and relationships with the Loop Current and associated warm- and cold-core eddies. U.S. Dept. of the Interior, Minerals Management Service, Gulf of Mexico OCS Region, New Orleans, LA. OCS Study MMS 2007-056. 98 pp.

Menzel, P.W. and J.F.W. Purdom. 1994. Introducing GOES-I: The first of a new generation of geostationary operational environmental satellites. Bull. Am. Met. Soc. 75:757-781.

Paluszkiewicz, T., L.P. Atkinson, E.S. Posmentier, and C.R. McClain. 1983. Observations of a Loop Current frontal eddy intrusion onto the west Florida Shelf. J. Geophys. Res. 88:9639-9651.

Schmitz, W.J., Jr. 2003. On the circulation in and around the Gulf of Mexico, a review. Available at: http://www.serf.tamus.edu/gomcirculation/.

Schmitz, W.J., Jr., D.C. Biggs, A. Lugo-Fernandez, L.-Y. Oey, and W. Sturges. 2005. A synopsis of the circulation in the Gulf of Mexico and on its continental margins. In: Sturges, W. and A. Lugo-Fernandez, eds. Circulation in the Gulf of Mexico: Observations and Models. American Geophysical Union, Washington, DC. Pp. 241-262.

Shay, L.K., G.G. Goni, P.G. Black. 2000. Effects of a warm oceanic feature on Hurricane Opal. Monthly Weather Review. 128:1366-1383.

Sturges, W. and R. Leben. 2000. Frequency of ring separations from the Loop Current in the Gulf of Mexico: A revised estimate. J. Phys. Ocean., 30:1814-1819.

Sturges, W. and A. Lugo-Fernandez. 2005. Circulation in the Gulf of Mexico: Observations and Models, American Geophysical Union, Washington, DC. 347 pp.

Vukovich, F.M., B.W. Crissman, M. Bushnell, and W. King. 1979. Some aspects of the oceanography of the Gulf of Mexico using satellite and in situ data. J. Geophys. Res. 84:7749-7768.

Vukovich, F.M. 1988. Loop Current boundary variations. J. Geophys. Res. 93:15585-15591.

Vukovich, F.M. and G.A. Maul. 1985. Cyclonic eddies in the eastern Gulf of Mexico. J. Phys. Ocean. 15:105-117.

Walker, N.D., A. Myint, A. Babin, and A. Haag. 2003. Advances in satellite radiometry for the surveillance of surface temperatures, ocean eddies and upwelling processes in the Gulf of Mexico using GOES-8 measurements during summer. Geophys. Res. Lett. 30. 1854, doi:10.1029/2003GL017555.

Walker, N.D., R.R. Leben, and S Balasubramanian. 2005. Hurricane-forced upwelling and chlorophyll a enhancement within cold-core cyclones in the Gulf of Mexico, Geophys. Res. Lett. 32. L18610, doi:10.1029/2005GL023716.

Walker, N., R.R. Leben, S.A. Hsu, A.S. Haag, S. Balasubramanian, B. Blanchard, and E. Weeks. 2006a. Potential role for real-time satellite infrared radiometry and altimetry in hurricane intensity prediction, AGU Ocean Sciences Meeting, Honolulu, Hawaii, February 2006 (Abstract in EOS Transactions).

Walker, N.D., A. Haag, S. Balasubramanian, R. Leben, I. van Heerden, P. Kemp, and H. Mashriqui. 2006b. Hurricane prediction: a century of advances. Oceanography 19:24-36.

Walker, N., S. Balasubramanian, R. Leben, S. Anderson, P. Coholan, and J. Feeney. 2008. Remote sensing of Loop Current frontal eddy cyclones. In: McKay, M. and J. Nides. Proceedings: Twenty-Fourth Gulf of Mexico Information Transfer Meeting, January 2007. U.S. Dept. of the Interior, Minerals Management Service, Gulf of Mexico OCS Region, New Orleans, LA. OCS Study MMS 2008-012. Pp. 190-195.

Wu, X., W.P. Menzel, and G.S. Wade. 1999. Estimation of sea surface temperatures using GOES-8/9 radiance measurements. Bull. Am. Met. Soc. 80:1127-1138.

Zavala-Hidalgo, J., S.L. Morey, and J.J. O'Brien. 2003. Cyclonic eddies northeast of the Campeche Bank from altimetry data. J. Phys. Ocean. 33:623-629.

6.0 APPENDIX A

A peer reviewed article on cold-core cyclonic eddies in the GoM was published with support from this funded study. This paper is included in its entirety beginning on the next page.

Clear skies, subsequent to Hurricane Ivan's passage across the Gulf of Mexico in September 2004, provided a unique opportunity to investigate upper ocean responses to a major hurricane. Oceanic cyclonic circulation was rapidly intensified by the hurricane's wind field (59-62 m s^{-1}), maximizing upwelling and surface cooling (3-7° C) in two large areas along Ivan's track. Upward isothermal displacements of 50-65 m, computed from wind stress and sea surface height changes, caused rapid ventilation of thermoclines and nutriclines, leading to phytoplankton blooms with peak concentrations 3-4 days later. Wind speed changes along Ivan's track demonstrated that the cool waters (20-26º C) provided immediate negative feedback to the hurricane's intensity. Although our study focused on a relatively small ocean area, it revealed that mesoscale cyclones, in addition to warm anticyclones, may play an important role in producing alongtrack hurricane intensity changes.

Hurricane-forced upwelling and chlorophyll *a* enhancement within cold-core cyclones in the Gulf of Mexico

Nan D. Walker

Department of Oceanography and Coastal Sciences/Coastal Studies Institute Earth Scan Laboratory, Louisiana State University, Baton Rouge, Louisiana, USA

Robert R. Leben

Colorado Center for Astrodynamics Research, University of Colorado, Boulder, Colorado, USA

Shreekanth Balasubramanian

Coastal Studies Institute Earth Scan Laboratory, Louisiana State University, Baton Rouge, Louisiana, USA

[1] Clear skies, subsequent to Hurricane Ivan's passage across the Gulf of Mexico in September 2004, provided a unique opportunity to investigate upper ocean responses to a major hurricane. Oceanic cyclonic circulation was rapidly intensified by the hurricane's wind field (59–62 m s^{-1}), maximizing upwelling and surface cooling (3–7°C) in two large areas along Ivan's track. Upward isothermal displacements of 50–65 m, computed from wind stress and sea surface height changes, caused rapid ventilation of thermoclines and nutriclines, leading to phytoplankton blooms with peak concentrations 3–4 days later. Wind speed changes along Ivan's track demonstrated that the cool waters (20–26°C) provided immediate negative feedback to the hurricane's intensity. Although our study focused on a relatively small ocean area, it revealed that mesoscale cyclones, in addition to warm anticyclones, may play an important role in producing along-track hurricane intensity changes. **Citation:** Walker, N. D., R. R. Leben, and S. Balasubramanian (2005), Hurricane-forced upwelling and chlorophyll *a* enhancement within cold-core cyclones in the Gulf of Mexico, *Geophys. Res. Lett.*, *32*, L18610, doi:10.1029/2005GL023716.

1. Introduction

[2] Hurricane Ivan was a classic hurricane that formed over the tropical Atlantic Ocean on 2 Sep 2004. Upon entering the southern Gulf of Mexico (GoM) as a category 4 hurricane on 14 Sep, it moved NNW towards New Orleans, LA, at 5.4 m s^{-1} with a maximum wind speed of 62 m s^{-1} (Figure 1). On 15 Sep, it altered course (as predicted) to the NNE, making landfall ten hours later near Gulf Shores, AL as a strong category 3 hurricane [*National Hurricane Center (NHC)*, 2004].

[3] Sea surface temperature (SST) above 26°C is essential for hurricane development and maintenance [*Buyers*, 1974]. Previous research has shown that GoM warm core rings (WCRs) can rapidly increase hurricane intensity due to the fluxes of latent and sensible heat from the warm (>28°C) and deep (>150 m) mixed layer [*Shay et al.*, 2000]. In contrast, negative oceanic feedback and hurricane weak-

ening has been documented over waters below 26°C [*Monaldo et al.*, 1997]. Hurricane-forced sea surface cooling results mainly from vertical mixing and entrainment, transient upwelling, and evaporative heat loss to the atmosphere [*Price*, 1981; *Sanford et al.*, 1987]. Previous observational and modeling studies have shown that an asymmetrical SST response to hurricane wind forcing is typical, with greatest cooling east of the hurricane's track. There, winds are strongest and the wind stress vector turns clockwise through time, maximizing surface divergence and upwelling [*Price*, 1981; *Stramma et al.*, 1986; *Monaldo et al.*, 1997]. Although hurricane-forced cooling can affect future storms that pass over the same area [*Brand*, 1971] and even the parent storm [*Black and Holland*, 1995], real-time SST information is not easily incorporated into hurricane intensity prediction models. This lack of crucial information is a contributing factor to the poor reliability in forecasting hurricane intensity changes [*Emanuel*, 1999].

[4] Clear skies, subsequent to Ivan's passage across the GoM, provided a unique opportunity to study physical and biological changes of the upper ocean using satellite data from both passive and active sensors. Integration of sea surface height (SSH) data with satellite-derived SSTs and chlorophyll *a* (Chla) enabled a comparison of ocean responses within cold-core cyclones and WCRs (anticyclones). Our analysis revealed sea surface cooling of 3–7°C and elevated Chla concentrations over two large areas of pre-existing cyclonic circulation along Ivan's track. Ivan's wind speeds decreased twice over the GoM [*NHC*, 2004], despite crossing the LC and a large WCR. Both intensity changes occurred subsequent to the evolution of 20–26°C SSTs along its track, suggesting rapid negative oceanic feedback from two cyclones.

2. Satellite Data

[5] SST was quantified using GOES-12 night-time composite images. A major advantage of GOES data is frequent repeat coverage (48 images/day) which enables removal of cloud cover, improving feature detection and SST accuracy [*Legeckis et al.*, 1999; *Walker et al.*, 2003]. Chla concentrations were computed from SeaWiFS data using the NASA OC2 algorithm [*O'Reilly et al.*, 1998]. Altimeter data from Jason-1, TOPEX/POSEIDON,
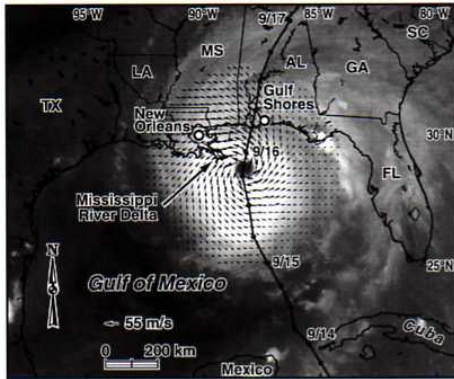
74

Figure 1. GOES-12 water vapor image on 15 Sep (2245 UT) showing Ivan, the GoM, and other pertinent locations. Ivan's 6-hour positions are depicted with black dots. NHC vector winds are superimposed (http://www.aoml.noaa.gov/).

and Geosat Follow-on were used to compute SSH using techniques described by *Leben et al.* [2002].

3. Upper Ocean Cooling and Relationship to Cyclones

[6] The GOES SST composite of 17 Sep revealed two large regions of cooling proximate to Ivan's track, where SSTs of 20–26°C were detected over 38,900 km^2 (Figure 2b). SSTs prior to the event (9 Sep) were 28–30°C (Figure 2a; Table 1). SST change averaged −3.8°C in the northern feature and −4.1°C in the southern feature, with respective maxima of −5.9° and −7.4°C (Table 1). Mean SST change of −1.9°C occurred within the WCR, which separated the areas of maximum cooling (Figures 2a and 2b; Table 1).

[7] SSH data showed pre-existing cyclonic circulation in the areas where the extreme cooling occurred (Figures 2a and 2b). The hurricane wind field (33–62 m s^{-1}) intensified cyclonic circulation in both areas, as SSH changes of −5 to −20 cm were detected between 9 and 17 Sep (Figures 2a–2c). North of the WCR, maximum cooling (SST change > −5°C) occurred 40 to 90 km east of Ivan's track in an area of maximum SSH change (Figure 2c). Its location agreed with results of *Price* [1981], who found that maximum cooling for rapidly moving hurricanes usually occurs 30–150 km to the right of the track. MODIS SST data (not shown) revealed a frontal eddy cyclone in this location before hurricane passage. South of the WCR, maximum cooling occurred within the area of cyclonic circulation, closest to Ivan's track (Figure 2b). The region of extreme cooling (SST change > −5°C) extended 20 km east of and 80 km west of Ivan's track. It extended further west than would be expected based on previous research. Some westward advection of upwelled waters may have occurred between Ivan's passage and image acquisition, as strong currents (~60 cm s^{-1}) occurred along the outer margin of the WCR on 17 Sep (Figure 3c). Extreme cooling was not observed further east as this was an area of positive SSH, connecting the WCR with the LC. Although cool wakes of

1–6°C have been detected after hurricane passage in several ocean areas [*Price*, 1981; *Stramma et al.*, 1986; *Monaldo et al.*, 1997], our results demonstrate maximum cooling in regions of cyclonic circulation along Ivan's track.

[8] Surface wind data, available every 6 hours from the National Hurricane Center [*NHC*, 2004], revealed that Ivan's winds decreased twice during its transit of the GoM (Figure 2c). The first intensity change (from 62 to 59 m s^{-1}) was observed on 15 Sep 1200 UTC, soon after evolution of 20–26°C water in the southern upwelling
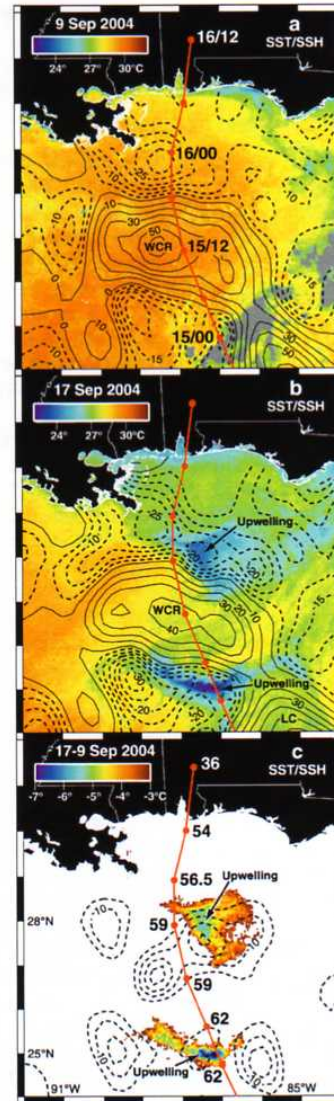

Figure 2. GOES SSTs (°C) with SSH 5 cm contours superimposed on (a) 9 Sep and (b) 17 Sep. Negative SSH indicates cyclonic circulation. (c) SST and SSH differences (17–9 Sep). Winds speeds at 10m (m s^{-1}) are shown along Ivan's track. Ivan's 6-hour positions are shown in a-c. Clouds are gray.

Table 1. SST (°C) for the Northern (UN) and Southern (US) Upwelling Regions, and WCR: September 2004

Region	9	17	19	ΔX Mean 17-9	ΔX Max 17-9
UN[a] (25,000 km²)	29.2	25.4	27.1	−3.8	−5.9
US[a] (14,000 km²)	28.9	24.8	26.4	−4.1	−7.4
WCR (19,000 km²)	29.4	27.5	28.3	−1.9	−3.6

[a]Statistics are for areas where SST change exceeded 3°C.

region. The second change (from 59 to 56.5 m s⁻¹) occurred between 15 Sep 1800 and 16 Sep 0000 UTC (Figures 2a and 2c), in close proximity to the northern upwelling feature. We conclude that the two large areas of cool water (<26°C over 38,000 km²) provided rapid negative feedback to Hurricane Ivan.

3.1. Cyclone Intensification and Upward Displacement of the Thermocline

[9] GoM cyclones are regions of vigorous sub-surface upwelling and upward doming of cool water where the top of the thermocline is typically 50–60 m below the sea surface [*Biggs and Muller-Karger*, 1994; *Zimmerman and Biggs*, 1999; *Gilligan and Blaha*, 2003]. The isopycnal displacement of the thermocline due to storm-induced upwelling can be computed as $\eta = \tau/\rho \, f \, U_h$; where τ is wind stress, ρ is water density, f is the Coriolis force, and U_h is hurricane transit speed [*Price et al.*, 1994; *Babin et al.*, 2004]. Based on maximum wind speeds of 59–62 ms⁻¹, τ values of 18.7–21.9, and a transit speed of 5.4 m s⁻¹ we estimated that the thermocline upwelled from depths of 53 to 62 m within the areas of maximum SST change. Using SSH data, we also computed isotherm upwelling (Δη) from the change in SSH anomaly (Δh) using the reduced gravity approximation $\Delta\eta = -g/g' \, \Delta h$ [*Shay et al.*, 2000]. Assuming a g' value of 0.03 ms⁻² that is representative of gulf-wide conditions we estimate upward displacement of an isotherm of 32.7 m for every −10 cm change in SSH. The observed −15 to −20 cm changes in SSH yielded isotherm displacements of 50–65 m, which are consistent with our estimates based on wind stress.

3.2. Chlorophyll *a* Changes Within Cyclones and Eddy Entrainment

[10] Time-sequence SeaWiFS imagery revealed large-scale enhancement of Chla concentrations within the two large upwelling regions (Figures 3a–3c). Peak concentrations occurred on 19 Sep (Figure 3c) (Table 2) when mean values above 1 mg m⁻³ covered 9000 km² and 6200 km² (in northern and southern features, respectively). Temporal Chla changes were assessed by including larger areas than those defined by 1 mg m⁻³, as the features were not stationary after generation. Within the northern area of cooling, concentrations increased from 0.36 mg m⁻³ (before Ivan) to 0.81 mg m⁻³ (on 19 Sep) over 27,000 km² (Table 2). In the southern region, mean concentrations increased from 0.24 mg m⁻³ to 0.99 mg m⁻³ over 13,000 km² (Table 2). Peak concentrations lagged Ivan's passage by 3 and 4 days in the northern and southern features, respectively. The predicted 50–65 m upward isotherm displacement would have injected high concentrations of nitrate into surface waters, since nitraclines within GoM cyclone centers are typically found near 50–70 m [*Biggs and Muller-Karger*, 1994; *Zimmerman and Biggs*, 1999].

[11] Hurricane-induced Chla enhancement can result from upward entrainment of phytoplankton to the surface from the deep Chla maximum or from new production [*Babin et al.*, 2004]. Our results indicate that both processes contributed to the enhancement in surface Chla. In the northern feature, mean Chla values increased from 0.36 mg m⁻³ on 8 Sep to 0.50 mg m⁻³ on 17 Sep, 1.5 days after Ivan's passage (Table 2). However, peak mean

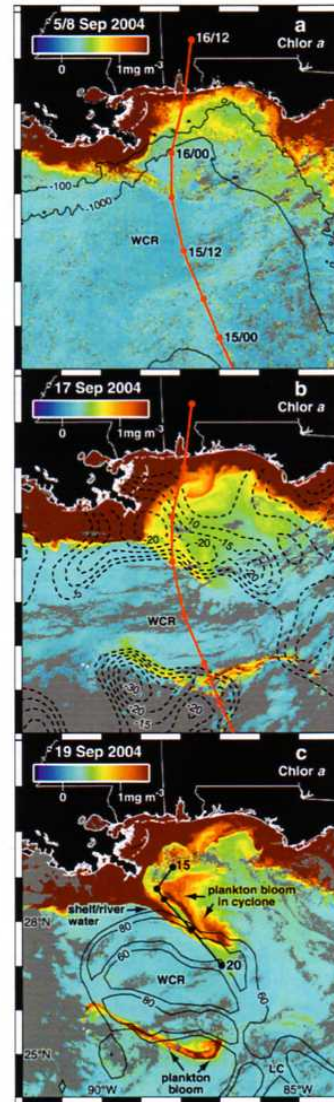**Figure 3.** Chla (mg m⁻³) computed from mean values on (a) 4 days (3, 5, 7, 8 Sep); (b) 17 Sep; and (c) 19 Sep. In (a) and (b), Ivan's 6-hour positions are shown. In (b), negative SSH data for 17 Sep are shown. In (c), SSH-derived 60 and 80 cm s⁻¹ speed isotachs for 17 Sep are superimposed. NDBC buoy positions, obtained at irregular intervals, from 15 to 20 Sep are also shown. Clouds are gray.

3 of 5

76

Table 2. Chla Changes (mg m^{-3}) for Northern (UN) and Southern Upwelling (US) Regions: September 2004

Region	3/8[a]	17	19	27/29[b]	ΔX Mean		
					17-8	19-17	19-8
UN (27,000 km^2)	0.36	0.50	0.81	0.45	+0.14	+0.31	+0.45
US (13,000 km^2)	0.24	0.46	0.99	0.24	+0.22	+0.53	+0.75

[a]Mean value for 3, 5, 7, and 8 September.
[b]Mean value for 27 and 29 September.

concentrations of 0.81 mg m^{-3} occurred a full 2 days later (Figures 3b and 3c). In the southern feature, mean Chla values increased from 0.24 mg m^{-3} to 0.46 mg m^{-3} between 8 and 17 Sep, reaching a maximum of 0.99 mg m^{-3} on 19 Sep. The initial increase is attributed to upward Chla entrainment, whereas the delayed increase is attributed to new production from ventilation of the nutricline. Based on these measurements we estimate that new production contributed about 70% to the total. By 27–28 Sep, Chla had decreased from 0.81 to 0.45 mg m^{-3} in the northern feature and from 0.99 to 0.24 mg m^{-3} in the southern feature (Table 2). Both blooms experienced horizontal entrainment around the WCR and mixing with adjacent waters due to strong currents (60–80 cm s^{-1}) (Figure 3c). The Chla response in GoM cyclones was larger than previous observations in the oligotrophic Atlantic [*Babin et al.*, 2004].

[12] On 19 Sep, a 200-km long filament of pigment-rich shelf and river water was detected in Chla imagery, extending SE from the Mississippi River delta along the north flank of the WCR (Figure 3c). Seaward entrainment of this coastal water mass was confirmed by NDBC buoy 42040, which broke free from its mooring and moved seaward at a mean speed of 66 cm s^{-1} from 17–20 Sep (Figure 3c). The buoy moved within relatively clear water, which separated the shelf filament from the plankton bloom within the cyclone (Figure 3c). The satellite-derived Chla estimates within the shelf filament (1–5 mg m^{-3}) may be overestimates of in-situ values due to high levels of river-borne suspended sediment and/or CDOM. Similar pigment-rich coastal filaments have been observed after hurricanes along the NE U.S. coast [*Davis and Yan*, 2004] and in the northern GoM [*Yuan et al.*, 2004]. Their importance in delivering carbon to deeper oligotrophic regions has been discussed [*Yuan et al.*, 2004].

4. Summary and Conclusions

[13] Satellite-derived SST, SSH, and Chla measurements clearly revealed rapid upwelling responses along and east of Ivan's path where pre-existing cyclonic circulation experienced intensification. Venting of thermoclines and nutriclines can explain the SST cooling response of 3–7°C and subsequent Chla enhancement. Although hurricane-forced SST change and augmentation in Chla have been reported in the Atlantic Ocean, an association with cold-core cyclones has not previously been made. Our results support the contention that wind-enhanced eddy pumping of nutrients into surface waters is an important process in biogeochemical cycling as discussed by *McGillicuddy et al.* [1998] and *Falkowski et al.* [1991]. Recent improvements in the repeat coverage from satellite altimeters will enhance capabilities for detecting cold-core cyclones, which can not easily be detected in satellite SST data until a wind event initiates upwelling and, in extreme cases such as this one, surface cooling.

[14] We observed evidence of rapid negative ocean-atmosphere feedback to Hurricane Ivan from the large areas of cooling where SSTs of 20–26°C were generated during hurricane passage. Thus, mesoscale ocean cyclones, in addition to warm anticyclones, may play an important role in along track hurricane intensity changes. We suggest that hurricane intensity forecasts may benefit from the inclusion of more accurate location and intensity information on oceanic cyclones. This could be accomplished by including an eddy-resolving data assimilative ocean modeling capability in coupled atmosphere/ocean hurricane simulations.

References

Babin, S. M., J. A. Carton, T. D. Dickey, and J. D. Wiggert (2004), Satellite evidence of hurricane-induced phytoplankton blooms in an oceanic desert, *J. Geophys. Res.*, *109*, C03043, doi:10.1029/2003JC001938.

Biggs, D. C., and F. E. Muller-Karger (1994), Ship and satellite observations of chlorophyll stocks in interacting cyclone-anticyclone eddy pairs in the western Gulf of Mexico, *J. Geophys. Res.*, *99*, 7371–7384.

Black, P. G., and G. J. Holland (1995), The boundary layer of tropical Cyclone Kerry (1979), *Mon. Weather Rev.*, *123*, 2007–2028.

Brand, S. (1971), The effects on a tropical cyclone of cooler surface waters due to upwelling and mixing produced by a prior tropical cyclone, *J. Appl. Meteorol.*, *10*, 865–874.

Buyers, H. R. (1974), *General Meteorology*, 314 pp., McGraw-Hill, New York.

Davis, A., and X. Yan (2004), Hurricane forcing on chlorophyll-a concentration off the northeast coast of the U.S., *Geophys. Res. Lett.*, *31*, L17304, doi:10.1029/2004GL020668.

Emanuel, K. A. (1999), Thermodynamic control of hurricane intensity, *Nature*, *401*, 665–669.

Falkowski, P. G., D. Ziemann, Z. Kolber, and P. K. Bienfang (1991), Role of eddy pumping in enhancing primary production in the ocean, *Nature*, *352*, 55–58.

Gilligan, M. J., and J. Blaha (2003), Gulf of Mexico Airborne Survey, January 2000: Dynamic height determination using airborne expendable bathythermographs, *Tech. Note TN 01-03*, Naval Oceanographic Office, Stennis Space Center, Miss.

Leben, R. R., G. H. Born, and B. R. Engebreth (2002), Operational altimeter data processing for mesoscale monitoring, *Mar. Geod.*, *25*, 3–18.

Legeckis, R., P. C. T. Zhu, and S. Chen (1999), Satellite animations reveal ocean surface dynamics for shortest timescales ever, *EOS Trans. AGU*, *80*(20), 229, 232–233.

McGillicuddy, D. J., A. R. Robinson, D. A. Siegel, H. W. Jannasch, R. Johnson, T. D. Dickey, J. McNeil, A. F. Michaels, and A. H. Knap (1998), Influence of mesoscale eddies on new production in the Sargasso Sea, *Nature*, *394*, 263–266.

Monaldo, F. M., T. D. Sikora, S. M. Babin, and R. E. Sterner (1997), Satellite imagery of sea surface temperature cooling in the wake of Hurricane Edouard, *Mon. Weather Rev.*, *125*, 2716–2721.

National Hurricane Center (2004), Tropical cyclone report: Hurricane Ivan, Natl. Weather Serv., Silver Spring, Md. (Available at http://www.nws.noaa.gov)

O'Reilly, J. E., S. Maritorena, B. G. Mitchell, D. Siegel, K. Carder, S. Garver, M. Kahru, and C. McClain (1998), Ocean color chlorophyll algorithms for SeaWiFS, *J. Geophys. Res.*, *103*, 24,937–24,953.

Price, J. F. (1981), Upper ocean response to a hurricane, *J. Phys. Oceanogr.*, *11*, 153–175.

Price, J. F., T. B. Sanford, and G. Z. Forristall (1994), Forced stage response to a moving hurricane, *J. Phys. Oceanogr.*, *24*, 233–260.

Sanford, T. B., P. G. Black, J. R. Haustein, J. W. Feeney, G. Z. Forristall, and J. F. Price (1987), Ocean response to a hurricane, Part I: observations, *J. Phys. Oceanogr.*, *17*, 2065–2083.

Shay, L. K., G. J. Goni, and P. G. Black (2000), Effects of a warm oceanic feature on Hurricane Opal, *Mon Weather Rev.*, *128*, 1366–1383.

4 of 5

Stramma, L., P. Cornillon, and J. F. Price (1986), Satellite observations of sea surface cooling by hurricanes, *J. Geophys. Res.*, *91*, 5031–5035.

Walker, N., S. Myint, A. Babin, and A. J. Haag (2003), Advances in satellite radiometry for the surveillance of surface temperatures, ocean eddies and upwelling processes in the Gulf of Mexico using GOES-8 measurements during summer, *Geophys. Res. Lett.*, *30*(16), 1854, doi:10.1029/2003GL017555.

Yuan, J., R. L. Miller, R. T. Powell, and M. J. Dagg (2004), Storm-induced injection of the Mississippi River plume into the open Gulf of Mexico, *Geophys. Res. Lett.*, *31*, L09312, doi:10.1029/2003GL019335.

Zimmerman, R. A., and D. C. Biggs (1999), Patterns of distribution of sound-scattering zooplankton in warm- and cold-core eddies in the Gulf of Mexico, from a narrowband acoustic Doppler current profiler survey, *J. Geophys. Res.*, *104*, 5251–5262.

S. Balasubramanian, Coastal Studies Institute Earth Scan Laboratory, Louisiana State University, Baton Rouge, LA 70803, USA.

R. R. Leben, Colorado Center for Astrodynamics Research, University of Colorado, Boulder, CO USA.

N. D. Walker, Department of Oceanography and Coastal Sciences/ Coastal Studies Institute Earth Scan Laboratory, Louisiana State University, Baton Rouge, LA 70803, USA. (nwalker@lsu.edu)

The Department of the Interior Mission

As the Nation's principal conservation agency, the Department of the Interior has responsibility for most of our nationally owned public lands and natural resources. This includes fostering sound use of our land and water resources; protecting our fish, wildlife, and biological diversity; preserving the environmental and cultural values of our national parks and historical places; and providing for the enjoyment of life through outdoor recreation. The Department assesses our energy and mineral resources and works to ensure that their development is in the best interests of all our people by encouraging stewardship and citizen participation in their care. The Department also has a major responsibility for American Indian reservation communities and for people who live in island territories under U.S. administration.

The Minerals Management Service Mission

As a bureau of the Department of the Interior, the Minerals Management Service's (MMS) primary responsibilities are to manage the mineral resources located on the Nation's Outer Continental Shelf (OCS), collect revenue from the Federal OCS and onshore Federal and Indian lands, and distribute those revenues.

Moreover, in working to meet its responsibilities, the **Offshore Minerals Management Program** administers the OCS competitive leasing program and oversees the safe and environmentally sound exploration and production of our Nation's offshore natural gas, oil and other mineral resources. The MMS **Minerals Revenue Management** meets its responsibilities by ensuring the efficient, timely and accurate collection and disbursement of revenue from mineral leasing and production due to Indian tribes and allottees, States and the U.S. Treasury.

The MMS strives to fulfill its responsibilities through the general guiding principles of: (1) being responsive to the public's concerns and interests by maintaining a dialogue with all potentially affected parties and (2) carrying out its programs with an emphasis on working to enhance the quality of life for all Americans by lending MMS assistance and expertise to economic development and environmental protection.